Streambed Stresses and Flow Around Bridge Piers

U.S. Geological Survey
Water-Resources Investigations Report 96-4142

Prepared in cooperation with the
UNIVERSITY OF LOUISVILLE, and
KENTUCKY TRANSPORTATION CABINET

Streambed Stresses and Flow Around Bridge Piers

By ARTHUR C. PAROLA[1], KEVIN J. RUHL[2], D. JOSEPH HAGERTY[1], BRIAN M. BROWN[1], DUFFY L. FORD[1], and ANTHONY A. KORVES[1]

[1]University of Louisville
[2]U.S. Geological Survey

U.S. Geological Survey
Water-Resources Investigations Report 96-4142

Prepared in cooperation with the
UNIVERSITY OF LOUISVILLE, and
KENTUCKY TRANSPORTATION CABINET

Louisville, Kentucky
1996

U.S. DEPARTMENT OF THE INTERIOR
BRUCE BABBITT, Secretary

U.S. GEOLOGICAL SURVEY
Gordon P. Eaton, Director

For additional information write to:

Chief, Kentucky District
U.S. Geological Survey
Water Resources Division
2301 Bradley Avenue
Louisville, KY 40217-1807

Copies of this report can be purchased from:

U.S. Geological Survey
Branch of Information Services
Box 25286
Denver, CO 80225-0286

CONTENTS

FIGURES

CONVERSION FACTORS

Multiply	By	To obtain
cubic foot (ft^3)	0.02832	cubic meter
cubic foot per second (ft^3/s)	0.02832	cubic meter per second
foot (ft)	0.3048	meter
mile (mi)	1.609	kilometer
square mile (mi^2)	2.59	square kilometer

Streambed Stresses and Flow Around Bridge Piers

By Arthur C. Parola, Kevin J. Ruhl, D. Joseph Hagerty, Brian M. Brown, Duffy L. Ford, *and* Anthony A. Korves

Abstract

Scour of streambed material around bridge foundations by floodwaters is the leading cause of catastrophic bridge failure in the United States. The potential for scour and the stability of riprap used to protect the streambed from scour during extreme flood events must be known to evaluate the likelihood of bridge failure. A parameter used in estimating the potential for scour and removal of riprap protection is the time-averaged shear stress on the streambed often referred to as boundary stress. Bridge components, such as bridge piers and abutments, obstruct flow and induce strong vortex systems that create streambed or boundary stresses significantly higher than those in unobstructed flow. These locally high stresses can erode the streambed around pier and abutment foundations to the extent that the foundation is undermined, resulting in settlement or collapse of bridge spans.

The purpose of this study was to estimate streambed stresses at a bridge pier under full-scale flow conditions and to compare these stresses with those obtained previously in small-scale model studies. Two-dimensional velocity data were collected for three flow conditions around a bridge pier at the Kentucky State Highway 417 bridge over the Green River at Greensburg in Green County, Ky. Velocity vector plots and the horizontal component of streambed stress contour plots were developed from the velocity data. The streambed stress contours were developed using both a near-bed velocity and velocity gradient method.

Maximum near-bed velocities measured at the pier for the three flow conditions were 1.5, 1.6, and 2.0 times the average near-bed velocities measured in the upstream approach flow. Maximum streambed stresses for the three flow conditions were determined to be 10, 15, and 36 times the streambed stresses of the upstream approach flow. Both the near-bed velocity measurements and approximate maximum streambed stresses at the full-scale pier were consistent with those observed in experiments using small-scale models in which similar data were collected, except for a single observation of the near-bed velocity data and the corresponding streambed stress determination. The location of the maximum streambed stress was immediately downstream of a 90 degree radial of the upstream cylinder (with the center of the upstream cylinder being the origin) for the three flow conditions. This location was close to the flow wake separation point at the upstream cylinder. Other researchers have observed the maximum streambed stress around circular cylinders at this location or at a location immediately upstream of the wake separation point.

Although the magnitudes of the estimated streambed stresses measured at the full-scale pier were consistent with those measured in small-scale model studies, the stress distributions were significantly different than those measured in small-scale models. The most significant discrepancies between stress contours developed in this study and those developed in the small-scale studies for flow around cylindrical piers on a

flat streambed were associated with the shape of the stress contours. The extent of the high stress region of the streambed around the full-scale pier was substantially larger than the diameter of the upstream cylinder, while small-scale models had small regions compared to the diameter of the model cylinders. In addition, considerable asymmetry in the stress contours was observed. The large region of high stress and asymmetry was attributed to several factors including (1) the geometry of the full-scale pier, (2) the non-planar topography of the streambed, (3) the 20 degree skew of the pier to the approaching flow, and (4) the non-uniformity of the approach flow.

The extent of effect of the pier on streambed stresses was found to be larger for the full-scale site than for model studies. The results from the model studies indicated that the streambed stresses created by the obstruction of flow by the 3-foot wide pier extended laterally, away from the pier face, approximately 3 times the pier width. The effect of the pier was approximately 8 times the width of the pier for the full-scale pier in this study. This large area of effect may be attributed in part to the 20 degree skew of the approach flow to the pier that was present for the three flow conditions.

A significant finding from the velocity measurements was the lack of a steady horseshoe vortex system at the upstream face of the pier. The horseshoe vortex system that normally forms upstream of piers is purported to be the primary cause of local scour. An explanation for the absence of the vortex is that the non-planar topography of the streambed around the base of the upstream end of the pier produced high values of bed roughness, and therefore disrupted formation of the vortex. Model studies that have been conducted with material mounded in front of the pier have shown that even a smooth mound can prevent horseshoe vortex formation.

INTRODUCTION

Bridges built over waterways collapse most commonly as a result of scour than from other causes; scour is the erosion of foundation material from around and beneath substructure components by flowing water. The erosion is a result of a combination of natural stream erosion processes and erosion processes induced by bridge components such as piers, abutments, roadway embankments, and the superstructure. Constriction of the channel by bridge substructure and superstructure components and debris that may accumulate on these structures can cause degradation across the entire channel. Local vortex systems induced by the bridge components cause scour of the streambed around bridge pier and abutment foundations and roadway embankments. This local scour can cause the streambed to be deepest around bridge pier and abutment foundations, potentially undermining these foundations. The effect of debris and ice accumulations against bridge elements, a common occurrence during flood events, further complicates this problem.

The design of bridge foundations that are not adversely affected by scour is possible. Current practice is to determine if the streambed material is classified as "erodible." If the streambed is considered erodible, then a scour depth is computed as though the streambed was composed entirely of sand. This approach may lead to conservative foundation designs that are expensive to construct. In the bridge design process, engineering judgment may be used to reduce the estimated scour depth (Richardson and others, 1991).

One alternative to designing the foundation for the maximum scour depth is to protect the streambed with an armor layer, such as a riprap system. However, the Federal Highway Administration (FHWA) recommends that, for an existing bridge, riprap should be used only as a countermeasure (Richardson and others, 1991). Equations exist to estimate the size of riprap required to protect streambeds around bridge piers and abutments. These equations were developed under laboratory conditions and their reliability under field conditions has not been examined.

A second alternative to designing for the maximum scour depth is to quantify the erodibility of the streambed material with respect to flow conditions, including the duration of those flow conditions. For either alternative, the resistance to flow of the armor layer or the streambed material must be known, and the erosion potential of the flow must be quantified. Both the erosion potential of the flow, and the resistive capacity of a streambed material to flow, can be expressed as a function of boundary shear stress on the streambed in the horizontal plane (referred to as streambed stress in this report). The critical boundary shear stress on the streambed is defined here as the lowest stress for which a material is susceptible to erosion. If this value is known, and if the stress created by a particular flow situation is known, then the potential for scour can be evaluated quantitatively. Boundary shear stress on the streambed around a model cylindrical pier has been investigated in the laboratory; however, boundary shear stress on the streambed around full-scale bridge piers and abutments has not been examined.

Purpose and Scope

The purpose of this study was to define streambed stresses around a full-scale bridge pier and compare that information with streambed-stress data collected in the laboratory on small-scale bridge piers. Both the magnitude and distribution of streambed stresses would be compared for the full-scale and small-scale bridge piers.

Two-dimensional velocity data were collected at up to 81 vertical locations around a cylindrical pier for three separate flow conditions. The velocity data was used to estimate streambed stresses and contours of the stress data were produced for the full-scale bridge pier. The study was a cooperative effort between the U.S. Geological Survey (USGS), the University of Louisville, and the Kentucky Transportation Cabinet.

Acknowledgments

The authors would like to acknowledge the assistance of Stewart Goodpaster of the Kentucky Transportation Cabinet for his help in locating data collection sites, the Study Advisory Committee (composed of State and Federal highway engineers) for their suggestions and guidance, Paul Roberson of the Louisville District Corps of Engineers for assistance in providing sustained flows from Green River Lake, and James Stahl, a University of Louisville Civil Engineering graduate student, for assistance in data collection.

PREVIOUS INVESTIGATIONS ON FLOW FIELDS AND STREAMBED STRESSES AROUND BRIDGE PIERS

Obstructions to flow, such as bridge piers and abutments, induce secondary currents that cause higher streambed stresses than in unobstructed flow. Consequently, the erosion capacity of the flow around piers and abutments is higher than the unobstructed flow, possibly causing local scour holes to form. The most frequent cause of catastrophic failure of bridges in the United States is scour of supporting material from around and below pier foundations (Makowski and others, 1989). Near bridges, streambed material is removed by a combination of natural erosion processes (channel scour); contraction of the natural channel by bridge components (contraction scour); and secondary currents induced by bridge piers and abutments (local scour). These combined elements may undermine the bridge substructure foundations and may lead to settlement and collapse of the bridge superstructure.

Common practice to solve the problem of scour at bridge sites is to place riprap on the streambed around the base of piers and abutments. Riprap that is sufficiently large and properly graded in size, protects the erodible materials of the streambed from the combined scouring forces. Riprap placed on the streambed alters the geometry and roughness of the streambed and therefore affects the flow around piers (Hjorth, 1975). As a result, the hydrodynamic forces on bed material are affected by riprap placement.

Flow Fields Induced by Bridge Piers

Local scour is caused by a combination of high fluid shear stresses, seepage forces, and diversion of bedload sediment on the streambed surrounding piers (Hjorth, 1975). These effects are caused by the flow system around the pier or and include (1) constriction of flow, (2) deflection of the downflow upstream of the pier, (3) formation of a horseshoe vortex system, and (4) formation of a flow separation spiral vortex and wake vortices in the wake of the pier. A schematic representation of the flow system is shown in figure 1.

The approach flow velocity distribution shown in figure 1 is typical of unobstructed flow conditions. The flow characteristics change abruptly as flow approaches the pier and accelerates to pass around it.

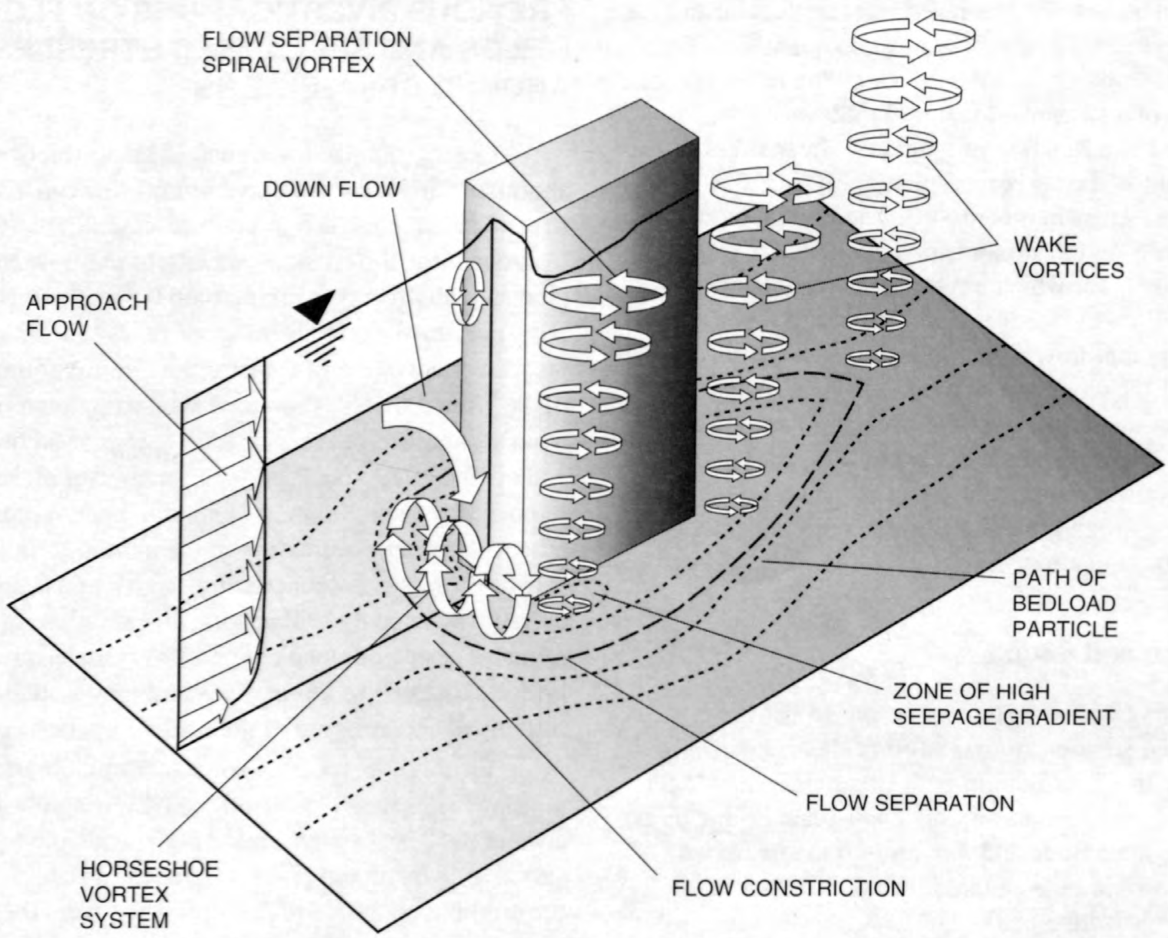

Figure 1. Flow system around a bridge pier.

The downflow, which occurs at the upstream face of the pier, resembles half of a vertical jet. Moore and Masch (1963) showed that the downflow is caused in part by the vertical velocity gradient of the approaching flow. The downflow also is caused by the curvature in the streamlines around the pier (Tison, 1937; Hjorth, 1975). The downflowing water causes flow constriction near the streambed, which impinges on the streambed, causing locally high fluid stresses. As shown in figure 1, streamlines of the approach flow at the base of the pier are deflected upstream and away from the pier by the momentum of the downward flowing water. In addition, the approach flow streamlines near the streambed are deflected by high pressure in a stagnation zone located immediately upstream from the pier, at approximately the same location of the horseshoe vortex shown in figure 1.

The complex system of vortices that develop upstream from the pier are caused by the disturbance of the flow field, and in particular from flow separation. Flow separation occurs where flows along a boundary converge, resulting in flow away from the boundary. The intersecting surface between these two flows is called the separation surface. A zone of flow separation forms on the streambed upstream of the pier. Shen and others (1966) explained the formation of this vortex system qualitatively in terms of changes in circulation.

A horseshoe vortex forms at the base of the upstream face of the pier. This is a result of the downflow along the upstream face of the pier attempting to propagate back upstream at the bed surface and the approaching flow forcing it downstream. The streamlines of the approach flow close to the streambed are deflected around the horseshoe vortex that forms in the separation zone. Hjorth (1975) postulated that bedload sediment is deflected away from the flow separation as well. The significance of this deflection of bedload sediment is that the potential for erosion of the bed around the pier may increase because of this localized loss in sediment load.

Wake vortices form along the sides of piers, particularly as a result of flow separation from the vertical edges of rectangular-shaped piers. Flow along the sides of the pier propagates back upstream toward the pier edge while flow along the upstream face of the pier is directed downward and out toward the pier edges. The upstream flowing water on each side of the pier converges at the pier edge with the flow from the upstream pier face. At this location, a surface of separation forms between both flows as they join and flow away from the pier corner. The surface of separation is the imaginary surface between the two converging flows. In addition, a boundary separation line forms where flow separates from the corner. The region between the side of the pier and the separation surface is called the wake region. Wake vortices form in this region as a result of abrupt changes in shape, as occurs with rectangular piers and foundations. Similar wake vortices form around cylindrical and round-nosed piers. However, the location of the separation from the boundary may change, depending on vortex shedding from the wake region. The wake vortex at the location of separation is called the flow separation spiral vortex. Once formed, the wake vortices are shed alternately from different sides of the pier and are carried downstream. The shedding of these wake vortices occurs downstream from abutments, but in slightly different ways from the vortex shedding around piers.

Vortex systems around a pier can generate fluctuations in the water pressures around the base of a pier. Using a small-scale pier in the laboratory, Hjorth (1975) measured pressure variations in the bed material around and below the pier near the flow separation points. Hjorth found reductions in water pressure just above the bed at these locations. Melville (1975) observed bursting of sediment particles from the streambed as wake vortices passed over them. He theorized that the wake vortices work in concert with the horseshoe vortices in removing bed materials. However, Dargahi (1987) found in similar experiments that wake vortices are shed at different frequencies than are horseshoe vortices. These observations indicate that the turbulent flow field around an obstruction generates very high local fluid shear stresses near the streambed that could become combined with locally severe uplift stresses caused by pressure fluctuations and seepage gradients.

Streambed Stress Around Bridge Piers

Because the flow field around an obstruction is so complex, it is difficult to predict even average shear and uplift stress values of the boundary between water and streambed around a bridge pier or abutment. Investigators have resorted to assumptions that simplify the flow system around bridge piers and abutments to analyze streambed stress and to predict time-averaged values of stress. For example, investigators have applied uniform flow similarity laws for the relation between streambed stress and velocity variation from the streambed. Because experimental laboratory data have been interpreted using such assumptions, values of streambed stresses can be used only to portray trends and qualitative changes in stress levels. Results of recently developed computational methods have shown that time-averaged streambed stresses may eventually be determined computationally for simple pier geometries and bed configurations (Mendoza-Cabrales, 1993; Olsen and Melaaen, 1993). However, no reliable estimates of streambed shear stresses have been developed to date for systems that incorporate full-scale bridge and stream geometries and actual flow conditions.

Melville (1975), Hjorth (1975), and Dargahi (1987) attempted to estimate the spatial variation of average streambed stresses around small-scale model piers from velocity measurements or Preston tube measurements. The Preston tube is a dynamic pressure sensing device that can be calibrated to measure shear stress over a smooth surface (Goldstein, 1983). In these studies, the investigators assumed a similarity relation between velocity profiles and streambed stress.

Melville (1975) used near-bed velocity and Preston tube measurements to determine streambed stresses on a fixed plane bed of homogeneous roughness around a circular cylinder. Melville found that the maximum streambed stress occurred beneath the edge of the wake zone and downstream of the flow separation from the pier. Using Preston tube measurements, Melville found that when a circular pier was present the streambed stress was approximately 4 times greater than without the pier. In addition, prior to scour hole development, the streambed stress under the horseshoe vortex upstream of the pier was less than the stress when no pier was present. After a scour hole had formed, the velocity measurements indicated that the region of maximum streambed stress shifted from the sides of the pier beneath the downstream flow separation zones, to the streambed area directly under the horseshoe vortex.

Hjorth (1975) approximated values of average streambed stress from Preston tube measurements. The spatial distribution and magnitude of average bed stresses determined by Hjorth were significantly different from those predicted by Melville (1975). In experiments involving a small-scale circular pier, Hjorth estimated that the streambed stress was as high as 12 times the stress of the undisturbed flow. However, when small-scale square-section piers were placed in the flow with their sides parallel to the flow direction, the measured data indicated that the streambed stress was approximately 4 times the stress generated in the model channel without the piers. When square-section piers were placed in the channel with their sides oriented at 45 degrees to the approaching flow, the measured data indicated that the streambed stress around the pier was as high as 11 times the stress in the channel without the piers.

In a similar study, Dargahi (1987) also used Preston tube measurements to evaluate the streambed stresses around a model circular pier. The measurements indicated that the mean streambed stress around the pier was approximately 3.5 times the stress that was determined at the bed surface in the approach flow outside the zone of affect of the pier. The zone of higher streambed stress extended upstream and downstream from the zone of flow separation.

For the purposes of providing guidance for riprap protection, Breusers and others (1977) recommended using a velocity at the pier equal to twice the approach flow velocity. This increase in velocity was based on potential flow around an infinite cylinder in the longitudinal direction. This recommendation also was based on observations reported by Nicollet and Ramette (1971) who found that the velocity at which particles just began to move at the sides of the model piers was the same as that which occurred when the flow velocity upstream of the piers was one-half of the velocity at which scour was first observed in the unobstructed channel. Other investigators such as Ettema (1980) have obtained similar results from model studies and observations of the start of erosion at the base of cylindrical piers. The increase in bed roughness caused by placement of riprap on the bed around a pier significantly changes the flow field and the streambed stresses. The changes in streambed stresses are highly dependent on roughness, therefore the presence of riprap around a pier must be considered.

Parola (1990) measured the approach flow conditions that caused displacement of model riprap mounded around small-scale model rectangular piers and placed within scour holes. These tests included variation in relative roughness of the bed from 0.004 to 0.4. Relative roughness of the approach flow is the ratio of the size of the bed material under the approach flow, D_o, to the depth of the approach flow, Y_o. Parola used these results to estimate the maximum streambed stress around the pier, assuming that the maximum streambed stress was equal to the value of critical shear stress that would just cause bed particles to begin to move in the model channel without piers. The critical shear stress to initiate particle motion was estimated from the Shields parameter (Raudkivi, 1990).

$$\tau_C = C_S(\gamma_S - \gamma)D_P \tag{1}$$

where

τ_c is the critical shear stress, in pounds per square foot,

C_s is the Shields parameter, dimensionless,

γ_s is the specific weight of rock, in pounds per cubic foot,

γ is the specific weight of water, in pounds per cubic foot, and

D_p is the equivalent particle diameter, in feet, around the pier.

A value of C_s of 0.06 was chosen on the basis of uniform flow, initial motion tests performed by Parola (1990) on the bed material. The same criteria for movement were used for each test.

The streambed shear stress of the approaching flow, upstream from, and outside of the affect of the pier was approximated from the log-velocity equation (Parola, 1990).

$$\tau_O = \frac{\rho U_O^2}{\left[5.75\log\left(5.53\frac{Y_O}{D_O}\right)\right]^2} \tag{2}$$

where

τ_o is the approach flow streambed shear stress, in pounds per square foot,

ρ is the density of water, in slugs per cubic foot,

U_o is the approach flow velocity averaged over the depth of flow, in square feet per second,

Y_o is the approach flow depth, in feet, and

D_o is the representative size of bed material, in feet, under the approach flow upstream of the pier.

If the maximum streambed shear stress around the pier is assumed to be equal to the critical shear stress for uniform unobstructed flow conditions, that is, $\tau_{max} = \tau_c$, the data collected by Parola (1990) can be used to approximate the ratio of maximum streambed shear stress around the model pier to the streambed shear stress upstream of the pier, τ_{max}/τ_o. The relation of this ratio to relative roughness D_o/Y_o is shown in figure 2 for all flow conditions for which Parola (1990) had conducted model tests on rectangular piers. Figure 2 shows that τ_{max}/τ_o varied considerably in Parola's tests ranging from about 1 to 18. The lowest value of τ_{max}/τ_o was found for flow conditions with very high bed relative roughness for the approach streambed. The highest value of τ_{max}/τ_o was found in the case of a relatively low bed roughness for the approach streambed. Tests were conducted using relatively small and large values of D_o/Y_o. While most of the observations contain values of D_o/Y_o of either <0.01 or >0.10, the observations with D_o/Y_o between 0.01 and 0.1 indicate a smooth transition between the two data clusters.

Johnson and Jones (1990) conducted experiments similar to Parola (1990) using marbles. They found maximum streambed stress at a small-scale cylindrical pier to be in agreement with those found by Parola (1990).

Effects of Seepage into and out of the Streambed

Near the streambed beneath the zones of separation in flow, the local variation in pressure can be substantial. Hjorth (1975) showed that pressure along the streambed can change by as much as ρU^2, from the front corner of a rectangular pier to the side of the pier, where ρ is the density of water and U is the unobstructed average flow velocity. When the pressure in the stream drops quickly by such high values, the instantaneous gradient causing seepage out of the streambed can be high. This rapid, substantial variation in pressure causes the entrainment of sediment particles from the streambed noted by Melville (1975). Posey (1973) stated that outflow seepage gradients would cause the removal of fine sandy material from

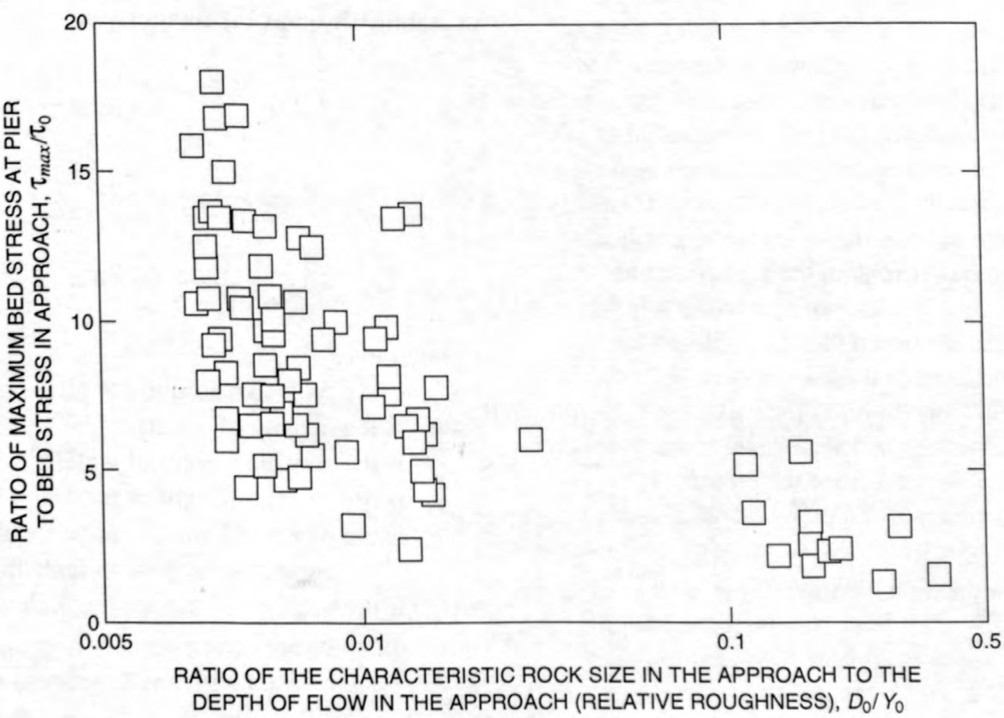

Figure 2. Maximum streambed-stress ratio and relative approach roughness for a rectangular pier.

beneath riprap protection and recommended that a filter should be provided to prevent removal of erodible fines. If such removal is severe, the loss of support can disrupt and undermine a riprap armor, layer.

Extent of Effect of the Flow Field at Bridge Piers

Laboratory experiments on small-scale models done by Hjorth (1975) provide a basis for determining the minimum extent that local vortex systems have on erosion of the streambed material around bridge piers. In those tests, a thin layer of sediment was placed over a plane bed to which a cylindrical model pier was attached. Flow velocity was increased until the streambed stresses caused ripples to form on the bed, and was then maintained at a slightly higher value during the remainder of the experiment. Hjorth measured the area of the streambed where the turbulence caused by the pier removed the sediment layer and exposed the plane undersurface. Hjorth suggested that the area of exposed undersurface would be the minimum area that is affected, which should be protected by an armor layer such as riprap.

Similar experiments were conducted by Parola (1993) using a rectangular pier, in which the angle between the approach flow direction and the long axis of the pier was varied from 0 to 90 degrees. The results of Parola's tests indicate that a protective layer (i.e., riprap) should extend upstream a distance *b* (*b* is the effective width of the pier, and is equal to the projected width of the pier perpendicular to the flow direction), and laterally for a distance of approximately *b*. If the formation of scour holes on the streambed downstream is to be prevented, the riprap should extend downstream a distance of approximately 5*b* measured from the upstream pier nose. When riprap is placed around the front of a pier, the stone armor prevents sediment from entering the wake zone. Hjorth (1975) found that wake vortices formed scour holes on the streambed downstream from the pier if the streambed downstream of the pier was not also protected.

The required extent of riprap protection is dependent on the overall flow system at the bridge crossing as well as the local flow fields around piers and abutments. If a possibility exists for the entire channel to degrade (general and contraction scour), then the riprap at the pier should be designed to accommodate this anticipated drop in bed level. The design of a protection system also should consider the extent of the high erosive stress region near the piers and abutments and the extent to which sediment is diverted around the piers and away from the abutments by the vortex systems.

Riprap Equations at Bridge Piers

The determination of the flow patterns and shear and pressure forces around bridge piers and abutments is important in bridge design or when attempting to reduce the risk of scour at existing structures. One method (although not recommended by the FHWA for design of new bridges) is the use of riprap: the placement of rock around a structural member or foundation to minimize bed material movement or loss.

Equations relating the rock size of riprap needed for stability around bridge piers were developed by Parola (1993), Parola and others (1989), Breusers and others (1977), Quazi and Peterson (1973), and Bonasoundas (1973). For rectangular piers Parola (1993) found that the rock size (equivalent diameter) required for stability varied relative to the ratio of the width of the pier face to the rock size, b/D_p; (basically a two-step solution). Parola (1993) provided the following equations to determine the size rock required for stability around a rectangular pier:

$$D_p = 1.25\rho \frac{U_o^2}{\gamma_s - \gamma} \quad for\ 20 < \frac{b}{D_p} < 33 \tag{3}$$

$$D_p = 1.0\rho \frac{U_o^2}{\gamma_s - \gamma} \quad for\ 7 < \frac{b}{D_p} < 14 \tag{4}$$

$$D_p = 0.83\rho \frac{U_o^2}{\gamma_s - \gamma} \quad for\ 4 < \frac{b}{D_p} < 7 \tag{5}$$

In equations 3–5, where

- D_p is the rock size around the pier,
- ρ is the density of water,
- γ is the specific weight of water,
- γ_s is the specific weight of rock (riprap),
- b is the pier width measured perpendicular to the approaching flow, in feet, and
- U_o is the velocity of the approach flow.

These equations are dimensionally homogeneous and therefore can be used with any consistent set of units.

Breusers and others (1977) recommended that Isbash's (1935) equation be used to size riprap, but that the design velocity be equal to two times the maximum approach flow velocity, U_o, to yield the relation.

$$D_p = 2.83 \frac{\rho U_o^2}{(\gamma_s - \gamma)} \tag{6}$$

Bonasoundas (1973) and Quazi and Peterson (1973) developed design equations based on the results of tests on small-scale cylindrical model piers. Bonasoundas (1973) gave the equation

$$D_p = 6 - 3.3\ U_o^2 + 4\ U_o^2 \tag{7}$$

for determining rock size for riprap around cylindrical piers. Quazi and Peterson (1973) developed a similar equation as

$$\frac{\rho\ U_o^2}{(\gamma_s - \gamma) D_p} = 1.14 \left(\frac{D_p}{Y_o}\right)^{-0.20} \tag{8}$$

Parola (1993) used the data from Quazi and Peterson (1973) and data from Parola (1990) to develop the equation

$$D_p = 1.4 \frac{\rho U_o^2}{(\gamma_s - \gamma)} \tag{9}$$

The relation between relative stone size and riprap stability for stones that are large relative to pier size (particularly width) requires further investigation. Likewise, further study should be given to the effect of mounding riprap around piers. Ettema (1980) found that scour depth was reduced significantly when bed-sediment size approached pier size. Likewise, Parola found that riprap mounded around a pier increased the stability of the streambed. The many small-scale model studies conducted to date have not taken into consideration (1) the effects of large bed forms (e.g., dunes on the streambed), (2) the stability of the bed material underlying riprap, (3) the effects of changes in riprap gradation, (4) the affect of different methods of placing riprap, (5) the effect of general degradation of the streambed, (6) the effects of ice blocking the stream or in contact with the riprap, or (7) the effects of debris collecting against piers or abutments. The lack of information about the affect of these factors on riprap stability indicates that the equations presented in this section should be used with extreme caution until additional information can be collected and interpreted.

THEORY OF STREAMBED SHEAR STRESS

Flow of water near bridge openings can be considered as flow of an incompressible and Newtonian fluid. The motion of the water is governed by mass and momentum conservation. The mass conservation equation for a steady flow of an incompressible fluid is

$$\frac{\partial u}{\partial x} + \frac{\partial v}{\partial y} + \frac{\partial w}{\partial z} = 0 \tag{10}$$

where u, v, and w are time-averaged components of velocity in the x-, y-, and z-coordinate directions, respectively. The time-averaged motion of turbulent flow can be modeled using the momentum conservation equation as

$$\rho\left(\bar{u}\frac{\partial \bar{u}}{\partial x} + \bar{v}\frac{\partial \bar{u}}{\partial y} + \bar{w}\frac{\partial \bar{u}}{\partial z}\right) = \rho g_x - \frac{\partial \rho}{\partial x} + \mu \nabla^2 \bar{u} - \rho\left(\frac{\partial \overline{(u')^2}}{\partial x} + \frac{\partial \overline{(u'v')}}{\partial y} + \frac{\partial \overline{(u'w')}}{\partial z}\right) \tag{11}$$

$$\rho\left(\bar{u}\frac{\partial \bar{v}}{\partial x} + \bar{v}\frac{\partial \bar{v}}{\partial y} + \bar{w}\frac{\partial \bar{v}}{\partial z}\right) = \rho g_y - \frac{\partial \rho}{\partial y} + \mu \nabla^2 v - \rho\left(\frac{\partial \overline{(v'u')}}{\partial x} + \frac{\partial \overline{(v')^2}}{\partial y} + \frac{\partial \overline{(v'w')}}{\partial z}\right) \tag{12}$$

$$\rho\left(\bar{u}\frac{\partial \bar{w}}{\partial x} + \bar{v}\frac{\partial \bar{w}}{\partial y} + \bar{w}\frac{\partial \bar{w}}{\partial z}\right) = \rho g_z - \frac{\partial \rho}{\partial z} + \mu \nabla^2 w - \rho\left(\frac{\partial \overline{(w'u')}}{\partial x} + \frac{\partial \overline{(w'v')}}{\partial y} + \frac{\partial \overline{(w')^2}}{\partial z}\right) \tag{13}$$

where

- ρ is the fluid density;
- μ is the dynamic viscosity in pound-second per square foot;
- g_x, g_y and g_z are the components of gravity in feet per square second in the directions denoted by the subscripts; and
- u', v', and w' are the turbulent fluctuations of velocity from the mean values (Schlichting, 1979).

The operator ∇^2 is defined as

$$\nabla^2 = \frac{\partial^2}{\partial x^2} + \frac{\partial^2}{\partial y^2} + \frac{\partial^2}{\partial z^2}.$$

The three right hand terms in each of equations 11, 12, and 13 represent the momentum transfer associated with fluctuating velocity components. The fluctuations of velocity can be conceptualized as artifacts of eddies that transport fluid momentum from the highest velocity portions of flow to the boundary. The fluctuation terms in the time-averaged equations represent this transfer of fluid momentum caused by eddies. In turbulent flow, the transfer of fluid momentum by this mechanism is an order of magnitude larger than that of fluid viscosity except close to the boundaries. For hydraulically rough boundaries the viscous stress terms (terms containing μ) are negligible compared to other terms.

In regions of separated flow, all terms in equations 11, 12, and 13 become important; however, in regions of small vertical velocity, the typical boundary layer assumptions can be used to examine the relation between flow and horizontal stress planes. Stresses on vertical fluid planes are assumed to be small except in regions close to the pier and in the fluid interface along the edge of wake regions. Therefore, equation 13 drops out and for purposes of describing the shear on a rough streambed the terms containing $u'v'$ and μ are considered negligible and equations 11 and 12 can be simplified to

$$\rho\left(\bar{u}\frac{\partial\bar{u}}{\partial x}+\bar{v}\frac{\partial\bar{u}}{\partial y}+\bar{w}\frac{\partial\bar{u}}{\partial z}\right) = -\frac{\partial\rho}{\partial x}-\rho\left(\frac{\partial\overline{(u')^2}}{\partial x}+\frac{\partial\overline{(u'w')}}{\partial z}\right) \quad (14)$$

and

$$\rho\left(\bar{u}\frac{\partial\bar{v}}{\partial x}+\bar{v}\frac{\partial\bar{v}}{\partial y}+\bar{w}\frac{\partial\bar{v}}{\partial z}\right) = -\frac{\partial\rho}{\partial y}-\rho\left(\frac{\partial\overline{(v'w')}}{\partial z}+\frac{\partial\overline{(v')^2}}{\partial y}\right). \quad (15)$$

The velocity fluctuation terms represent the variation of apparent stresses referred to as Reynolds stresses (Schlichting, 1979). These stresses are written

$$\tau_{xz} = \rho\,\overline{u'w'} \quad (16)$$

$$\tau_{zy} = \rho\,\overline{w'v'} \quad (17)$$

$$\sigma_{xx} = \rho\,\overline{(u')^2} \quad (18)$$

$$\sigma_{yy} = \rho\,\overline{(v')^2} \quad (19)$$

where

τ_{xz} and τ_{zy} are the two components of bed stress considered parallel to the water surface and

σ_{xx} and σ_{yy} are apparent normal stresses.

Because of the strong adverse pressure gradient of the flow caused by the pier, the effect of the fluctuating normal stresses is considered negligible, and therefore, the apparent normal stresses are considered negligible. The final equations of motion for flow in a horizontal place close to the streambed are

$$\rho\left(\bar{u}\frac{\partial\bar{u}}{\partial x}+\bar{v}\frac{\partial\bar{u}}{\partial y}+\bar{w}\frac{\partial\bar{u}}{\partial z}\right) = -\frac{\partial\rho}{\partial x}-\frac{\partial\tau_{xz}}{\partial z} \quad (20)$$

and

$$\rho\left(\bar{u}\frac{\partial\bar{w}}{\partial x}+\bar{v}\frac{\partial\bar{w}}{\partial y}+\bar{w}\frac{\partial\bar{w}}{\partial z}\right) = -\frac{\partial\rho}{\partial z}-\frac{\partial\tau_{zy}}{\partial z}. \quad (21)$$

Equations 20 and 21 are the reduced equations of motion describing the relation between stress planes parallel to the water surface and the fluid motion.

Streambed Stress and Velocity Gradient

Boundary stresses, and therefore streambed stresses, have been related to the gradient of the flow velocity near those boundaries. Relations such as those provided by Prandtl and Von Karman (Schlichting, 1979) relate boundary stress to the velocity distribution in the boundary layer. These relations assume that pressure gradients are negligible. These relations have been applied to conditions of nonuniform flow within 15 percent of the boundary layer thickness.

Von Karman's boundary layer equation (Schlichting, 1979) is

$$\frac{U-u}{u_*} = -\frac{1}{\kappa}\left\{\ln\left[1-\sqrt{\frac{z}{\delta}}\right]+\sqrt{\frac{z}{\delta}}\right\} \quad (22)$$

where

U is the free-stream undisturbed velocity outside the boundary layer,

u is the velocity at a distance z from the boundary,

z is the distance from the boundary,

δ is the boundary layer thickness, in ft,

κ is Von Karman's Universal Constant (0.4), dimensionless, and

u_* is the shear velocity defined as

$$u_* = \sqrt{\frac{\tau_o}{\rho}} \tag{23}$$

where

τ_o is the shear stress and

ρ is the fluid density.

Prandtl assumed a different shear distribution and developed an equation that can be expressed as

$$\frac{u}{u_*} = \frac{1}{\kappa} \ln (z) + C \tag{24}$$

where

C is a constant of integration.

Using equation 24 and values of u and y for two points along the velocity profile, the boundary shear stress can be expressed as

$$\tau_o = \frac{\rho (u_2 - u_1)^2}{\left(5.75 \log \frac{z_2}{z_1}\right)^2}. \tag{25}$$

A simpler relation that is essentially the same as Prantdl's equation is the one-seventh power law (Schlichting, 1979) given as

$$\frac{u}{u_*} = K z^{\frac{1}{7}} \tag{26}$$

where

K is a constant that must be determined empirically.

Other similar relations, termed similarity laws, between velocity profile and boundary stress have been developed (Schlichting, 1979). The similarity laws were developed for uniform flow in flume channels and pipes. The relations given above provide accurate estimates of streambed stress from velocity profile data of flow with negligible pressure gradients. In flow situations with significant pressure gradients, such as flow around piers and abutments, the characteristics of the boundary layer must be examined more extensively.

Origin of Velocity Profiles

The origin for determining distance from the boundary is necessary for determining velocity gradients for an indirect measurement of streambed stress. For hydraulically rough flow, the origin lies within the roughness elements. For streambeds with very high relative roughness, which is common where riprap protection is used, the precise location of the bottom is not well defined. The computed streambed stress is sensitive to the location of the origin for flow conditions with high relative roughness. Researchers have used hemispheres of diameter D mounted to a plane bed to determine the origin for depth as some fraction of D below the top of the hemispheres. Bayazit (1976) performed such a study and determined that the origin was located at 0.35 D.

Boundary Layer Characteristics

Boundary layer thickness δ can be defined as the distance where the velocity differs by only 1 percent from the external velocity (Schlichting, 1979). Displacement thickness δ^* is the distance where the external streamlines are shifted by the boundary layer and is defined by Schlichting (1979) as

$$\delta^* = \int_o^{\delta} \left(1 - \frac{u}{U}\right) dz \tag{27}$$

where

U is the free-stream velocity and

u is the x-component velocity a distance z from the boundary.

The momentum thickness θ, in ft, is the distance where the momentum of the external flow is affected by the boundary layer and is defined as (Schlichting, 1979)

$$\theta = \int_o^{\delta} \frac{u}{U}\left(1 - \frac{u}{U}\right) dz. \tag{28}$$

A dimensionless shape factor was defined to characterize velocity profiles in pressure gradients as (Schlichting, 1979)

$$H = \frac{\delta^*}{\theta}. \tag{29}$$

Given these characteristics of the boundary layer, an approximate solution to the momentum integral for a two-dimensional boundary layer is (Schlichting, 1979)

$$\frac{\tau_o}{\rho U^2} = \frac{d\theta}{dx} + (H + 2)\frac{\theta}{U}\frac{dU}{dx}. \tag{30}$$

For a turbulent boundary layer, H ranges from 1.3 in a zero pressure gradient to 2.5 at a separation region (Schlichting, 1979).

Dargahi (1987) used the method introduced by Clauser (1954) to determine streambed stresses from vertical velocity profiles measured in the plane of flow symmetry about a cylindrical pier model. Dargahi found that along the plane of symmetry the distribution of flow velocity agreed well with the logarithmic and wake universal law. In the region of significant adverse pressure gradient caused by the cylinder, the profiles deviated significantly from these laws. Dargahi defined a somewhat universal distribution for the boundary layer thickness, δ, for the entire region:

$$\Delta = \int_{o}^{\delta}\left(\frac{U-u}{u_*}\right)dz \qquad (31)$$

Streambed-Stress Measurement

Streambed-stress measurement techniques have been categorized as direct and indirect. Direct methods involve the actual measurement of force over a section of streambed. A section of the bed is allowed to move longitudinally and strain gages measure the deflection. Wall shear is then determined from this deflection. The details of isolating this section of streambed and preventing flow through the edges of the isolated section of the streambed make direct measurement impractical even under most laboratory conditions where three-dimensional flow is dominant; however, the method is still used in laboratory studies.

Indirect methods utilize a relation between velocity and boundary or streambed shear stress. The relation between velocity and streambed stress is based on similarity laws (Schlichting, 1979) as mentioned previously. Indirect methods to estimate streambed stress in the laboratory include use of the Stanton tube, Preston tube, and three-dimensional laser-doppler anemometer. The Stanton and Preston tubes are basically dynamic pressure sensing devices that can be calibrated to measure shear stress in flows without significant adverse pressure gradients (Goldstein, 1983). Melville (1975), Hjorth (1975), and Dargahi (1987) used Preston tubes to approximate streambed stresses around model bridge piers. Laser-doppler anemometry has been used to measure velocity fluctuations to determine Reynolds stresses in uniform flow in open channels. The three-dimensional laser doppler anemometer is capable of measuring practically instantaneous three-dimensional velocity; however, published papers on the measurement of streambed stress using this technique were not found in the literature. Melville (1975) used hot film anemometry to measure velocity at 2 mm (millimeters) from the streambed and developed a qualitative method to describe high streambed stress areas from these measurements. In addition, sonar acoustic doppler current profiler technology is developing rapidly to provide high frequency, three-dimensional velocity measurements. At the time of this study, however, these techniques were not developed sufficiently to provide accurate velocity measurement over a sufficiently small measurement volume in regions near the streambed, particularly in areas close to obstructions such as piers.

SITE SELECTION, INSTRUMENTATION, DATA COLLECTION, AND DATA REDUCTION

Site Selection

The criteria used for selecting a full-scale bridge site to collect data were that (1) flow velocity in the approach section be greater than 1.0 foot per second during the measurement, (2) skew of the approach flow to the pier be a minimum, (3) flow during the measurement be relatively constant, (4) pier diameter or width of from 1 to 4 ft, (5) manageable flow depths, and (6) minimal debris accumulation on the pier face. A reconnaissance was performed in the fall of 1991. It was anticipated that sites below reservoirs would have superior measuring conditions even though the travel time to the site would be extensive. In all, over 100 sites were evaluated, but only three sites had characteristics deemed suitable to meet accessibility and data collection needs. The three sites were located on the Green River downstream of Green River Lake. The Green River Lake is a multi-purpose project operated and maintained by the U.S. Army Corps of Engineers (COE), Louisville District office.

The three sites chosen for possible study were (1) Green River at State Highway 55 near Campbellsville, Ky., (2) Green River at U.S. Highway 68 at Greensburg, and (3) Green River at State Highway 417 at Greensburg, Ky. Each of the three sites consisted of two piers, one of which would experience velocities and depths appropriate for study conditions. The piers at the State Highway 55 and U.S. Highway 68 sites consisted of three 4-foot square concrete columns connected by concrete webs. The 21-foot long piers at the State Highway 417 site consisted of two 3-foot diameter circular concrete columns connected by a concrete web 1.3 ft wide. Operational U.S. Geological Survey (USGS) gaging stations were located at the State Highway 55 and U.S. Highway 68 sites, and the State Highway 417 site was located just 3 miles upstream of the U.S. Highway 68 site. The locations of the three bridge sites and the two USGS gaging stations are shown in figure 3. The stations would make it possible to monitor stage and streamflow conditions at the measurement sites. Stage records, previous discharge measurements, and the latest stage-discharge relation at each gaging station provided information from which the optimal measurement period was determined. Previous records indicated that sustained flow occurs each spring from about March to mid-May as a result of controlled releases from the dam after rainfall events, and from mid-October to early December when the Lake is lowered to winter pool level. The fall period was chosen as the measurement period. In the fall, water availability is quite certain because summer pool must be lowered in anticipation of winter and spring rains. In addition, precipitation amounts in the fall are generally small. Therefore, larger releases from the dam than those needed for the measurements would be unlikely. By contrast, spring releases are rainfall dependent, and because of the 1988 drought in Kentucky, the COE multi-purpose projects have operated on an early-fill schedule since 1989. In addition, measurement activities could be preplanned more easily during the fall drawdown than during the spring, because rainfall would not be a prerequisite to measurement activities. By using sites below the dam, debris accumulation on the pier would be minimized, particularly during the drawdown cycle. The mid-October to early December time period limited data collection, but the measurement conditions were considered superior to those in the spring or at other sites where flow is uncontrolled.

Instrumentation and Data-Collection Equipment

The data acquisition system, including the software used to collect and store the laboratory velocity data was developed by Parola (1990). At the full-scale bridge site, measurements were to be made from a boat secured in position by a cable stretching across the stream and by ropes tied to eyelets mounted in the pier face. A Marsh-McBirney 511 two-dimensional, high sensitivity current meter with a 1.5 in. diameter sensor was used to determine longitudinal and lateral point velocities, and at a few locations the sensor was reoriented to collect vertical velocity readings as well. The sensor was attached to a 13 ft aluminum rod that was positioned manually. So that the sensor would always be oriented in the same direction in the flow, a digital compass was attached to the aluminum rod. A digital display allowed the person taking the measurement to orient the sensor in a particular direction and continuously monitor the value. As the velocity was being measured and recorded, the orientation was also being sampled at 20 hertz and recorded by the data acquisition software. The output of the compass was 0.0 to 1.9 volts, and was converted to 0.0 to 359.9 degrees. A prism was attached to the aluminum rod, and a total station accurate to within 5 seconds of arc was used to determine the sensor location in a predefined horizontal grid and to determine bed elevation. The prism was positioned so that it was directly above the velocity sensor when the rod was held vertical.

The 13 ft aluminum rod consisted of two poles; one fixed and one movable. The fixed pole was 3/4 in. aluminum stock graduated every 0.1 ft with a 3 in. diameter base plate and a bracket near the top to mount the digital compass and prism. The movable rod was 1/2 in. round aluminum stock graduated every 0.1 ft and had a bracket near the bottom for mounting the velocity probe. A groove was machined into the movable rod to accommodate the cable that ran from the sensor to the top of the rod and then to the meter. Ties were used to secure the cable to the rod and prevent the cable from vibrating in the flow. A schematic of the rod is shown in figure 4.

During testing of the Marsh-McBirney current meter, it was observed that vibrating the cable from the probe to the meter resulted in a fluctuation of the signal.

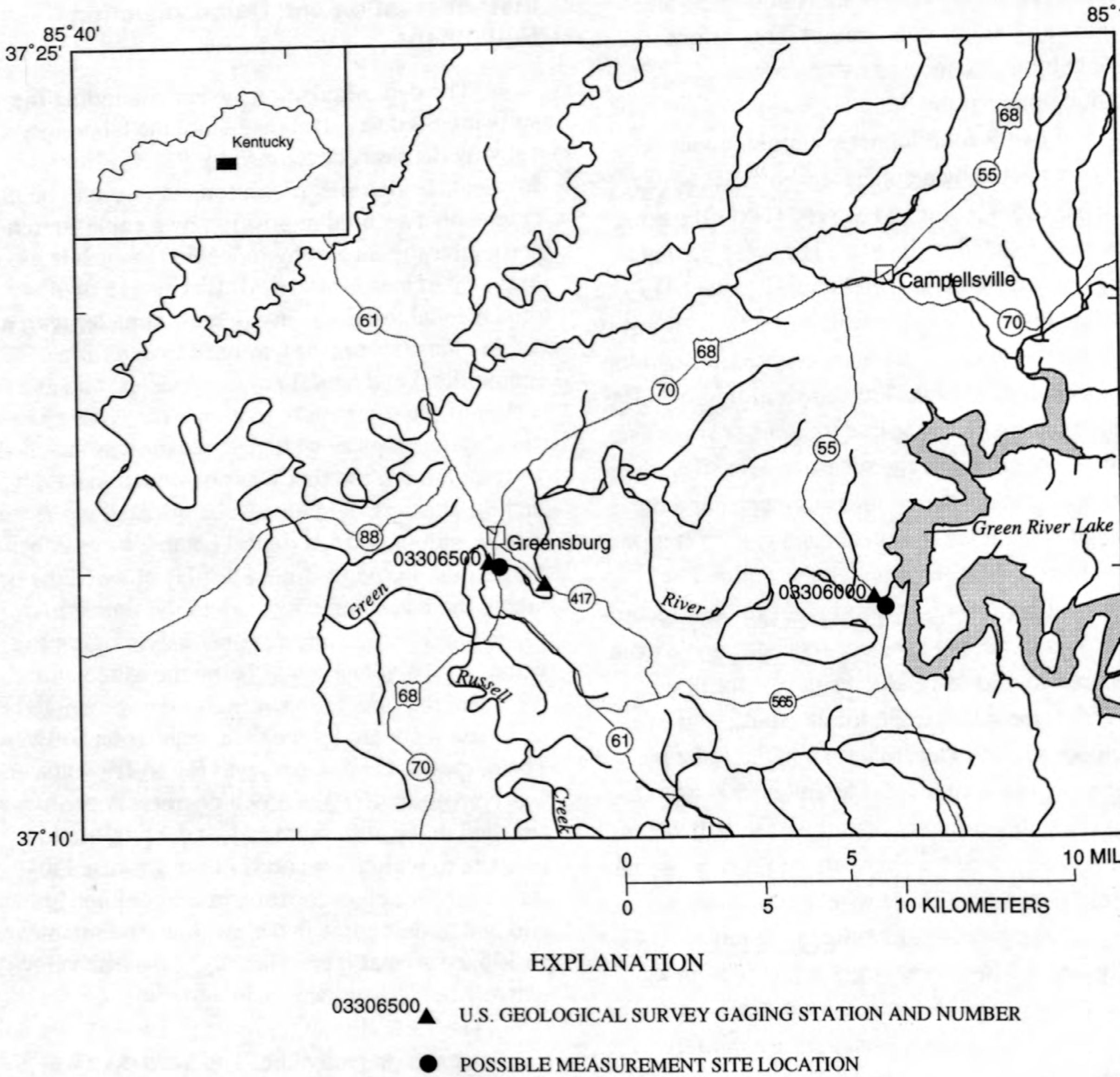

Figure 3. Location of streamflow-gaging stations and possible measurement sites on the Green River.

Therefore, precautions were taken during measurements to minimize cable vibration. These included positioning the cable in the groove in the round rod and securing it with ties, and placing the meter in the boat. The excess cable was neatly stowed in the boat to prevent movement. The signal cable from the meter was then suspended above the water and over to the streambank to the data acquisition equipment. The ±1.0 volt output for both velocity components of the current meter were amplified to ±5.0 volts and converted to a digital signal using a Metrabyte DAS-8 analog to digital converter. The DAS-8 card was controlled by a Dell 320sl 80386 laptop computer and Labtech Notebook software. The two velocity components were recorded at 20 Hz in ASCII format and compressed before being stored on 1.44 megabyte diskettes. The computer was powered by a 12-volt, deep-cycle marine battery.

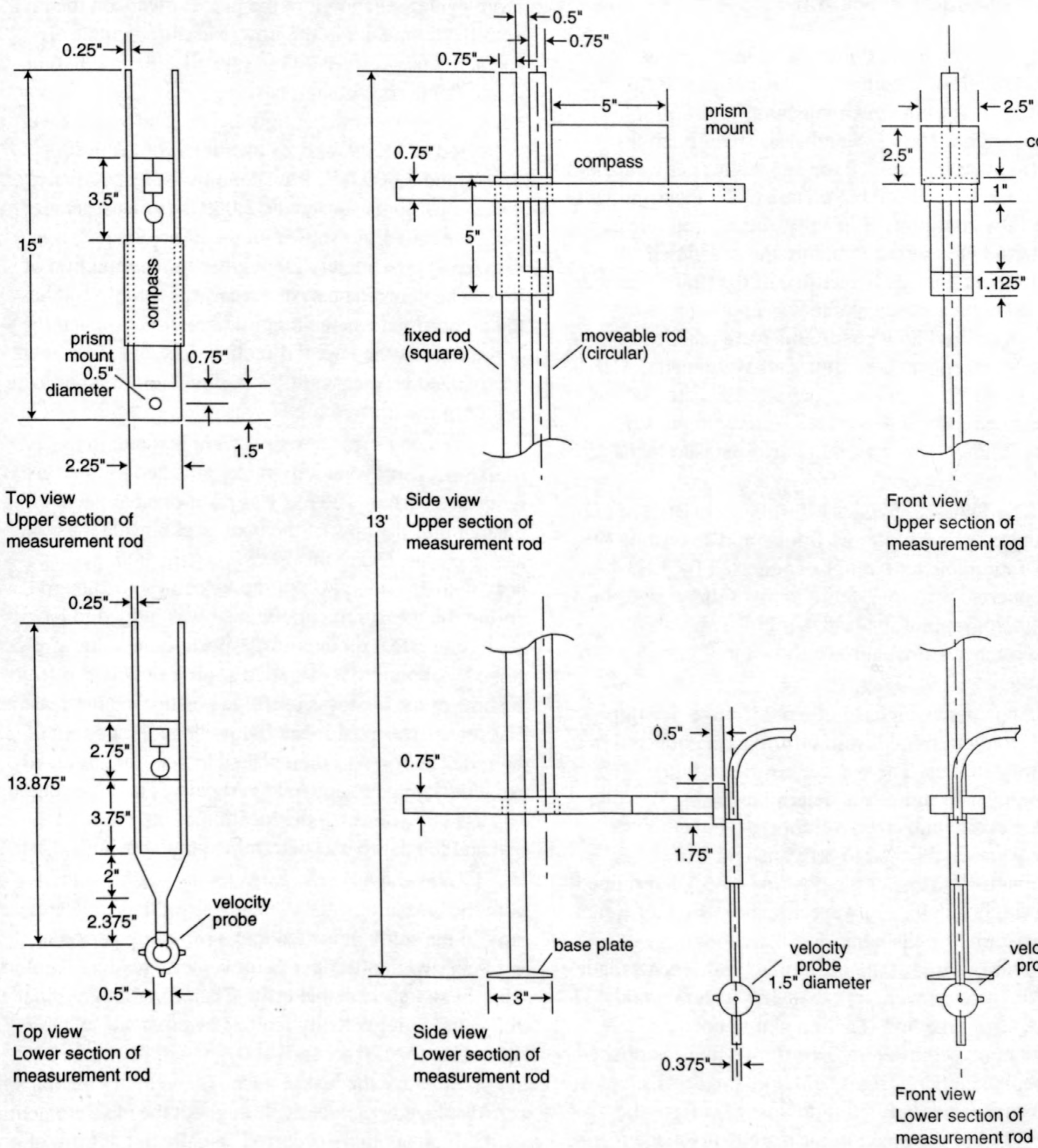

Figure 4. Measurement rod and electromagnetic velocity probe, compass, and prism mounts.

Data-Collection Procedure

Two-dimensional measurements were made under three flow conditions at the east pier at the State Highway 417 bridge in Greensburg, Ky., during the period October 15 to December 8, 1992. Each flow condition was maintained for 3 to 4 days per week, and 7 to 8 days were needed to complete the measurements at one flow condition. Typically, the desired release was started the afternoon before the scheduled measurement period. Traveltime of the flow from the Lake to the measurement site was about 4 hours, therefore desired flow conditions were reached at least 12 hours before any measurements were made. After the 3 to 4 day measurement period, the Lake outflow was reduced to match estimated inflow to the Lake, thereby holding water until the next measurement period.

The State Highway 417 bridge consisted of two identical piers, each pier 21 ft long and consisting of two, 3-foot diameter columns connected by a 1.3-foot wide concrete web. A location map of the bridge site and a photograph of the bridge pier where measurements were made are shown in figures 5 and 6, respectively.

Approximate measurement locations for this study were determined from information collected in laboratory studies. The precise position of the measurement location was determined using the total station. Several hubs (recoverable survey reference marks) were established to reference position determinations. Most of the positions were determined from a single hub located approximately 40 ft upstream of the east pier on the bank (left bank looking downstream). Most of the position measurements made from this location were less than 100 ft (horizontal distance) from the hub. The remaining position measurements were determined from a hub established on the opposite bank (right bank looking downstream) that was approximately 50 ft downstream from the bridge. Most of the position measurements made from this location were about 200 ft (horizontal distance) from the hub.

The velocity measurements were collected from a 17 ft john boat. A bracket mounted on the boat accepted a steel cable that was stretched from bank to bank. The bracket pinched the cable to keep the boat stationary once at the measurement location. Ropes from eyelets anchored in the pier to cleats on the boat, stabilized the boat in the flow. Measurements were made at three different flow rates: 1,800, 2,230, and 3,000 ft^3/s. The actual measurement locations for each set of data are shown in figures 7, 8, and 9. Data were collected at 81, 79, and 23 locations for the 1,800, 2,230, and 3,000 ft^3/s flow conditions, respectively. Time constraints caused the 3,000 ft^3/s measurement to be abbreviated. As shown on the plots, the pier was skewed approximately 20 degrees to the direction of flow. The coordinate system that was established has the x-coordinate as the longitudinal direction and the y-coordinate as the lateral direction. The distances were normalized by pier width (3 ft. diameter piers) and the center of the upstream pier was selected as the origin.

Velocity measurements were made with the Marsh-McBirney velocity meter attached to the rod as described earlier. The rod was positioned either upstream of the bow of the boat or alongside the boat near the bow. Using this measuring method, particularly with consideration of the velocities encountered during the measurement, the boat was judged to have negligible effect on the flow, especially near the streambed. A boom that extended approximately 3 ft from the bow of the boat was useful in positioning the sensor. The sensor was positioned 0.4 ft above the bottom of the rod. The rod was then placed in position, oriented using the compass, and held vertically. The total station was used to determine the location of the probe in the grid and the depth was determined to the nearest 0.1 ft.

An average horizontal velocity was computed from the measurements. An analysis of data collected early in the study indicated that a sampling period of less than two minutes per point velocity reading would result in an unacceptable error. Therefore, longitudinal and lateral point velocity readings were made at a rate of 20 hertz for 120 seconds at 0.4, 0.6, 0.8, 1.3, 2.3, 4.3, and 6.3 ft above the bed surface. The velocity readings were displayed graphically throughout the measurement period. If an anomaly occurred, usually in the form of a velocity spike resulting from debris (leaves or sticks) covering or striking the probe, the measurement was usually repeated. If the measurement was not repeated, the spike was noted, and was removed during data reduction. At selected locations in the grid, vertical velocity readings were made only for the 2 or 3 points nearest the streambed.

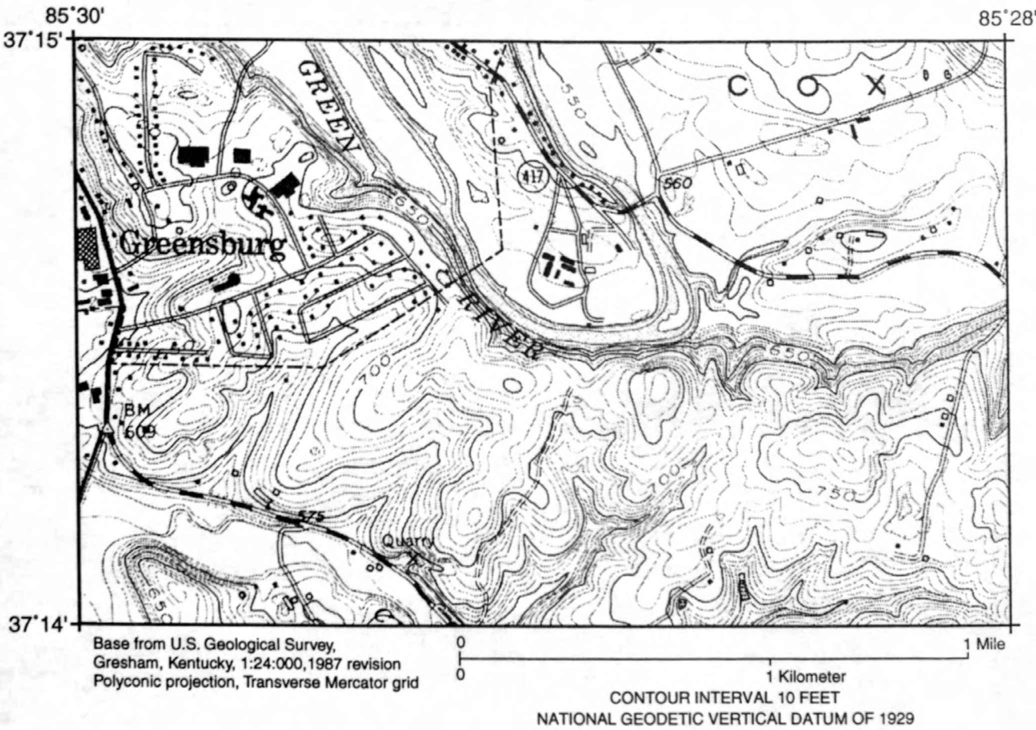

Figure 5. Stream reach, which includes the study area (flow is from right to left).

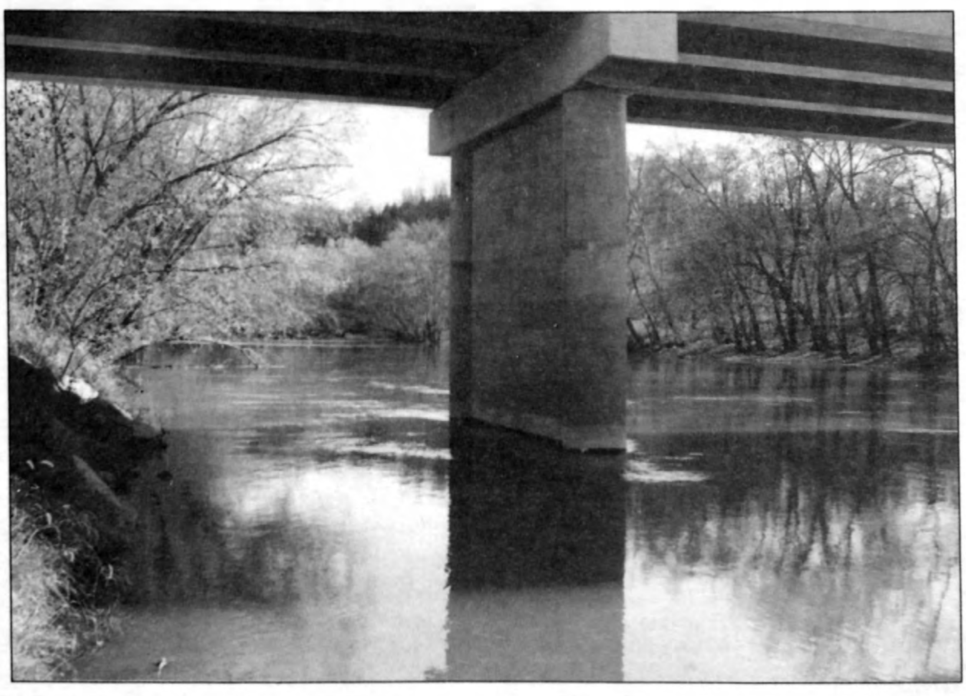

Figure 6. Upstream face of the pier where data were collected.

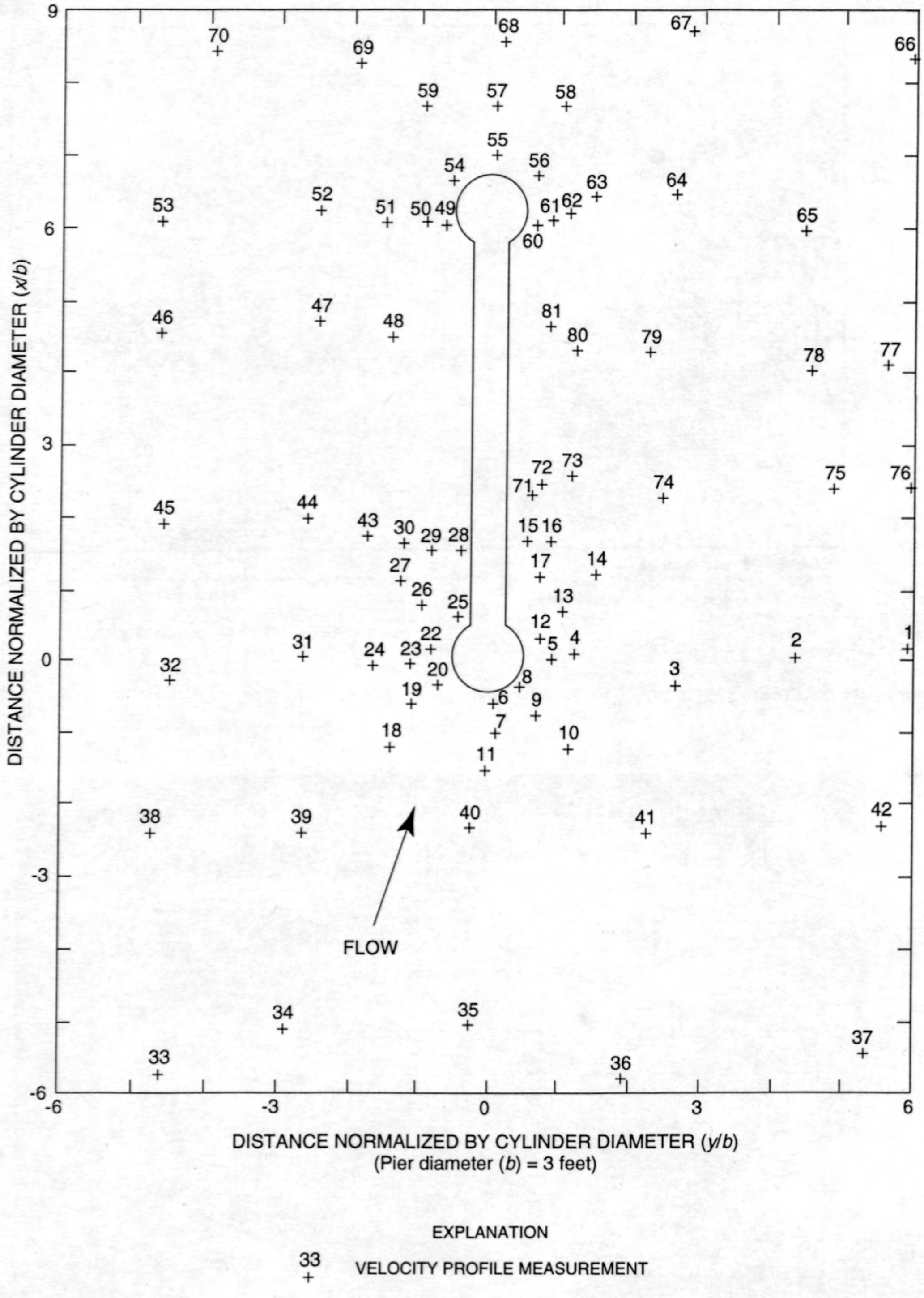

Figure 7. Location of velocity profile measurements for the 1,820 cubic feet per second flow condition at the study site [(0,0) is at the center of the upstream cylinder].

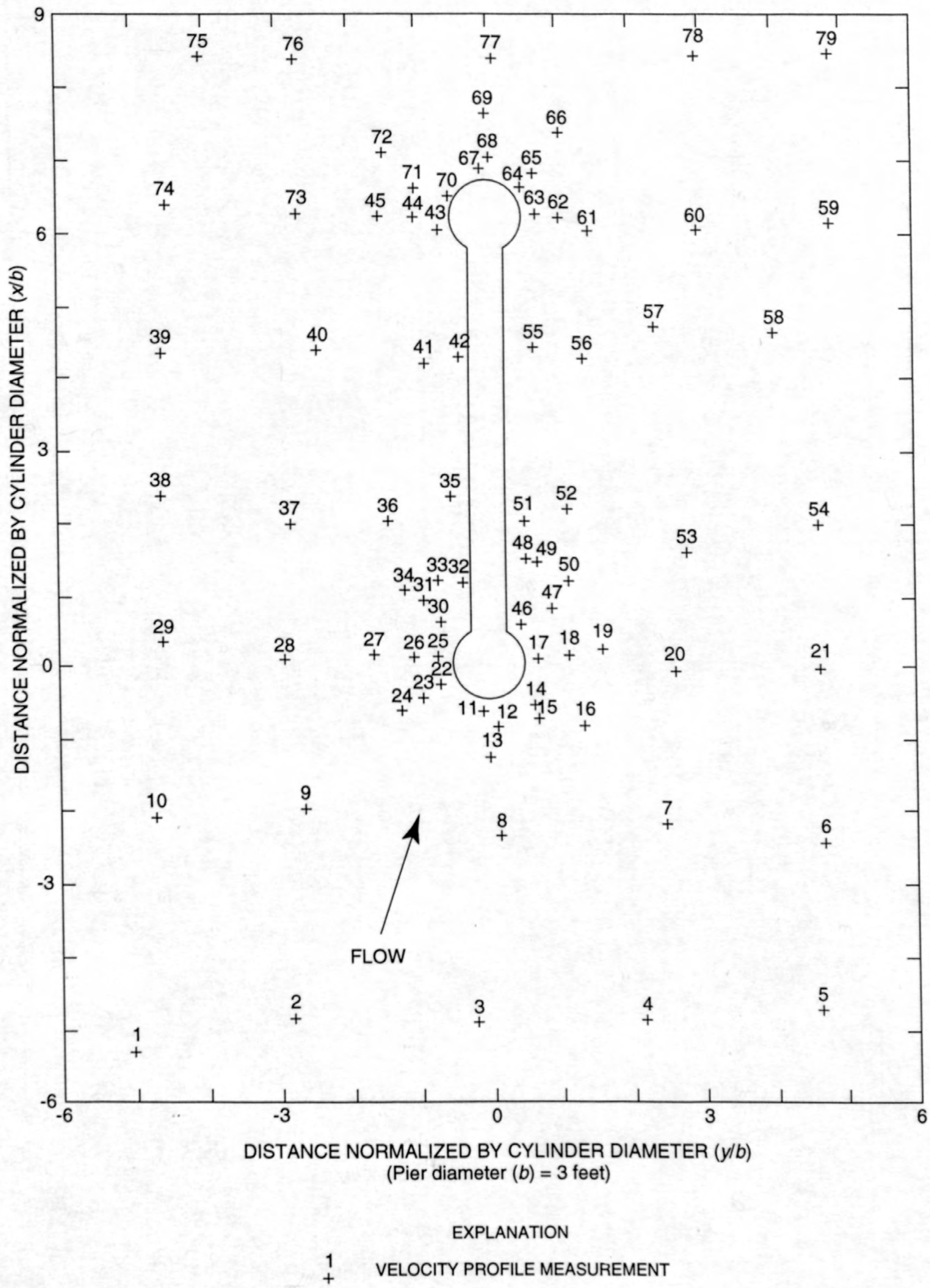

Figure 8. Location of velocity profile measurements for the 2,230 cubic feet per second flow condition at the study site [(0,0) is at the center of the upstream cylinder].

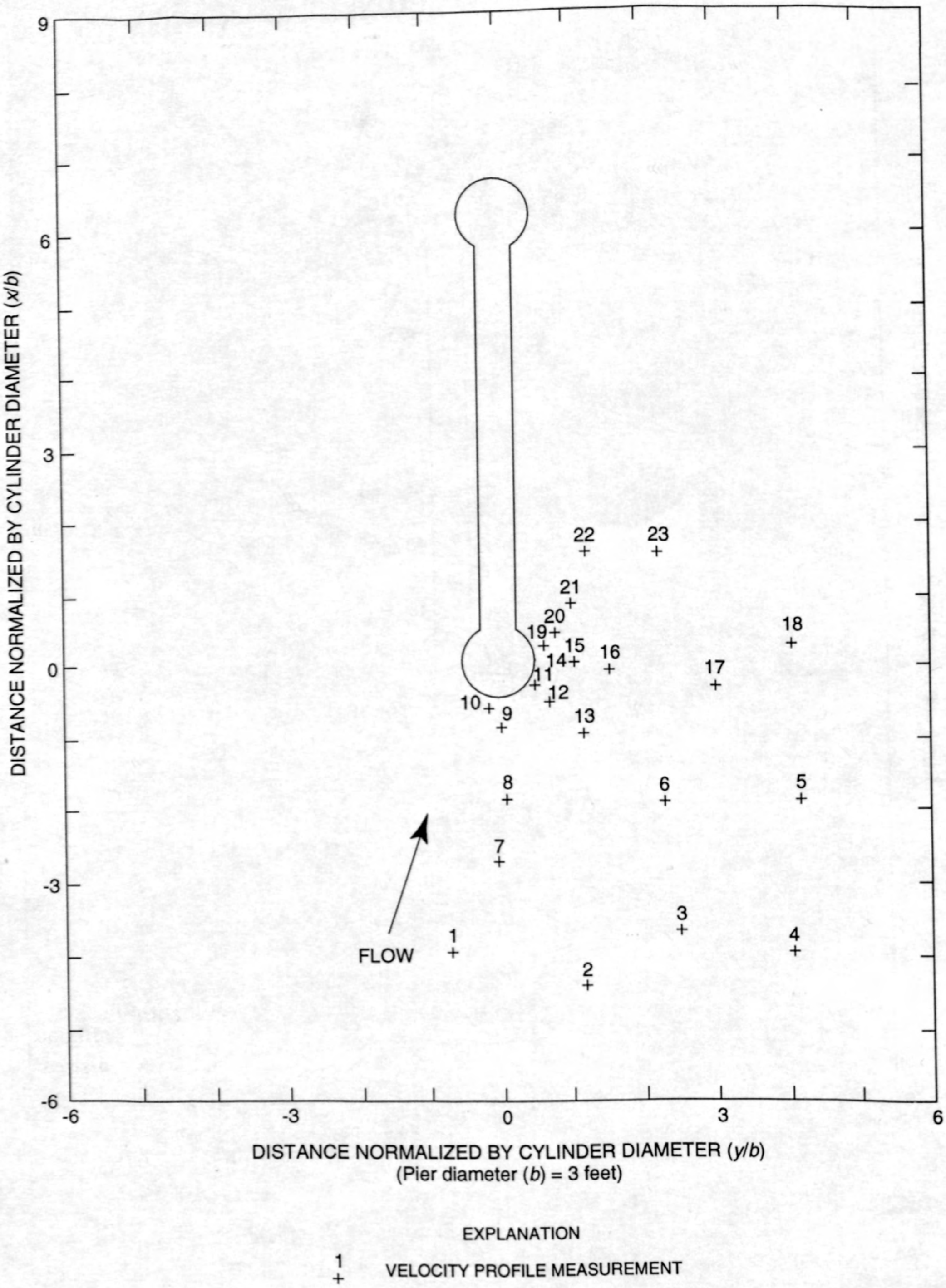

Figure 9. Location of velocity profile measurements for the 3,000 cubic feet per second flow condition at the study site [(0,0) is at the center of the upstream cylinder].

Data Reduction

Streambed elevations were measured during February 1991 and concurrently with the velocity readings during the three flow conditions. All data were combined to produce a contour plot of the streambed surface (fig. 10). As previously mentioned, the coordinate system was established with the x-coordinate as the longitudinal direction parallel to the streambank, the y-coordinate as the lateral direction perpendicular to the streambank, and the z-coordinate as the vertical direction. The center of the upstream cylinder of the pier was selected as the origin of the coordinate system. Peaks in the surface plots were caused by the rod being placed on the top of riprap. High regions along the left side of the pier represent areas where riprap mounds were located. Riprap was present around the upstream and downstream faces of the cylinders with scattered pieces present along both sides of the web section. Peaks and troughs of the surface plot at the upstream cylinder illustrate the high roughness of the streambed in this area. The rod was difficult to position near the pier because of the riprap. The contour plot (fig. 10) also shows that the streambed was relatively flat upstream of the pier where the approach flow was measured.

The velocity data were examined to determine unreasonably high velocity accelerations that appeared as spikes in the data. These data spikes were likely caused by probe vibration or by debris colliding with the probe. Point velocity data with accelerations in excess of 5 square feet per second were removed from the data set. Average component velocities, velocity vector magnitudes, velocity vector angles, and other standard statistics for the velocity measurements were computed and are provided in Appendix A, tables A.1, A.2, and A.3 for the 1,820 ft^3/s, 2,230 ft^3/s, and 3,000 ft^3/s flow conditions, respectively. Streambed-elevation data collected at each profile measurement location are provided in Appendix B, tables B.1, B.2, and B.3 for the 1,820 ft^3/s, 2,230 ft^3/s, and 3,000 ft^3/s flow conditions, respectively. Streambed-elevation data from the February 1991 survey are provided in Appendix C, table C. Pier coordinate data are provided in Appendix D, table D.

STREAMBED STRESSES AND FLOW AROUND BRIDGE PIERS

Average velocity vectors and magnitudes at each measurement profile were analyzed to determine the extent of effect of the flow on the streambed and the effect of the pier on local boundary (streambed) stress. Near-bed velocity and geometric values were normalized for the purpose of comparing full-scale bridge pier data to the small-scale model data. Distances are represented in units of the pier cylinder diameter, b, with the center of the upstream cylinder as the origin. Velocity magnitudes are represented as multiples of the near-bed approach velocity taken from the central three profiles, located approximately 5.5 pier diameters upstream of the origin (15 ft upstream from the nose of the pier). The streambed stresses also are represented as multiples of the average approach flow streambed stresses computed from the stresses measured at 5.5 cylinder diameters upstream of the origin.

Upon initiation of the study the researchers hypothesized that Reynolds stresses could be computed from measurements of the turbulent fluctuations near the streambed. Data were collected for this purpose; however, the data provided unrealistic estimates of streambed stresses. Two reasons for the unrealistic estimates were (1) the difficulty in aligning the sensor with the local velocity vector to collect velocity components in a vertical plane and (2) the difficulty in obtaining velocity fluctuation measurements sufficiently accurate to compare Reynolds stresses. Based on the analysis of preliminary data, the electromagnetic meter values of average velocity were judged to be accurate to within 5 percent. The root mean square (rms) of the velocity fluctuations ranged from 10 to 20 percent of the point mean velocity, making the error of each fluctuation value unacceptably high for Reynolds stress computations. Because of the difficulty in obtaining adequate information to determine Reynold stresses from the velocity data, streambed stresses were estimated from the average velocity data only.

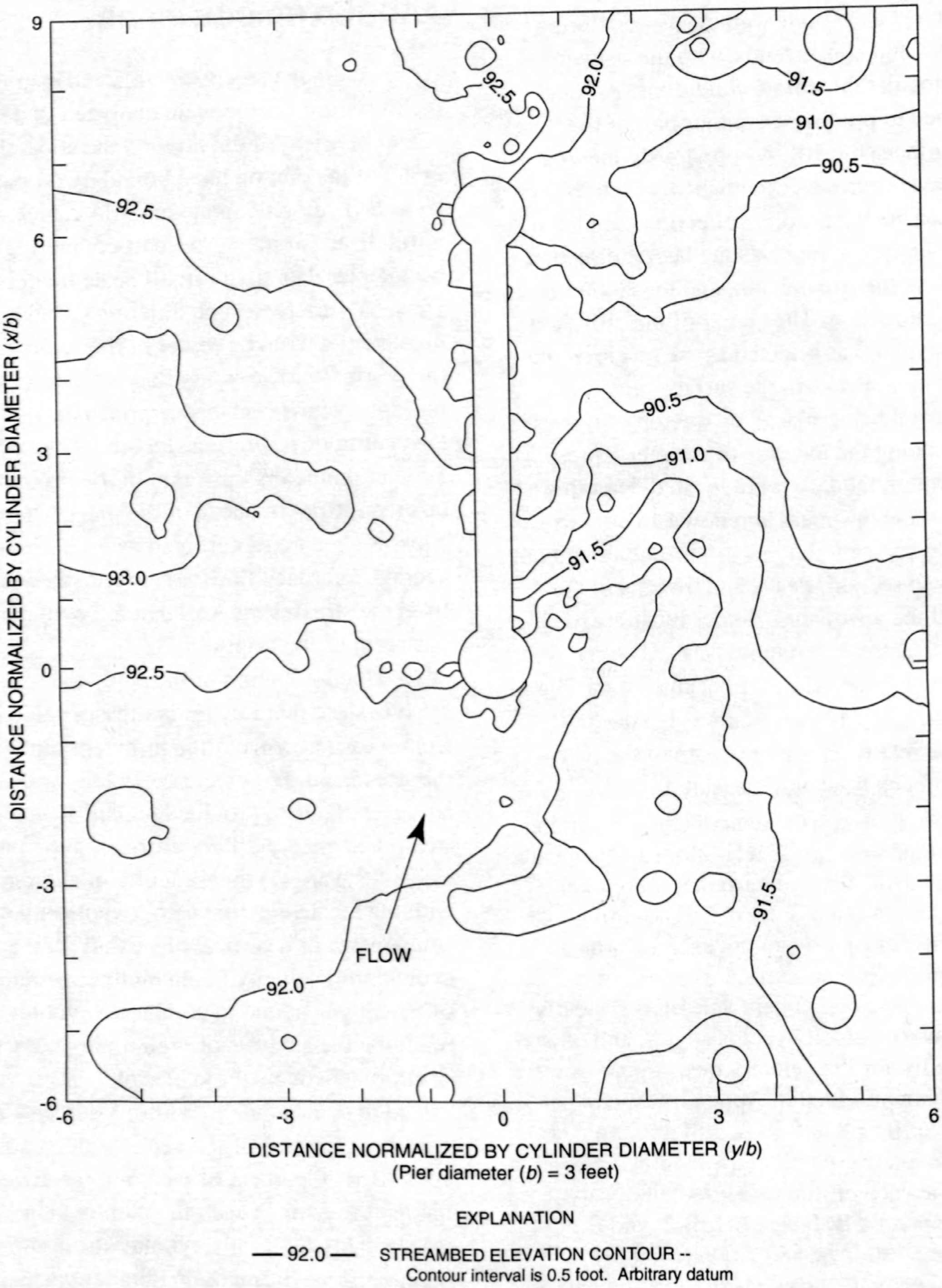

Figure 10. Streambed-elevation contours around the pier [(0,0) is at the center of the upstream cylinder].

Near-Bed Velocity Vectors

The velocity measured closest to the streambed, 0.4 ft from the streambed, for each profile was used to determine the extent of the affect of the pier on the flow field. This velocity was termed the "near-bed velocity." The variation of the near-bed velocities indicated high stress areas and the extent of the affect of the pier. The near-bed velocity vector fields for the three flow conditions are listed in Appendix E, table E.1, and are plotted in figures 11, 12, and 13.

The upstream velocity vectors show that the approach flow near the streambed was skewed to the pier by about 20 degrees for the three flow conditions. The skew was postulated to be the result of a complex interaction caused by the bend in the river, located approximately 500 ft upstream from the bridge, and the bank and bed geometry. High velocity regions were found on the sides of and immediately downstream from the upstream cylinder. Figures 11 and 12, for the 1,820 and 2,230 ft^3/s flow conditions, respectively, show that large wake separation regions with reverse flow occurred along the webwall on the right side (looking downstream) of the pier and relatively small wake separation regions formed downstream of the upstream cylinder on the left side. The asymmetric wake separation regions were caused by the combination of bed topography and the 20 degree skew angle of the approaching flow. As shown in figure 10, higher bed elevations existed around the entire pier, except in a region along the right side of the webwall, because of the presence of riprap. The abrupt change in streambed topography caused flow separation regions near the streambed on the right side. Because the area of lower streambed elevation is located in the wake of the upstream cylinder, adverse pressure gradients caused upstream flow along the face of the webwall.

Although the overall near-bed velocity fields for the three flow conditions showed many similarities, the size of the wake separation region and the magnitudes and locations of the maximum near-bed velocities were different for each flow condition. For the 1,820 ft^3/s flow condition (fig. 11), the highest velocities around the pier at elevation 0.4 ft were found downstream of the upstream cylinder just outside the wake separation zone (profiles 4, 8, 30, and 74 in fig. 7 and table E.1). The high velocity region on the right side of the pier extends further downstream and farther away from the pier than the high velocity region on the left side of the pier. The asymmetry of the high velocity regions can be attributed to the skew of the approach flow direction and the pier axis. The maximum velocities at elevation 0.4 ft were 1.45 and 1.50 times the average approach velocity at elevation 0.4 ft on the left and right side of the pier, respectively. The velocity values at the downstream end of the pier were low in comparison to the upstream velocities. Upstream flow near the streambed of the pier was not observed, indicating that a steady horseshoe vortex did not form.

The 2,230 ft^3/s flow condition (fig. 12), was similar to the 1,820 ft^3/s flow condition, but high near-bed velocities were observed further downstream and around the downstream cylinder. Evidence of a horseshoe vortex was not observed at the upstream face of the pier. The highest near-bed velocities around the pier were found at profiles 25, 27, 28, and 34 on the left side of the pier and profiles 14 and 18 on the right side of the pier (fig. 8 and table E.2). The maximum near-bed velocity on the left and right sides of the pier were 1.59 and 1.42 times the average approach near-bed velocity, respectively. The highest near-bed velocity regions were located near the wake separation zone from the upstream cylinder.

Data for the 3,000 ft^3/s flow condition was collected to describe the approaching flow and the high velocity region near the upstream cylinder (fig. 13). The velocity field for the region shown in figure 13 was similar to that of the other two flow conditions (figs. 11 and 12). Evidence of a horseshoe vortex was not observed at the upstream face of the pier. The highest velocity at 0.4 ft from the streambed around the pier was measured at profile 14 on the right side of the pier (fig. 9 and table E.3). Near the wake flow separation from the pier surface, the maximum velocity at 0.4 ft from the streambed was found to be about 2.04 times the average approach velocity at 0.4 ft from the streambed.

Near-bed velocity vectors along the sides of the upstream cylinder show the effects of convective acceleration and downflow for the three flow conditions. The ratio of the measured maximum near-bed velocities around the pier to the average near-bed approach flow velocity are similar to the near-bed velocity ratios measured by Parola (1990) in a small-scale model study of near-bed velocities around cylindrical and rectangular piers.

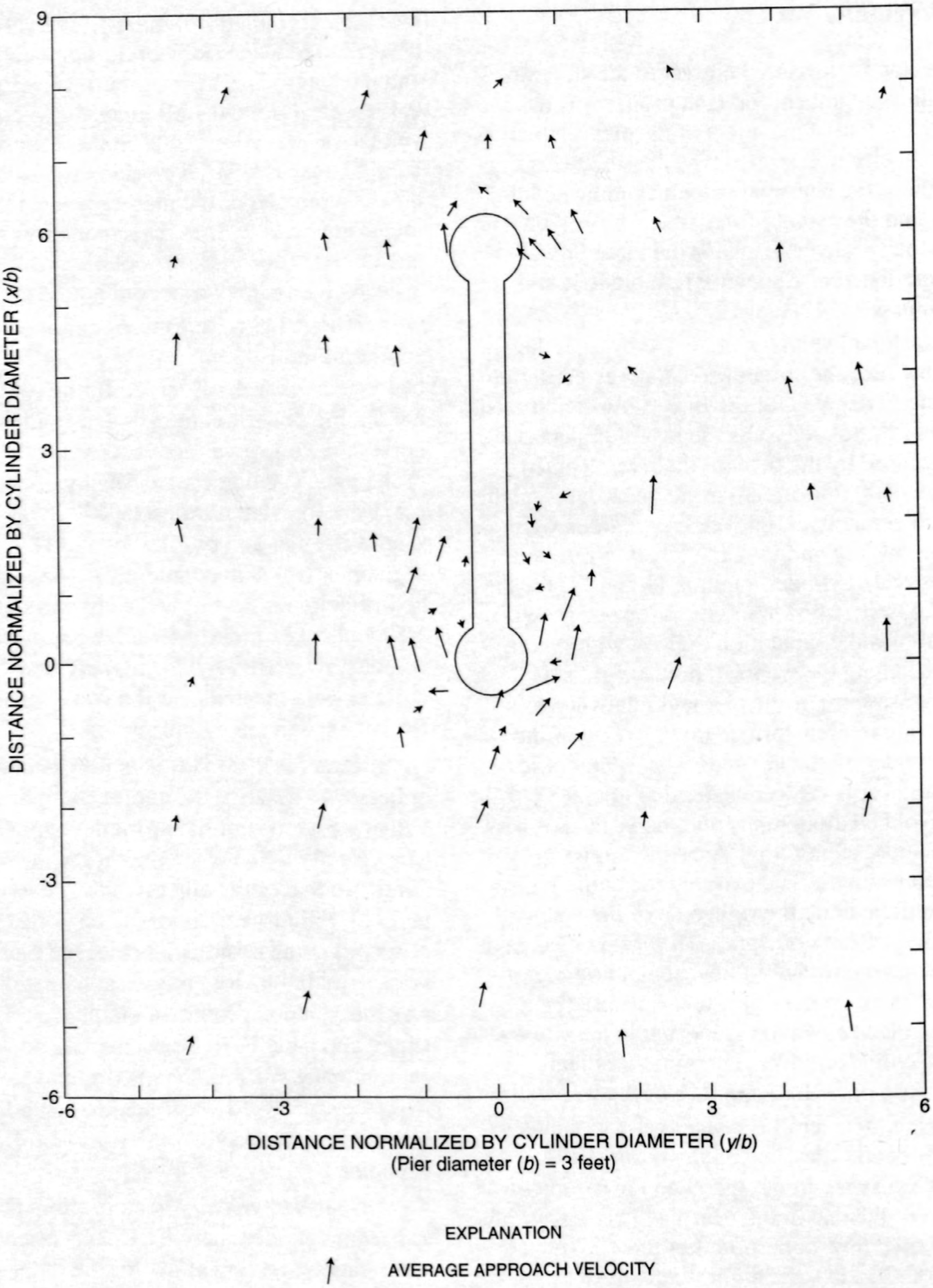

Figure 11. Vector representation of velocities measured at 0.4 foot above the streambed for the 1,820 cubic feet per second flow condition [(0,0) is at the center of the upstream cylinder].

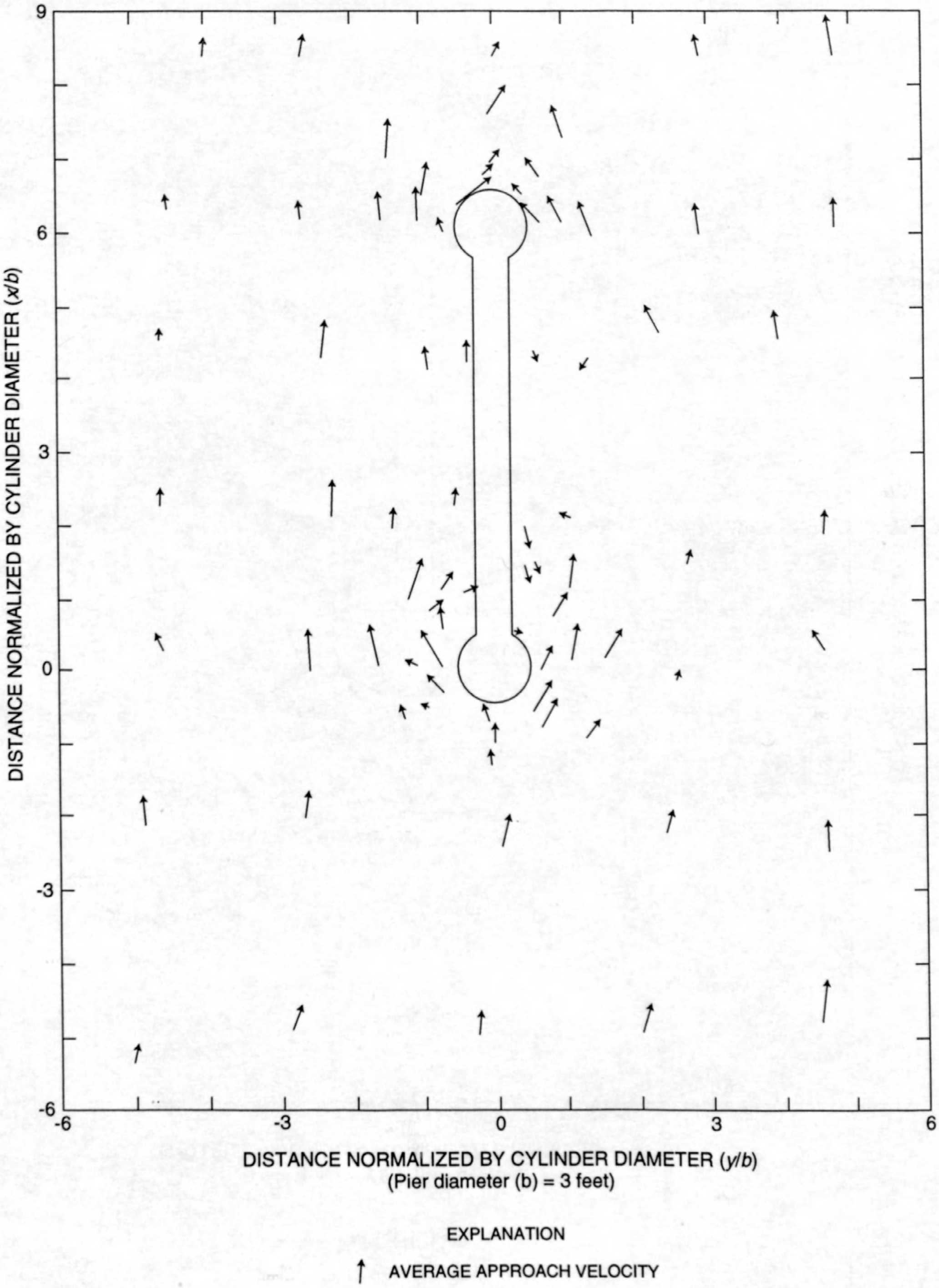

Figure 12. Vector representation of velocities measured at 0.4 foot above the streambed for the 2,230 cubic feet per second flow condition [(0,0) is at the center of the upstream cylinder].

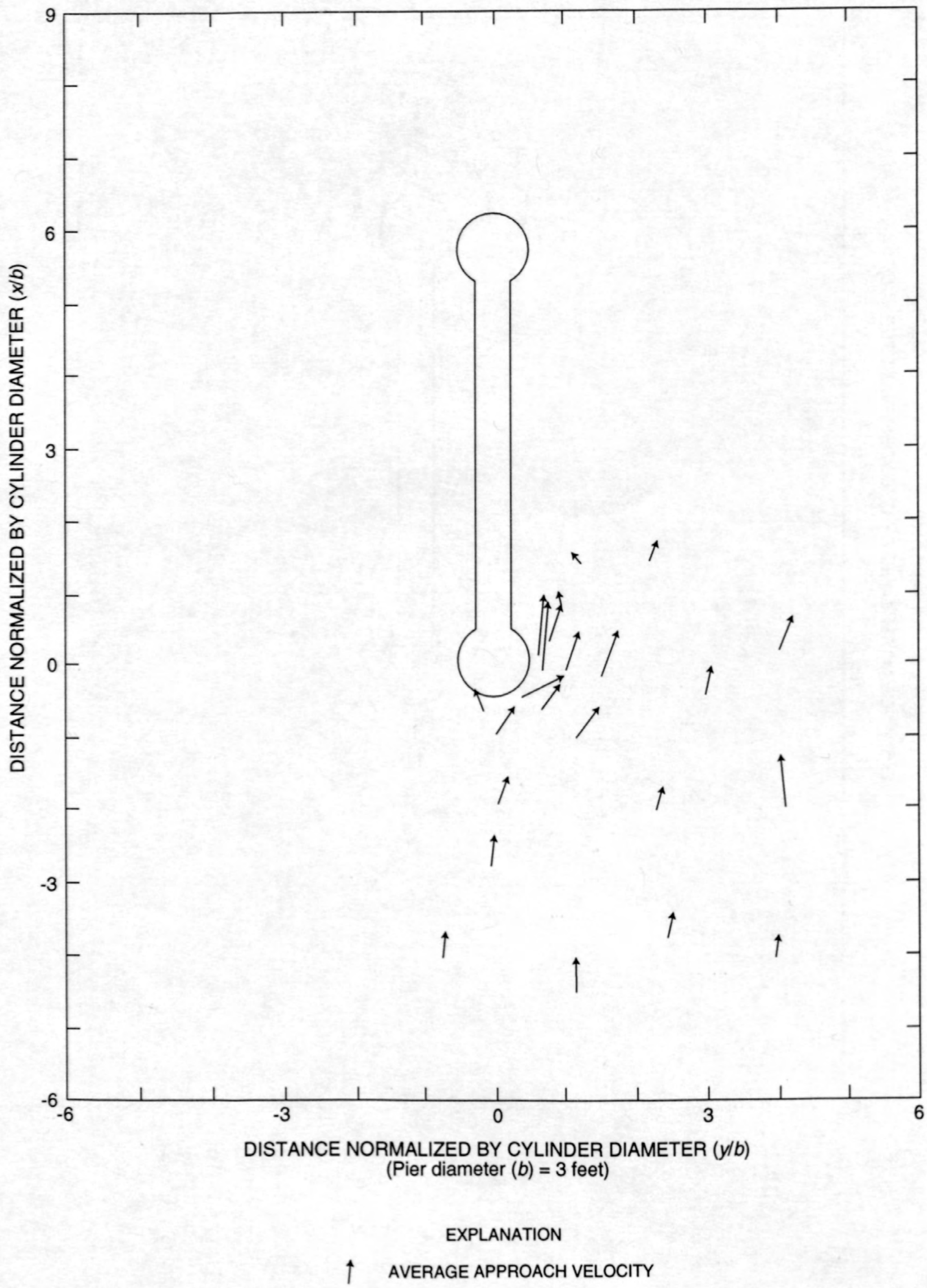

Figure 13. Vector representation of velocities measured at 0.4 foot above the streambed for the 3,000 cubic feet per second flow condition [(0,0) is at the center of the upstream cylinder].

The ratio of maximum near-bed velocity measured around cylindrical and rectangular piers by Parola (1990) was 1.6 and 1.7, respectively. At the full-scale site, mounds were present around the upstream and downstream ends of the cylinder, the pier was skewed 20 degrees to the approaching flow, and the pier consisted of a web wall in addition to a cylinder. Using available data from Melville (1975), Ford (1994) has shown that the ratio of maximum near-bed velocity to approach near-bed velocity was approximately 1.52 for Melville's hot film anemometry data collected 2 mm from the surface of a flat sand bed around a cylindrical pier.

The maximum near-bed velocity at the full-scale site was located near the vertical separation line for the wake vortex system on the right side of the upstream cylinder. The location of the maximum near-bed velocity was affected by the skew of the approach flow, the geometry of the riprap mound and its roughness, and the webwall. Melville (1975) also measured highest near-bed velocities in approximately the same location as this study. Parola (1990) measured the highest near-bed velocities immediately upstream of the wake separation zone.

Although flow reversal was measured in the wake region of the upstream cylinder, no such flow reversal was measured at the bed at the upstream face of that cylinder. The lack of time-averaged flow reversal upstream of this cylinder indicated that the horseshoe vortex system was not sufficiently persistent to provide upstream average velocity components. Further analysis of the point measurements indicated that some instantaneous near-bed velocity vectors were directed upstream, indicating the presence of at least a temporary horseshoe vortex system. The stress and pressure variation caused by the shape and roughness of the riprap around the pier combined to prevent a sustained horseshoe vortex system from developing. A horseshoe vortex is common under flat and relatively smooth bed conditions. Ettema (1980) found that scour depth was reduced significantly when bed sediment size approached the pier size. Parola (1993) found that mounding riprap around a pier increased the stability of the riprap.

Streambed-Stress Contours from Averaged Near-Bed Velocity Magnitudes

An approximate representation of the ratio of streambed stresses around the pier to that of the approaching flow was developed from the average of the three velocity measurements closest to the streambed at each profile location of the three flow conditions. Three point-velocity measurements at distances of 0.4, 0.6, and 0.8 ft from the streambed were averaged to develop an average near-bed velocity value at each profile location. An approximation of streambed stress given boundary layer characteristics and their variation could be developed from equation 30; however, the steep velocity gradient and the high roughness of the bed material prevented meaningful computation of boundary layer characteristics such as the displacement thickness (equation 27), the momentum thickness (equation 28), and shape factor (equation 29) that would enable the use of equation 30.

A gross estimate of the variation of streambed stress from the approach flow to the pier was enabled by considering the right hand side of equation 30 to be a constant, C, giving

$$\frac{\tau_o}{\rho U^2} = C. \tag{32}$$

The variable U in equation 32 represents the free-stream velocity at the edge of the boundary layer.

The location of the velocity at the edge of the boundary layer, considered the free-stream velocity here, was difficult to define. Velocity gradients near the pier are caused by both streambed stress and pressure gradients induced by the pier. The region of flow near the streambed dominated by the effects of streambed stress and consisting of high positive velocity gradients (velocity magnitude increasing with distance from the boundary) was considered to be the boundary layer. The error associated with individual depth measurement of the bed and the variation in the boundary layer thickness contribute error in the measurement of "free-stream velocity," In addition, the location of the upper limit of the boundary layer was difficult to define. To provide consistent results that could be qualitatively compared to research results of Melville (1975) and Parola (1990), an average of three velocity measurements was used as the free-stream velocity in equation 32. This technique provided more consistent results than using velocity measurements from a single distance measurement.

Normalized streambed stress, τ^*, was computed as

$$\tau^* = \frac{\tau_o}{\tau_{oa}} = \frac{U^2}{U_a{}^2} \tag{33}$$

where

U_a is the average approach flow value obtained from the averaged near-bed velocity, and

τ_{oa} is the average approach flow streambed stress.

The value of U_a was obtained from the average of the center three profiles at the upstream end of the velocity measurement grid.

The averaged near-bed velocity values were used to produce a grid of normalized streambed stress values spaced at 0.10 b in each direction. Contours were developed from the grid values. The interpolated values that make up the grid were developed using the inverse squared distance method.

Normalized streambed stress contours are shown in figures 14–16. Figures 14 and 15 show areas of high normalized stress areas of the bed in the region of the wake separation on both sides of the upstream cylinder of the pier but only on the one side for the 3,000 ft^3/s flow condition. Reverse flow occurred in the area alongside the webwalls (figs. 11–13) resulting in low streambed stresses (figs. 14–16). The maximum normalized streambed stress computed for the 1,820 ft^3/s flow condition was 2.3 ($(1.51)^2$) times the approach flow average stress at profiles 12 and 13 (fig. 7 and table E.1) on the right side of the pier at approximately the coordinates (0.8, 0.5) in figure 14. On the left side of the pier the maximum normalized streambed stress was 1.9 times the approach flow boundary stress and was determined for profile 23.

For the 2,230 ft^3/s flow condition (fig. 15) the highest streambed stress region was on either side of the upstream cylinder. Two other regions also experienced high stress values: the left side of the pier and an area immediately downstream of the downstream cylinder. The highest normalized streambed stresses were found at profiles 17 and 18 on the right side of the pier and profiles 25 and 27 on the left side of the pier (fig. 8). The maximum normalized streambed stress on the right side of the pier was found to be about 2.4 ($(1.55)^2$) times the average streambed stress of the approach flow (table E.2) and was located at approximately the coordinates (0.7, 0.0) in figure 15. The maximum normalized streambed stress on the left side of the pier was measured as 2.2 ($(1.50)^2$) times the average approach flow streambed stress and was located at approximately the coordinates (-1, 0.1) in figure 15. A region of high stress extends along the side of the pier at y/b = -2.5.

For the 3,000 ft^3/s flow condition (fig. 16) the number of data points collected was insufficient to provide information on the complete streambed stress pattern. The highest normalized streambed stress computed around the pier was at profile 14 (fig. 9) on the right side of the pier. The maximum normalized streambed stress was computed as 4.4 ($(2.11)^2$) times the average approach streambed stress and was located at approximately the coordinates (0.7, 0.0), figure 16, near the flow separation from the pier surface. At the upstream pier for the three flow conditions, the maximum stress values were located within approximately 2-cylinder diameter of the center of the upstream pier.

The normalized streambed stress contour plots generated from the full-scale bridge data (figs. 14–16) were compared with those developed from Melville's (1975) hot film anemometry near-bed velocity data (fig. 17) and Preston tube data (fig. 18). The contours in the region of highest stress in figures 14–16 are similar in configuration to those of figure 17. The principal differences are in the wake regions, primarily on the right side. The change in the stress contours is more abrupt in this region for the full-scale data than for Melville's (1975) (fig. 17). The depression on the right side of the web (fig. 10) and the skew of the flow cause lower near-bed velocities, resulting in lower stress values.

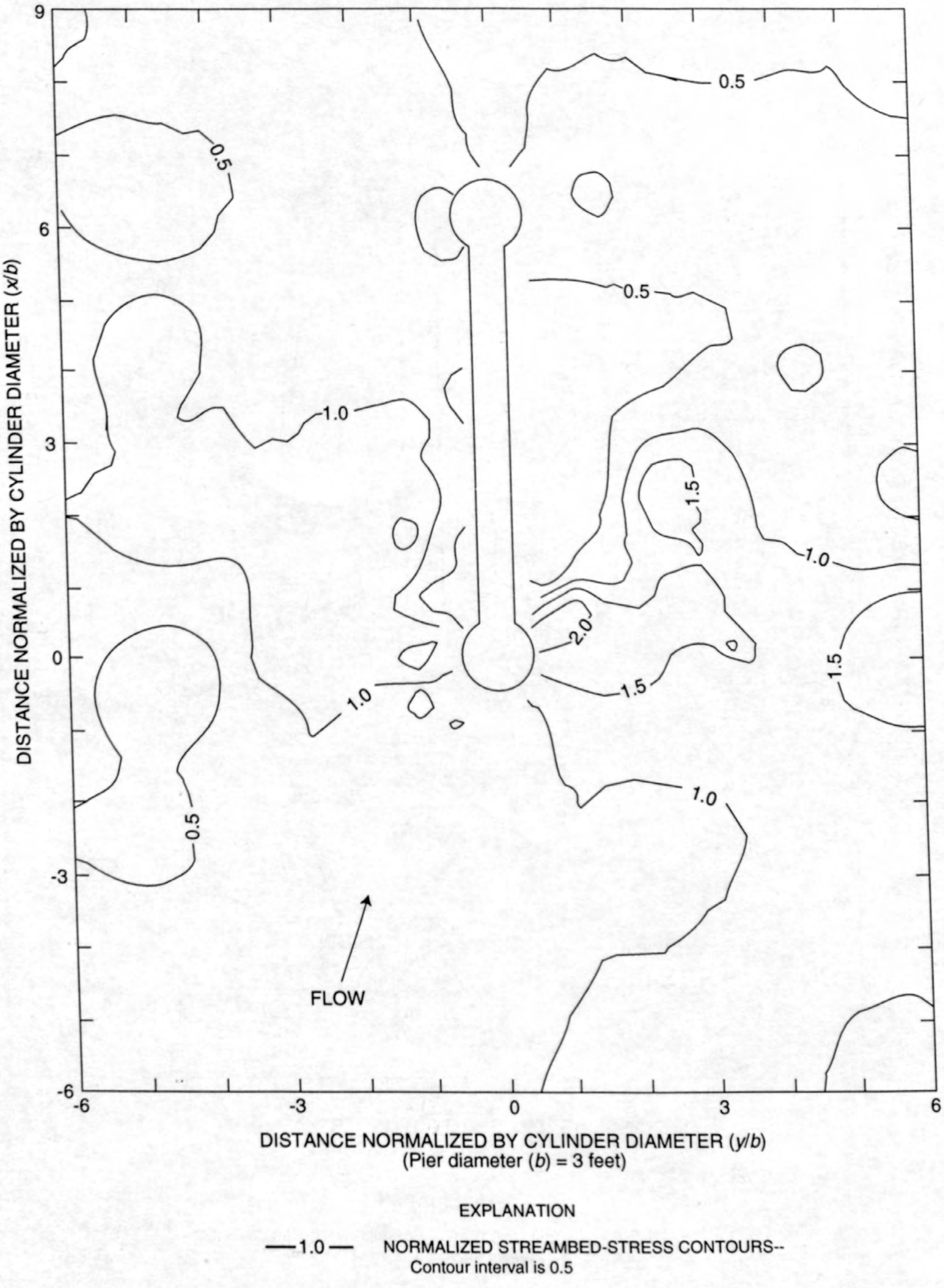

Figure 14. Normalized streambed-stress contours developed from the average magnitude of velocity measurements at 0.4, 0.6, and 0.8 foot above the streambed for the 1,820 cubic feet per second flow condition [(0,0) is at the center of the upstream cylinder].

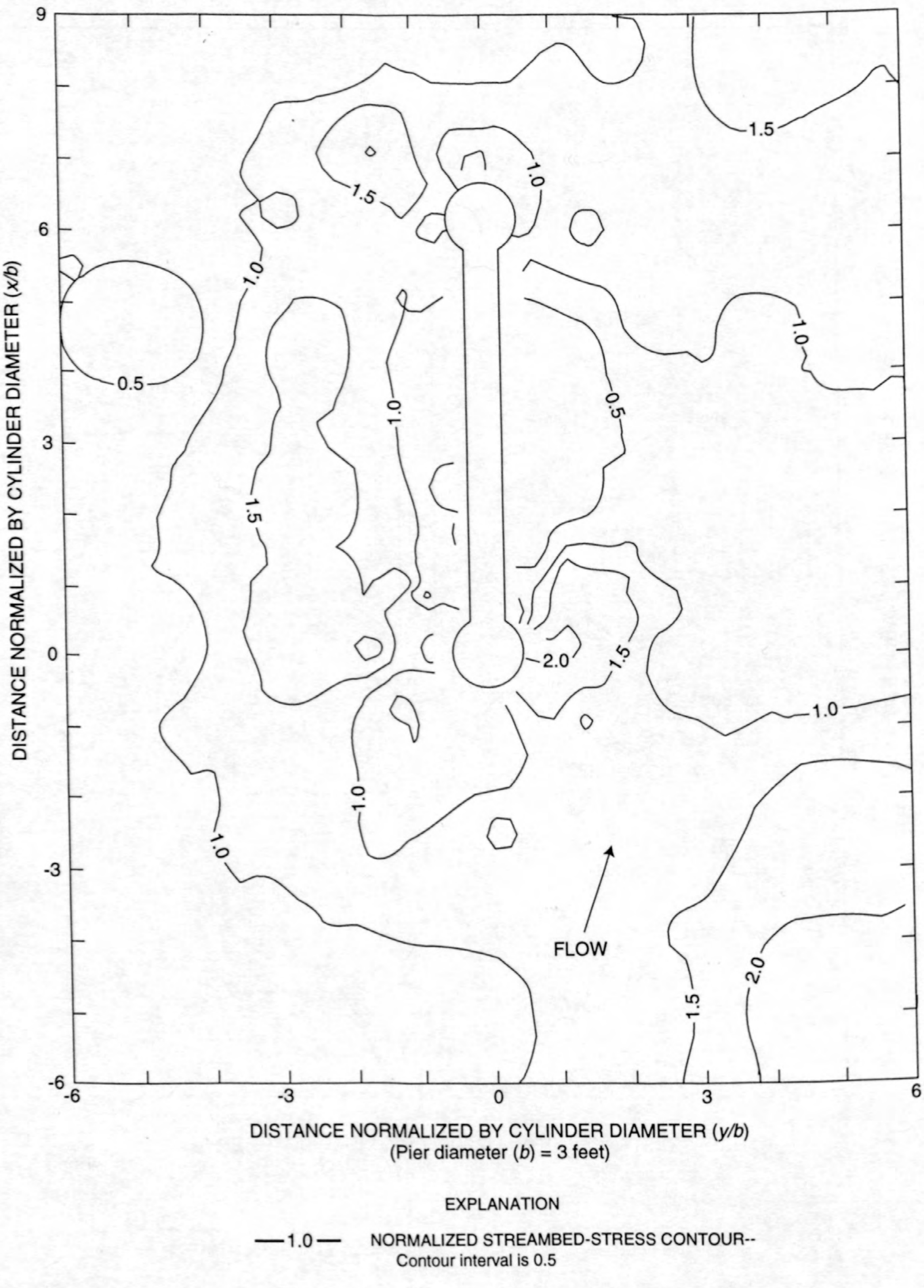

Figure 15. Normalized streambed-stress contours developed from the average magnitude of velocity measurements at 0.4, 0.6, and 0.8 foot above the streambed for the 2,230 cubic feet per second flow condition [(0,0) is at the center of the upstream cylinder].

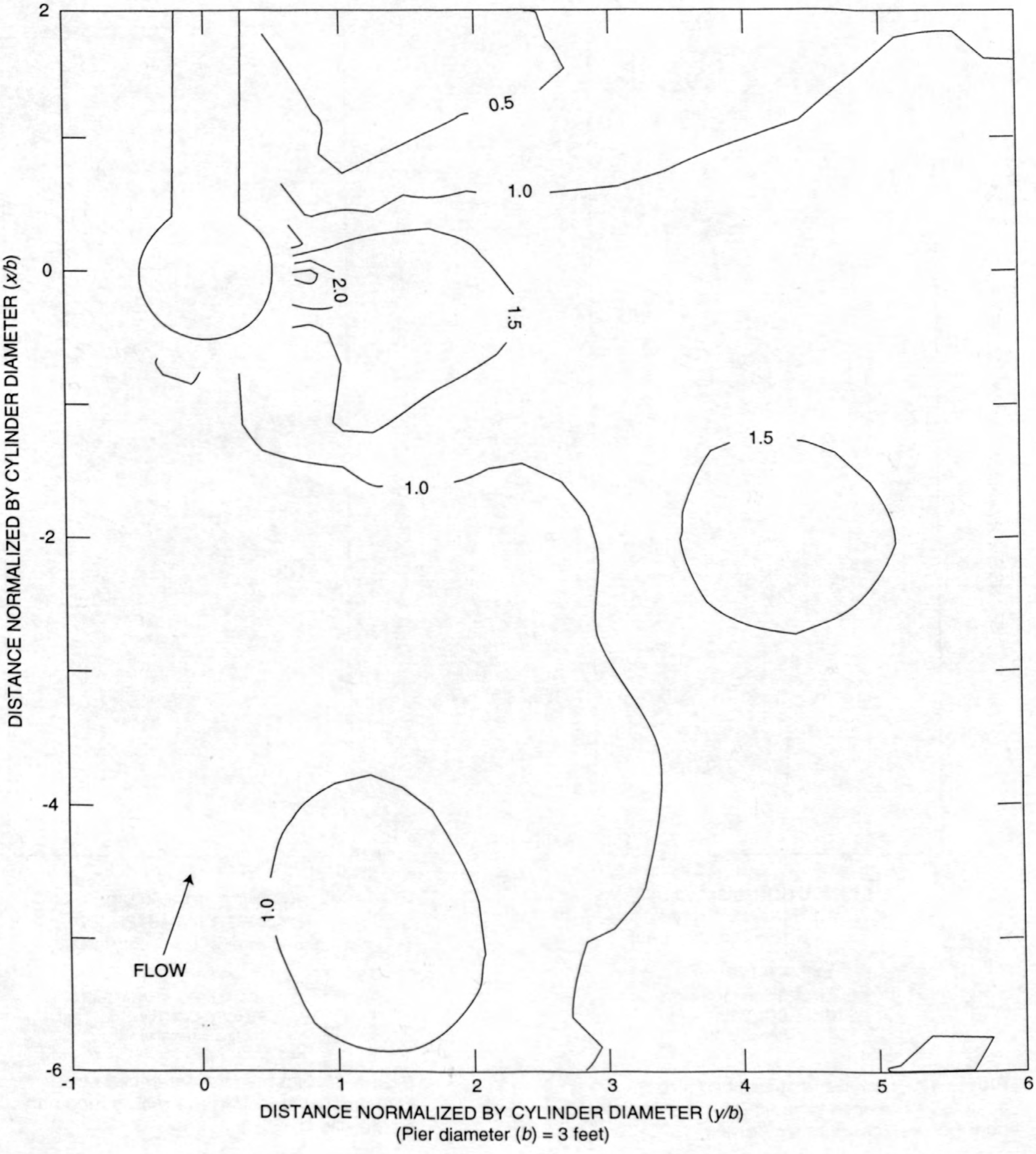

EXPLANATION

—1.0— NORMALIZED STREAMBED-STRESS CONTOURS--
Contour interval 0.5

Figure 16. Normalized streambed-stress contours developed from the average magnitude of velocity measurements at 0.4, 0.6, and 0.8 foot above the streambed for the 3,000 cubic feet per second flow condition [(0,0) is at the center of the upstream cylinder].

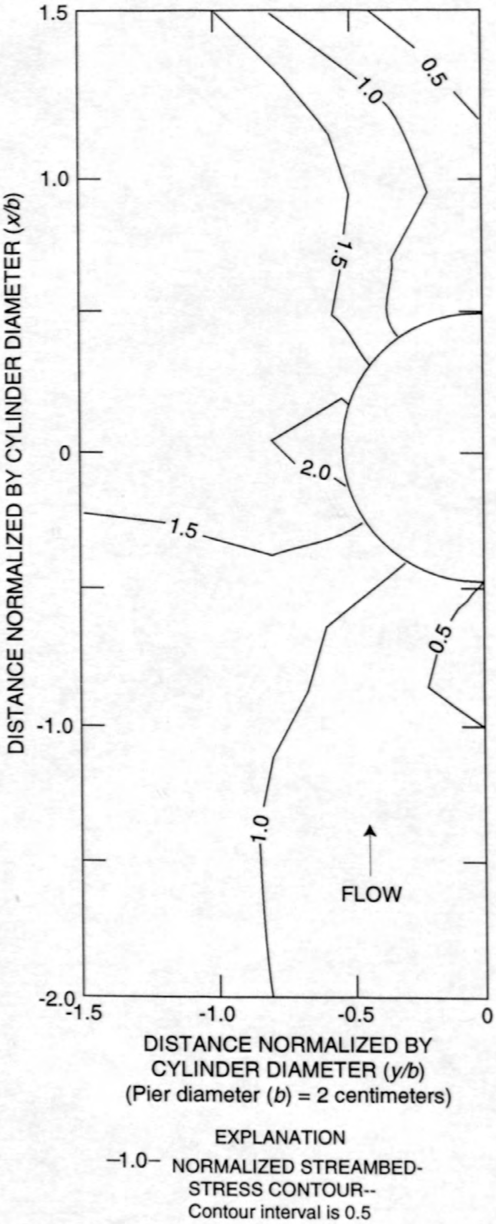

Figure 17. Normalized streambed-stress contours developed from hot-film anemometry near-bed velocity data by Melville (1975).

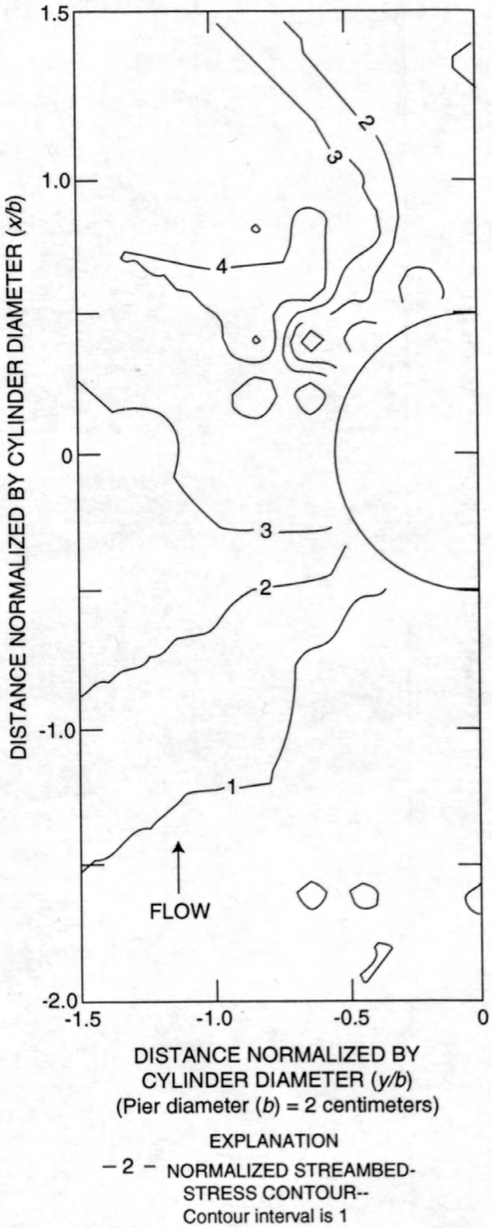

Figure 18. Normalized streambed-stress contours developed from Preston-tube data by Melville (1975).

Contours developed from Preston tube measurements by Melville (1975) (fig. 18) show the location of the maximum stress (τ_{max}) to be slightly downstream of the flow separation line. The magnitude of the maximum stress is approximately 4.9 times the approach flow streambed stress (τ_o). The contour pattern in the zone of high streambed stress in figure 17 more closely resembles the full-scale patterns than those of figure 18.

The streambed stress contours developed by Hjorth (1975) using data from Preston tube measurements around cylinders of various height, although not shown here, have significantly different contour patterns and significantly higher maximum streambed stresses. Hjorth (1975) reported streambed stresses upstream of the wake separation from the pier that were measured as high as 12 times those of the approach flow.

Streambed-Stress Contours from Averaged Near-Bed Velocity Gradients

Streambed stress at each measurement profile was approximated assuming that the velocity profile and fluid shear stress within the boundary layer were related by Prandtl's logarithmic velocity relation (equation 25). Equation 25 can be rearranged as

$$\tau_o = \frac{\rho}{5.75^2}\left(\frac{\Delta U}{\Delta \log z}\right)^2 \qquad (34)$$

where

τ_o is the streambed stress,

ρ is the density, and

z is the elevation of the horizontal velocity magnitude U given by

$$U = \sqrt{u^2 + v^2} \qquad (35)$$

and u and v are the measured average velocity components in the longitudinal and lateral directions. Relations between velocity and shear such as Von Karmen's equation (equation 22) and other relations (Clauser, 1954; Dargahi, 1987) were considered. However, the number of velocity measurements within the boundary layer was insufficient to use these methods for evaluating the streambed stress. The boundary layer was considered to be the region of fluid above the streambed in which velocity magnitude increased with increased distance from the boundary. Although the velocity measurements were collected at vertical distances of 0.2 ft intervals near the streambed and at distances starting at 0.4 ft from the streambed, typically less than three velocity measurement points were located within the boundary layer. This problem was associated with the high bed roughness and the relatively thin boundary layer near the pier.

Velocity magnitude measurements within 1.3 ft of the streambed were considered in determining velocity gradients. Because of the complex flow patterns associated with flow acceleration over individual pieces of riprap and wake flow downstream of pieces of riprap, velocity measurements did not always produce profiles that continuously increased with increasing distance from the streambed. Only velocity measurements with magnitudes that produced a positive velocity gradient were used to compute streambed shear stresses.

The lack of a positive velocity gradient indicated that the velocity measurements were most likely above the boundary layer created by the streambed. This type of profile was found most frequently in the wake zone on the sides of the pier. Because Equation 34 is only valid within the boundary layer of the streambed, shear stresses for velocity profiles that did not include data within the boundary layer of the streambed were not calculated using this equation. A value of zero stress was assumed because of the low velocity magnitudes measured at most of these profiles (tables F.1, F.2, and F.3). Profiles 5, 8, 21, 24, 29, 30, 49, and 54 were removed from the 1,820 ft^3/s flow condition; profiles 10, 21, 28, 37, and 39 were removed from the 2,230 ft^3/s flow condition. No profiles were removed from the 3,000 ft^3/s flow condition; however, profile 19 was found to have a virtually vertical profile but represented an area of high streambed stress. In addition, the elevations at which velocities were measured were substantially higher than surrounding elevations indicating the base of the measurement rod was positioned on a rock. Profile 20 was located less than 1 ft from profile 19 in the downstream direction and appeared to be in the wake of the rock under profile 19. In order to provide a stress approximation in this important region of flow, the two profiles were combined using the elevation data and the origin of the bed of profile 20. The combined information is shown as profile 24 in table F.3.

Velocity gradients were computed using the two to four velocity observations judged to be within the boundary layer of the streambed. Gradients at profiles with three or four usable velocity observations were computed using a least-squared-distance regression with U as the dependent variable and log z as the independent variable. Tables F.1, F.2, and F.3 provide the observed data, the computed streambed shear stress, and the ratio of streambed stress at each profile to streambed stress in the approach flow for the three flow conditions. The streambed stress in the approach was determined using the average value from the central profiles upstream from the pier; at profiles 34, 35, and 36 for the 1,820 ft^3/s flow condition, profiles 2, 3, 4 for the 2,230 ft^3/s flow condition, and profiles 1 and 2 for the 3,000 ft^3/s flow condition.

Contours were developed from the stress computed at the measurement points using a grid of interpolated points spaced at 0.10 b in each direction. The interpolation grid was developed using the inverse squared distance method.

For the 1,820 ft^3/s flow condition shown in figure 19, maximum stress regions on the streambed were located between radials of 80 degrees and 140 degrees from a radial of zero degrees extending in the upstream direction along the axis of the pier if skew is considered (60 to 120 degrees from the negative x-axis of the coordinate system). The maximum stress in this region was approximately 15 times the approach flow average streambed stress.

For the 2,230 ft^3/s flow condition shown in figure 20, maximum stress regions on the streambed were located between radials of 80 degrees and 160 degrees from a radial extending in the upstream direction (60 to 140 degrees from the negative x-axis of the coordinate system). The maximum stress measured was located along a radial of approximately 110 degrees (90 degrees from negative x-axis) and was 36 times the approach flow average streambed stress. The computed stress at this point was the highest for this study. The next highest computed stress was about 17 times the approach flow streambed stress. The extent of the high stress region laterally was approximately 8 times the diameter of the upstream cylinder in the cross- stream direction. A high stress region was found on the left side of the downstream cylinder. The maximum stress in this region was approximately 12 times that of the approach flow average bed stress.

For the 3,000 ft^3/s flow condition shown in figure 21, maximum stress regions of the streambed were located along a radial of approximately 140 degrees, as measured from a radial of zero degrees extending in the upstream direction along the axis of the pier (120 degrees from the negative x-axis of the coordinate system if skew is considered). The maximum stress measured was approximately 10 times the approach flow average bed stress. As with the stresses developed from the velocity magnitudes, the maximum stress values for the three flow conditions of the upstream pier were located within approximately 2-cylinder diameters of the center of the upstream pier.

Significant differences were found between the contours developed from near-bed velocities and those generated from velocity-gradient. The reason for the difference is the effect of roughness on velocity magnitudes and velocity gradients. Because the velocity measurements were collected at the upper regions of the boundary layer of flow on the streambed, the velocity magnitudes reflect the effects of pressure gradients more than streambed shear stress. On the other hand, velocity gradients near the boundary are effected significantly by both pressure gradient and streambed shear stress, and are not affected to the same degree by boundary roughness.

Several sources of error significantly affect the accuracy of the stresses reported here. Two sources of error are associated with the differences in the measured values of depth and velocity. The origin of the distance from the streambed, z, was used as the baseplate of the measuring device. For hydraulically rough flow, especially for flow over riprap, this origin is not well defined. The differences in average velocity magnitude in the boundary layer are small except in a region closer to the boundary than could be measured in this study.

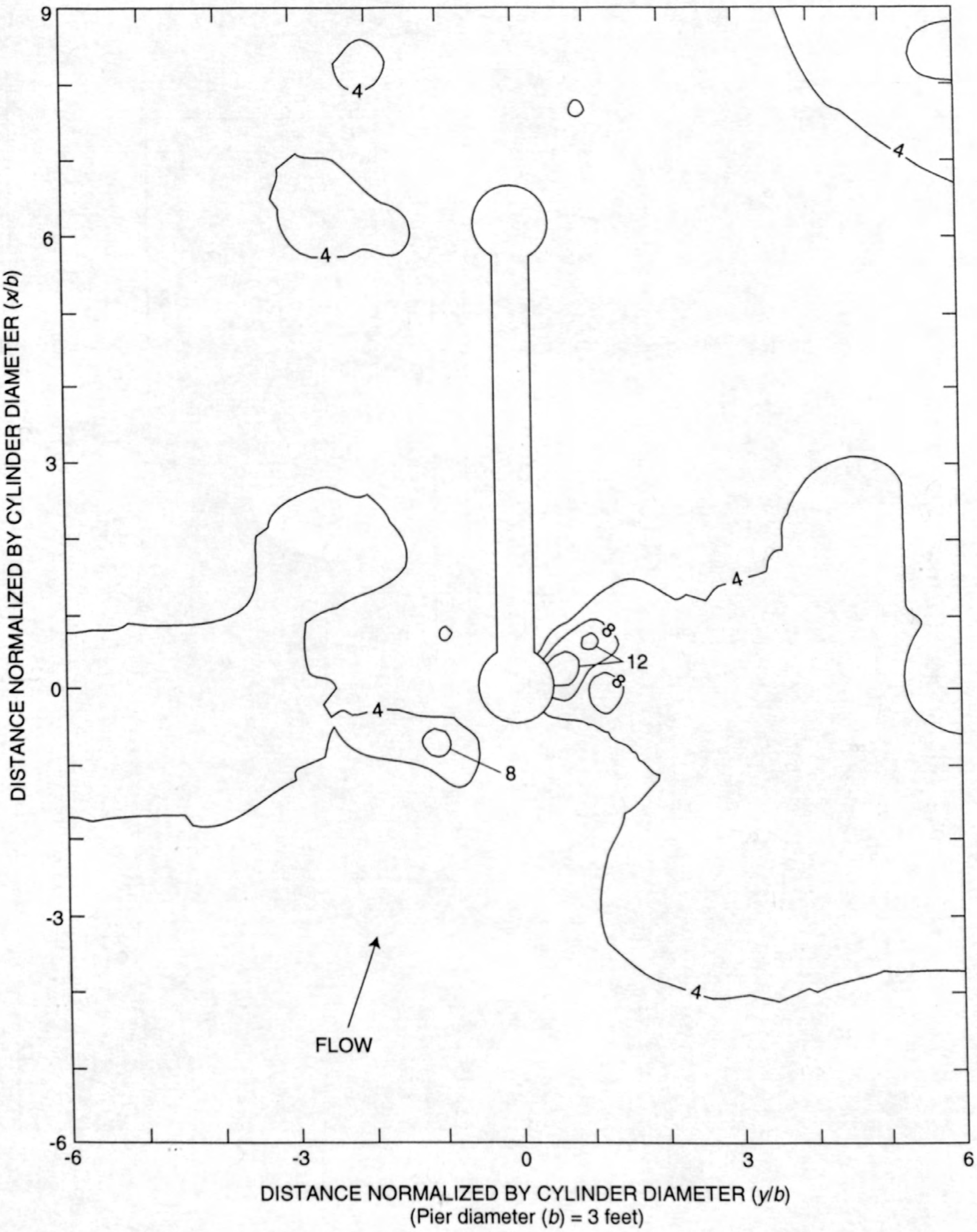

EXPLANATION

— 4 — NORMALIZED STREAMBED-STRESS CONTOURS--
Contour interval is 4

Figure 19. Normalized streambed-stress contours developed from average velocity gradient for the 1,820 cubic feet per second flow condition [(0,0) is at the center of the upstream cylinder].

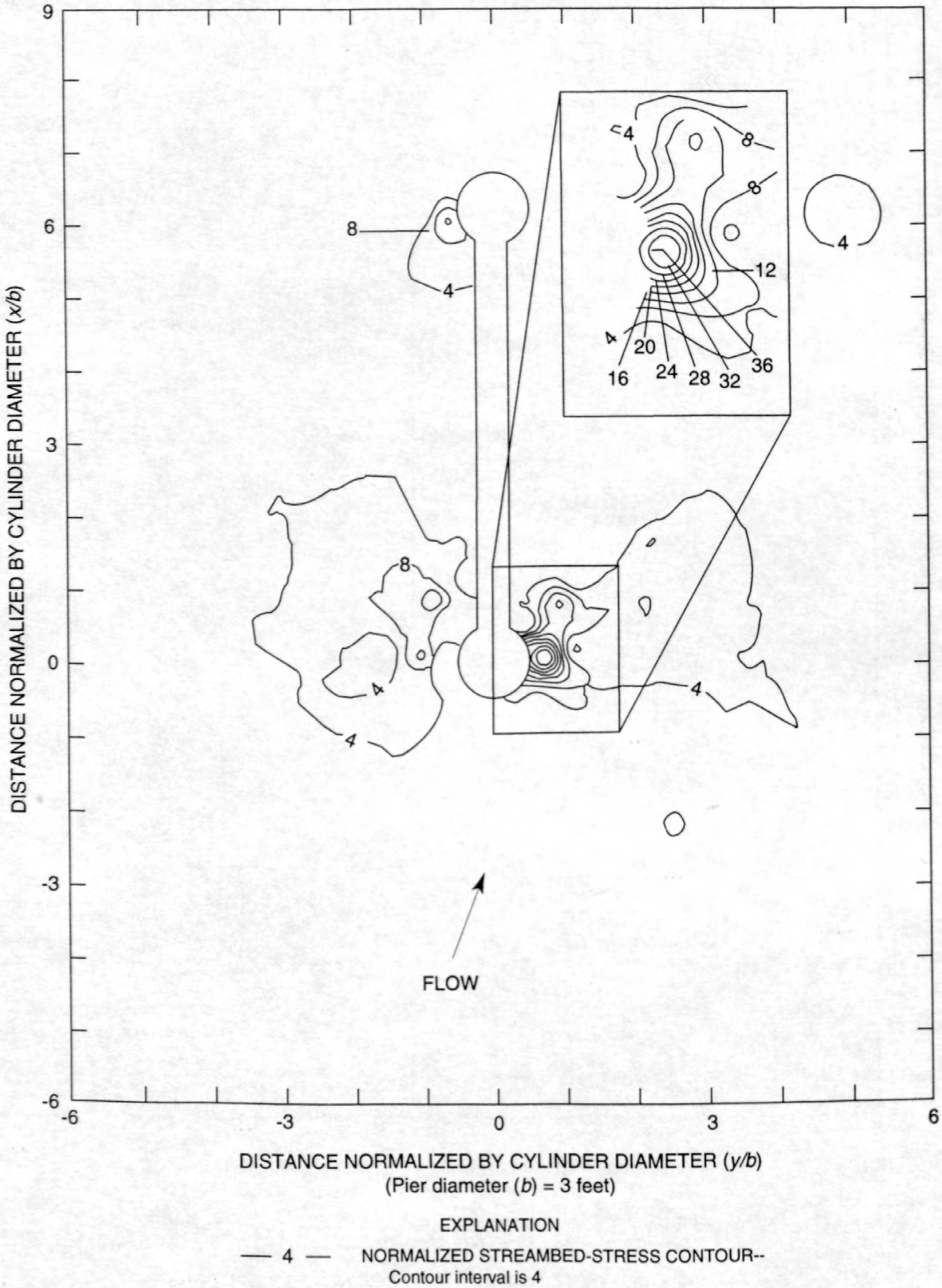

Figure 20. Normalized streambed-stress contours developed from average velocity gradient for the 2,230 cubic feet per second flow condition [(0,0) is at the center of the upstream cylinder].

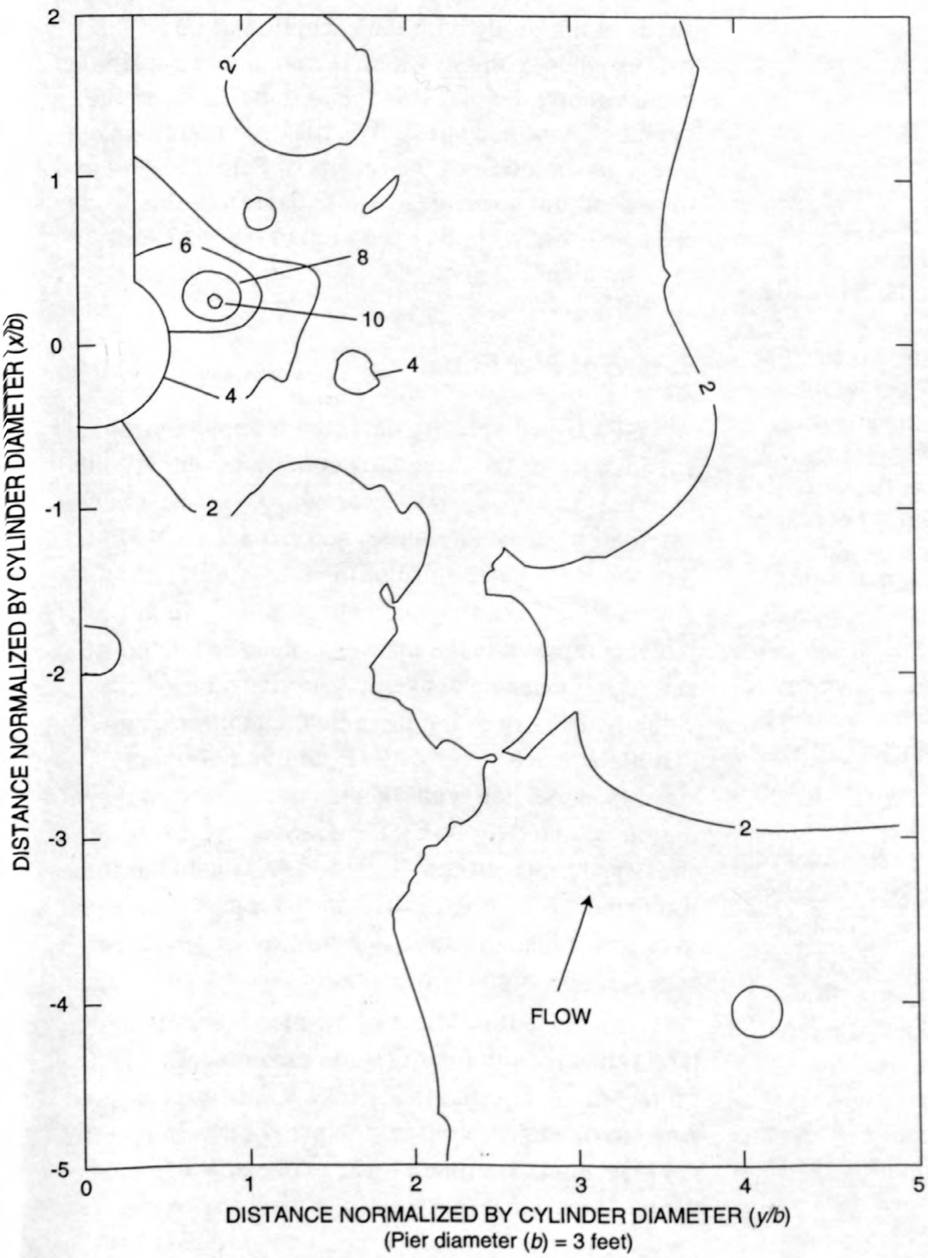

EXPLANATION

— 2 — NORMALIZED STREAMBED-STRESS CONTOUR-- Contour interval is 2

Figure 21. Normalized streambed-stress contours developed from average velocity gradient for the 3,000 cubic feet per second flow condition [(0,0) is at the center of the upstream cylinder].

The percentage error in the depth measurement and velocity measurements are magnified because of the differences used in the computation of velocity gradient. The measurement rod baseplate may have been placed on top of a piece of riprap. Adjacent profile measurements may have been made when the baseplate was positioned between several pieces of riprap.

The normalized streambed stress contours developed here were compared to normalized stress contours developed from near-boundary measurements by Hjorth (1975) and Melville (1975). Both studies were conducted on small-scale model cylindrical piers on flat streambeds with homogeneous bed roughness. The locations of maximum streambed stress determined from this study were similar to those found by Melville (1975). Hjorth (1975) found maximum streambed stress upstream of the flow separation on the sides of the cylinder.

The magnitude of the maximum normalized streambed stress found in this study was significantly higher than indicated by data from Melville (1975) and Hjorth (1975). The differences between the model study normalized streambed stress values can be explained, at least in part, by considering the differences between the model study test conditions and the conditions present for this study.

The bed topographies of the model studies were essentially flat and composed of a homogeneous material. Therefore, the bed roughness for the model studies was the same around the cylinder as in the upstream approach channel. At the full-scale site riprap mounds were present around the upstream and downstream cylinders and the roughness caused by the riprap at the pier was considerably higher than the roughness of the approach channel. The model studies were conducted using a single, circular cylinder. However, the full-scale pier consisted of two circular cylinders connected by a webwall. The webwall separated the flow in the wake zone of the upstream cylinder. Conversely, at the downstream cylinder the approach flow was diverted as a result of the web. Also, no skew was present in the laboratory because a single, circular cylinder was used. However, the webwall of the full-scale bridge was skewed to the flow by approximately 20 degrees for the three flow conditions. In addition, depth average velocity in the flume upstream of the models was essentially uniform across the channel. However, depth average velocity varied across the river channel at the full-scale pier.

Although the axis of the pier as parallel to the channel banks, the approach flow was skewed 20 degrees to the axis of the pier. A submerged mound of material between the pier and the streambank created an adverse pressure gradient causing flow to deflect toward the center of the channel upstream of the pier. Unlike flow around a pier in which the entire flow field away from the pier maintains its skew, the flow over the mound and confined by the pier and the streambank was essentially parallel to the pier and streambank. Consequently, flow around the downstream end of the pier behaved similar to flow around an aligned pier. The mound induced an approach flow skew and flow field around the pier quite different from that which would be created by a pier in an unconfined flow skewed 20 degrees on a planar streambed.

The maximum streambed stresses developed from model riprap studies around a small-scale rectangular pier (Parola, 1990) were shown to be as much as 18 times the approach flow streambed stress where relatively low bed roughness existed for the approach streambed (fig. 2). The maximum streambed stresses for all flow conditions were found to be between 10 and 17 times the approach flow streambed stress in this study with the exception of one measurement point in which the maximum streambed stress around the pier was found to be 36 times the approach flow bed stress. The maximum normalized stress generated from the results of Parola (1990) and the maximum normalized stress data from this study are consistent with the exception of one bed stress measurement.

Extent of Pier Effect

Near-bed velocity data (0.4 ft above the streambed) for the three flow conditions were plotted in figure 22 from the data near $x/b = 0$ (greatest lateral extent of upstream cylinder) and $x/b = 2$ (approximately one-third of the pier length downstream from the upstream cylinder). In these plots, U represents the measured near-bed velocity, and U_a represents the average approach near-bed velocity. Data from the three flow conditions show that high near-bed velocity regions and boundary stresses associated with the pier were found in the region bounded by $-4 < y/b < 4$. (See figs. 14-16 for stress patterns between $-4 < y/b < 4$). Outside of these limits the stresses associated with the pier were equal to or lower than the approach flow average values accept in the streambed region of the central channel.

The extent of affect of the pier is significantly larger than the minimum region recommended for protection by Hjorth (1975) for a single circular pier equal in diameter to the upstream cylinder. In Hjorth's (1975) model experiments, the total extent of effect of the pier was equal to 3 times the diameter of the cylinder in the direction perpendicular to the approach flow direction. In contrast, the extent of near-bed velocity affect found in this study was 8 times the diameter of the upstream cylinder (approximately 24 ft total, or 12 ft either side of the center of the pier). The difference in the extent of effect between the single cylinder model and the two-cylinder and webwall pier is attributed, at least partially, to the effects of the skew of the bridge to the approach flow, the riprap around the pier, and the webwall on the stress distribution.

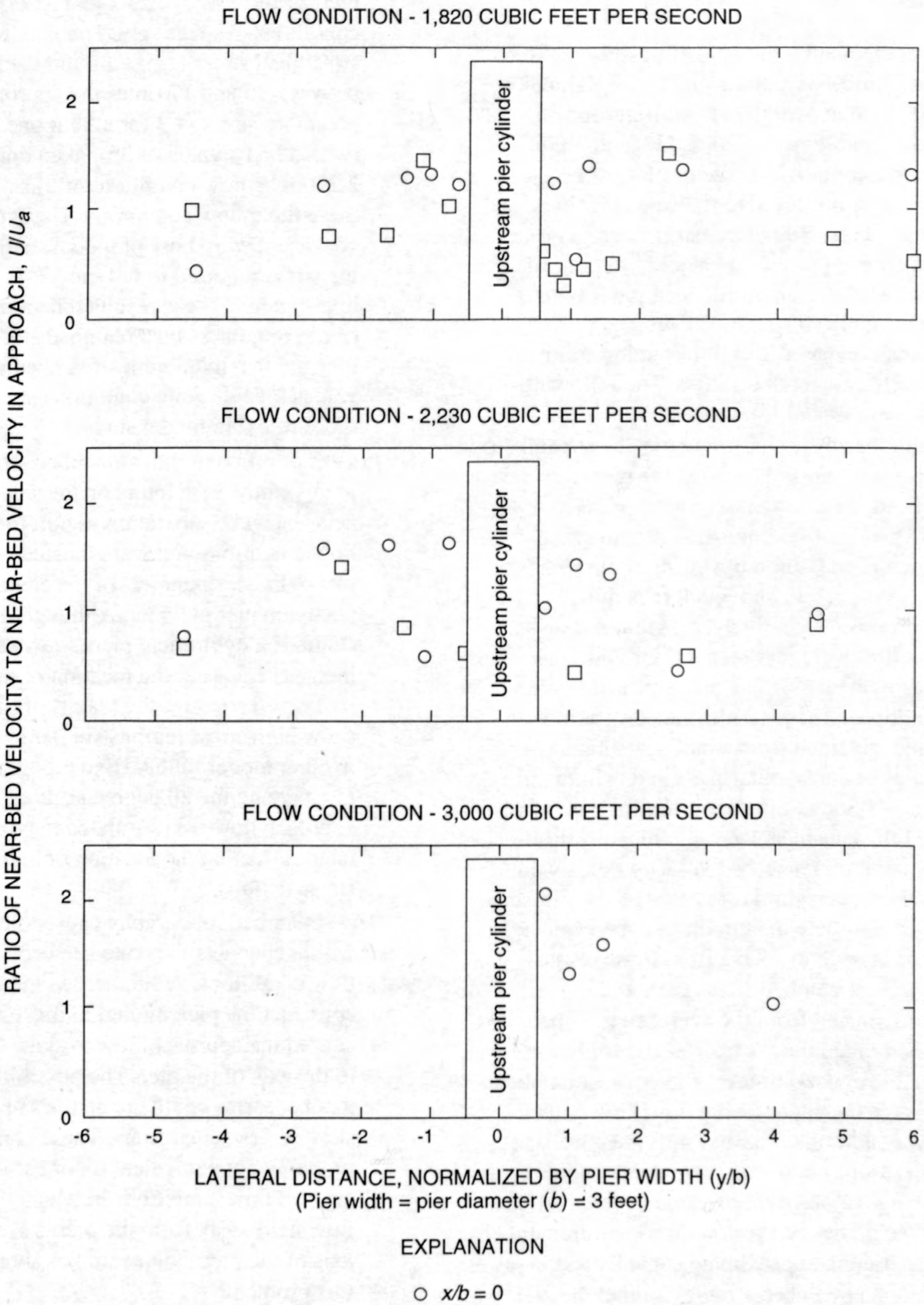

Figure 22. Lateral variation of velocity ratio along x/b=0 for the 1,820 and 2,230 cubic feet per second flow conditions, and along x/b=2 for the 1,820, 2,230, and 3,000 cubic feet per second flow conditions [x/b is the longitudinal distance normalized by pier width, with (0,0) at the center of upstream cylinder].

CONCLUSIONS

Two-component point velocities were measured along vertical profiles around a pier at the Kentucky Highway 417 bridge over the Green River for three different flow conditions; 1,820, 2,230, and 3,000 cubic feet per second (ft^3/s). Vector plots of near-bed velocity data were produced to indicate magnitude and direction of the flow. Boundary (streambed) stresses were estimated from near-bed velocities and from velocity gradients at each profile location. Contour plots of the normalized streambed stresses were developed and compared with information from previous small-scale model studies. The following conclusions were drawn from this study:

1. Maximum near-bed (0.4 ft above the streambed) velocities measured around the pier were 1.5, 1.6, and 2.0 times the average approach flow near-bed (0.4 ft above the streambed) velocities measured upstream of the pier for the 1,820, 2,230, and 3,000 ft^3/s flow conditions, respectively. Maximum near-bed velocities were less than 1.6 for all but two measurements for this pier under these flow conditions. These results are consistent with results obtained from small-scale model studies on rectangular piers and cylindrical piers. Although the conditions for the model and full-scale piers were significantly different, the maximum near-bed velocity ratios were not. However, similarity between the full-scale and small-scale maximum near-bed velocity ratios is not conclusive from these results.
2. Maximum streambed stresses around the pier approximated from the averaged near-bed velocity magnitudes from each profile were 2.3, 2.4, and 4.4 times the average streambed stress of the approaching flow for the three flow conditions. These results are consistent with results obtained from model studies on rectangular and cylindrical piers in which near-bed velocities or Preston tube measurements were used to approximate streambed stresses.
3. Maximum streambed stresses around the pier approximated from averaged near-bed velocity gradients were 15, 36, and 10 times the streambed stresses of the flow approaching the pier for the 1,820, 2,230, and 3,000 ft^3/s flow conditions, respectively. The maximum streambed stress (τ_{max}) around the pier was between 10 and 17 times the approach flow boundary stress (τ_o) for all but one profile (which had a value of 36) taken during the 2,230 ft^3/s flow condition for this pier under these three flow conditions. These results are consistent with those of model studies in which the stress required to fail model riprap was investigated. These results reflect the effect of riprap roughness on streambed stresses and indicate that maximum streambed stress ratio values for full-scale conditions are similar to those found in model studies.
4. Locations of maximum streambed stresses found in this study were found on the sides of the pier near the wake separation region for the three flow conditions and were located within 2.0 pier cylinder diameters of the center of the upstream pier cylinder. Although model studies on cylindrical piers show some inconsistencies in the location of maximum streambed stresses, the results of this study show high stress regions similar to those found in other model studies. Bed topography around the pier and the 20 degree skew of the approach flow are postulated to be a significant factor affecting the location of high streambed stress regions.

   The streambed topography caused flow to shift within channels to create skewed approach flow conditions. A submerged mound used to construct the pier studied in this investigation caused the approach flow to skew 20 degrees to the axis of the pier. The possibility exists that bedforms could create the same type of skewed flow conditions. These conditions are probably not equivalent to, or as severe as, the skewed flow conditions in which the entire flow field away from the pier is skewed to the axis of the pier. Future studies should consider this problem.
5. Streambed stress distributions found in this study were significantly different than those of small-scale model studies of cylindrical and

rectangular piers. These differences could be attributed to (1) the differences in streambed topography, pier geometry, and approach flow velocity distributions between the full-scale studies and the small-scale model studies; (2) the 20 degree skew of the approach flow to the pier alignment and the presence of a web; and (3) the effects of scale.

6. The extent of effect of the pier on the near-bed velocity found in this study was approximately 8 times the diameter of the upstream cylinder as compared with 3 times the diameter observed in laboratory studies. The difference in the extent of effect is attributed, as least partially, to the effects of the skew of the bridge to the approach flow, the riprap around the pier, and the webwall on the stress distribution.
7. Evidence of a steady horseshoe vortex system, regarded as the primary cause of local scour, was not found in this study. The high roughness and greatly varying topography of the streambed and riprap mound around the pier prevented the formation of the vortex system.

The streambed around the pier in this study was covered with riprap, particularly around the upstream and downstream circular columns. As a result, the information from this study is most applicable to streambeds that are rough. In small-scale model studies, mounding of riprap around the base of piers was shown to increase the stability of foundation material around a pier. This study showed that a sustained horseshoe vortex was not present upstream of the pier because of the varying streambed topography and riprap mounded around the pier. The mounding of riprap may be an effective method of preventing the horseshoe vortex formation and therefore may prevent scour at the upstream face of a pier. In addition, mounded riprap is easy to place and is easy to inspect. Current recommendations are for riprap to be placed at or below the streambed level to reduce vulnerability of the riprap to horseshoe vortex systems. Further consideration should be given to the practical benefits of mounding riprap around bridge piers.

REFERENCES CITED

Bayazit, M., 1976, Free surface flow in an open channel of large relative roughness: Journal of Hydraulic Research, v. 14, no. 2, p. 115–126.

Bonasoundas, M., 1973, Flow structure and problem at circular bridge piers: Munich, West Germany, Oskar V. Miller Institute, Munich Technical University, Report no. 28, 191 p.

Breusers, H.N.C., Nicollet, G., and Shen, H.W., 1977, Local scour around cylindrical piers: Journal of Hydraulic Research, v. 15, no. 3, p. 211–252.

Clauser, F.H., 1954, Turbulent boundary layers in adverse pressure gradients: Journal of Aeronautical Sciences, v. 21, no. 2, p. 91–108.

Dargahi, B., 1987, Flow field and local scouring around a cylinder: Stockholm, Sweden, The Royal Institute of Technology, Hydraulics Laboratory Bulletin TRITA-VBI-137, 129 p.

Ettema, R., 1980, Scour at bridge piers: Aukland, New Zealand, University of Aukland, Ph.D. dissertation, 522 p.

Ford, D.L., 1994, Boundary stress in the vicinity of bridge piers: Louisville, Ky., University of Louisville, Master of Engineering Thesis, 65 p.

Goldstein, R.J., 1983, Fluid mechanics measurements: Hemisphere Publishing Corporation, 630 p.

Hjorth, P., 1975, Studies of the nature of local scour: Sweden, University of Lund, Department of Water Resources Engineering, Bulletin ser. A, no. 46, 191 p.

Isbash, S.V., 1935, Construction of dams by dumping stones in flowing water: English translation by Dorijikow, A., Eastport, Maine, U.S. Army Engineer District, p. 123–136.

Johnson, P.A., and Jones, J.S., 1990, Shear stress at base of bridge piers: Washington, D.C., Transportation Research Board, National Research Council, Transportation Research Record, no. 1350, p. 90–92.

Makowski, D.B., Thompson, P.L., and Yew, C.P., 1989, Scour assessment at bridges, *in* Proceedings of the American Society of Civil Engineers National Conference on Hydraulic Engineering, New Orleans, La., 1989, p. 1–6.

Melville, B.W., 1975, Local scour at bridge sites: Aukland, New Zealand, University of Aukland, Ph.D. dissertation, 227 p.

Mendoza-Cabrales, C., 1993, Computation of flow past a cylinder mounted on a flat plate, *in* Proceedings of the American Society of Civil Engineers Hydraulic Division National Meeting, San Francisco, Calif., 1993, p. 899–904.

Moore, W.L., and Masch, F.D., 1963, The influence of secondary flows on local scour at obstructions in a channel *in* Proceedings of the Federal Interagency Sedimentation Conference, 1963, Miscellaneous Publication no. 970, Agricultural Research Service, U.S. Department of Agriculture, Washington, D.C., no. 36, p. 314–319.

Nicollet, G., and Ramette, M., 1971, Affouillements au voisinage de piles de pont cylindiques circulaires *in* Proceedings of the 14th International Association of Hydraulic Research Congress, Paris, France, 1971, v. 3, p. 315–322.

Olsen, N.R.B., and Melaaen, M.C., 1993, Three dimensional calculation of scour around cylinders: American Society of Civil Engineers, Journal of Hydraulic Engineering, v. 119, no. 9, p. 1048–1054.

Parola, A.C., 1990, The stability of riprap used to protect bridge piers: University Park, Penn., Pennsylvania State University, Ph.D. dissertation, 112 p.

_____1993, Stability of riprap at bridge piers: American Society of Civil Engineers, Journal of Hydraulic Engineering, v. 119, no. 10, p. 1081–1097.

Parola, A.C., Jones, J.S., and Miller, A.C., 1989, Sizing riprap at bridge piers: Washington, D.C., Transportation Research Board, National Research Council, Transportation Research Record, no. 1290, v. 2, p. 276–280.

Posey, C.J., 1973, Test of scour protection for bridge piers: American Society of Civil Engineers, Journal of Hydraulic Engineering, v. 100, no. 12, p. 1773–1783.

Quazi, M.E., and Peterson, A.W., 1973, A method for bridge pier riprap design, *in* Proceedings of the 1st Canadian Hydraulics Conference, University of Alberta, Edmonton, Canada, 1973, p. 96–106.

Raudkivi, A.J., 1990, Loose Boundary Hydraulics (3d ed.): New York, Perganon Press, 538 p.

Richardson, E.V., Harrison, L.J., and Davis, S.R., 1991, Evaluating scour at bridges: Federal Highway Administration Hydraulic Engineering Circular No. 18 (HEC 18), Publication No. FHWA-IP-90-017, 105 p.

Schlichting, Hermann, 1979, Boundary layer theory (7th ed.): McGraw-Hill, Inc., 817 p.

Shen, H.W., Schneider, V.R., and Karaki, S.S., 1966, Mechanics of local scour: Fort Collins, Colo., Colorado State University, Report CER66, HWS22, 56 p.

Tison, L.J., 1937, Erosion autour de piles de ponts and riviere: Annales des Travaux Publiques de Belgique, v. 41, no. 6, p. 813–871.

APPENDIX A:
Two-Component Velocity Data

Explanation for Appendix A

y = distance of velocity measurement from streambed, in feet;

n = number of sampling points;

$$\bar{u} = \sum_{i=1}^{n} \frac{u_i}{n}$$ = average x-component velocity, in feet per second;

u_i = x-component velocity for sampling point i, in feet per second;

$$\bar{v} = \sum_{i=1}^{n} \frac{v_i}{n}$$ = average y-component velocity, in feet per second;

v_i = y-component velocity for sampling point i, in feet per second;

$$\bar{U} = \sum_{i=1}^{n} \frac{U_i}{n}$$ = average horizontal velocity magnitude, in feet per second;

$$|U_i| = \sqrt{u_i^2 + v_i^2}$$ = horizontal velocity magnitude of sample i, in feet per second;

$$\text{RMS } u = \sqrt{\frac{\sum_{i=1}^{n} (u_i')^2}{n-1}}$$ = root mean square error of u, the x-component velocity, in feet per second;

$$u_i' = u_i - \bar{u}$$ = deviation of the x-component velocity for sample i, in feet per second;

$$\text{RMS } v = \sqrt{\frac{\sum_{i=1}^{n} (v_i')^2}{n-1}}$$ = root mean square error of v, the y-component velocity, in feet per second;

$$v_i' = v_i - \bar{v}$$ = deviation of the y-component velocity for sample i, in feet per second;

$$\text{RMS } U = \sqrt{\frac{\sum_{i=1}^{n} (U_i')^2}{n-1}}$$ = root mean square error of U, the horizontal velocity magnitude, in feet per second;

$$U_i' = U_i - \bar{U}$$ = deviation for sample i, in feet per second;

MIN U = minimum value of U, the horizontal velocity magnitude (feet per second);

MAX U = maximum magnitude of U, the horizontal velocity magnitude (feet per second);

ϕ = direction of U from the negative x-axis (degrees)

Table A-1. *Two-component velocity data for 1,820 cubic feet per second flow condition*

Profile	y (ft)	FILE	n	$\bar{u}$ (ft/s)	$\bar{v}$ (ft/s)	$\bar{U}$ (ft/s)	RMS u (ft/s)	RMS v (ft/s)	RMS U (ft/s)	MIN U (ft/s)	MAX U (ft/s)	ϕ
1	0.4	0	2,400	-1.530	0.425	1.614	0.329	0.281	0.325	0.661	2.755	164.5
	.6	1	2,400	-1.652	.486	1.747	.300	.297	.304	.993	2.719	163.6
	.8	2	2,400	-2.074	.519	2.153	.346	.269	.354	1.109	3.377	166.0
	1.3	3	2,400	-2.243	.651	2.359	.427	.316	.414	1.232	3.728	163.8
	2.3	5	2,394	-2.316	.891	2.504	.350	.339	.357	1.656	3.337	159.0
	3.3	6	2,392	-2.237	.892	2.426	.273	.298	.277	1.488	3.326	158.3
	4.3	7	2,400	-2.718	.993	2.904	.316	.247	.317	2.017	3.767	159.9
2	.6	9	2,400	-1.160	.040	1.180	.290	.203	.285	.245	2.106	178.0
	.8	10	2,384	-.984	.055	1.010	.350	.216	.346	.173	1.904	176.8
	1.3	11	2,400	-1.410	.284	1.459	.400	.202	.374	.308	2.593	168.6
	2.3	12	2,400	-1.654	.599	1.776	.295	.244	.294	1.051	2.697	160.1
	3.3	13	2,400	-1.278	.459	1.388	.212	.270	.183	.305	2.038	160.2
	4.3	16	2,400	-2.242	.862	2.412	.306	.239	.320	1.530	3.382	159.0
3	.4	17	2,400	-1.658	-.197	1.689	.280	.263	.287	.974	2.681	186.8
	.6	18	2,400	-1.269	-.032	1.285	.346	.190	.342	.474	2.315	181.4
	.8	19	2,400	-1.676	-.098	1.697	.288	.249	.287	1.005	2.861	183.3
	1.3	20	2,400	-1.889	.144	1.910	.385	.244	.383	.979	3.105	175.6
	2.3	21	2,400	-2.134	.474	2.209	.399	.302	.386	1.295	3.420	167.5
	3.3	22	2,400	-2.368	.697	2.485	.315	.301	.322	1.535	3.351	163.6
	4.3	23	2,400	-2.514	.699	2.628	.241	.327	.256	1.881	3.534	164.5
4	.4	26	2,400	-1.684	.093	1.705	.237	.258	.241	1.098	2.416	176.9
	.6	27	2,400	-1.751	.036	1.765	.257	.218	.255	.972	2.514	178.8
	.8	28	2,400	-1.946	.150	1.965	.274	.221	.272	1.296	2.754	175.6
	1.3	29	2,400	-1.882	.506	1.961	.357	.245	.375	1.177	3.025	164.9
	2.3	30	2,400	-2.073	.727	2.210	.219	.239	.215	1.568	2.740	160.7
	3.3	31	2,400	-2.186	.673	2.297	.295	.207	.294	1.378	3.054	162.9
	4.3	32	2,392	-2.259	.631	2.359	.247	.260	.249	1.764	3.226	164.4

Table A-1. Two-component velocity data for 1,820 cubic feet per second flow condition—*Continued*

Profile	y (ft)	FILE	n	$\bar{u}$ (ft/s)	$\bar{v}$ (ft/s)	$\bar{U}$ (ft/s)	RMS u (ft/s)	RMS v (ft/s)	RMS U (ft/s)	MIN U (ft/s)	MAX U (ft/s)	ϕ
5	0.4	33	2,400	0.242	0.575	0.651	0.187	0.212	0.212	0.096	1.391	67.2
	.6	34	2,395	-2.154	-.051	2.188	.304	.380	.304	1.380	2.974	181.4
	.8	35	2,390	-2.150	.043	2.170	.272	.287	.272	1.442	3.135	178.9
	1.3	37	2,362	-1.696	-.028	1.719	.352	.267	.343	.827	2.897	180.9
	2.3	39	2,400	-2.453	.077	2.495	.310	.443	.300	1.632	3.440	178.2
	3.3	41	2,377	-2.468	.636	2.569	.257	.315	.244	1.855	3.219	165.5
	4.3	43	2,360	-2.087	.651	2.195	.219	.206	.222	1.600	3.061	162.7
6	.4	44	2,400	-.808	-.017	.865	.263	.301	.256	.157	1.605	181.2
	.6	45	2,400	-.847	-.208	.925	.270	.302	.263	.158	1.771	193.8
	.8	46	2,400	-.852	-.163	.921	.261	.308	.260	.132	1.682	190.8
	1.3	47	2,400	-.964	-.254	1.043	.275	.323	.295	.258	1.982	194.8
7	.4	48	2,400	-.521	-.120	.584	.242	.225	.233	.034	1.326	193.0
	.6	49	2,400	-.753	-.282	.897	.356	.344	.293	.058	1.956	200.5
	.8	50	2,394	-.971	-.305	1.083	.310	.353	.289	.305	1.994	197.4
	1.3	51	2,394	-1.226	-.002	1.282	.270	.381	.280	.394	2.210	180.1
8	.4	52	2,400	-1.084	-1.373	1.763	.211	.269	.267	.850	2.490	231.7
	.6	53	2,400	-1.169	-1.029	1.584	.263	.342	.323	.776	2.475	221.4
	.8	54	2,400	-1.065	-.838	1.369	.238	.267	.303	.672	2.470	218.2
	1.3	55	2,400	-1.705	-1.349	2.188	.293	.281	.323	1.282	3.225	218.4
	1.8	56	2,400	-1.469	-.944	1.758	.224	.267	.281	1.217	2.879	212.7
9	.4	58	2,400	-1.059	-.485	1.204	.314	.281	.290	.396	2.126	204.6
	.6	59	2,400	-1.137	-.381	1.232	.268	.265	.248	.494	1.926	198.5
	.8	60	2,384	-1.433	-.322	1.507	.285	.330	.279	.684	2.435	192.7
	1.3	61	2,375	-1.656	-.117	1.694	.285	.323	.269	.901	2.908	184.1
	1.8	62	2,400	-2.059	.010	2.085	.358	.322	.352	1.358	3.093	179.7

Table A-1. Two-component velocity data for 1,820 cubic feet per second flow condition—*Continued*

Profile	y (ft)	FILE	n	$\bar{u}$ (ft/s)	$\bar{v}$ (ft/s)	$\bar{U}$ (ft/s)	RMS u (ft/s)	RMS v (ft/s)	RMS U (ft/s)	MIN U (ft/s)	MAX U (ft/s)	ϕ
10	0.4	0	2,400	-0.948	-0.490	1.088	0.191	0.227	0.207	0.402	2.205	207.3
	.6	1	2,394	-1.451	-.287	1.508	.337	.291	.338	.544	2.324	191.2
	.8	2	2,400	-1.673	-.300	1.730	.279	.325	.281	.846	2.698	190.2
	1.3	4	2,400	-1.917	-.033	1.954	.408	.357	.391	.971	3.378	181.0
	2.3	5	2,400	-1.791	.007	1.819	.288	.320	.286	1.152	2.646	179.8
	4.3	8	2,400	-2.011	.312	2.051	.306	.261	.308	1.279	2.921	171.2
11	.4	9	2,400	-1.131	-.062	1.173	.363	.303	.361	.247	2.627	183.2
	.6	10	2,400	-1.029	.032	1.070	.261	.301	.268	.384	1.955	178.2
	.8	11	2,400	-1.317	-.104	1.355	.256	.302	.255	.298	1.995	184.5
	1.3	12	2,400	-1.567	-.032	1.611	.340	.370	.338	.820	2.601	181.2
	2.3	13	2,400	-1.527	.349	1.600	.269	.330	.274	.626	2.819	167.1
	4.3	14	2,400	-1.561	.684	1.718	.213	.241	.240	1.116	2.611	156.3
12	.4	15	2,376	-1.526	.118	1.580	.767	.361	.751	.104	3.483	175.6
	.6	16	2,400	-2.127	.197	2.195	.780	.429	.735	.217	3.730	174.7
	.8	17	2,400	-2.072	.222	2.129	.676	.439	.676	.116	3.684	173.9
	1.3	18	2,400	-1.542	.172	1.572	.237	.246	.233	.719	2.505	173.6
	1.8	19	2,400	-1.646	.319	1.695	.234	.234	.214	1.099	2.496	169.0
	2.3	20	2,383	-1.660	.428	1.724	.229	.183	.224	1.005	2.524	165.5
13	.4	21	2,400	-1.543	-.161	1.661	.773	.427	.653	.105	3.500	186.0
	.6	22	2,400	-2.206	.154	2.234	.269	.320	.273	1.292	3.028	176.0
	.8	23	2,400	-1.991	-.004	2.021	.294	.337	.285	1.061	2.979	180.1
	1.3	24	2,400	-1.921	.368	1.972	.324	.253	.323	1.076	2.852	169.2
	1.8	25	2,400	-1.475	.230	1.503	.409	.164	.404	.806	3.041	171.2
	2.3	26	2,400	-1.211	.276	1.247	.185	.098	.179	.773	1.857	167.2

Table A-1. Two-component velocity data for 1,820 cubic feet per second flow condition—*Continued*

Profile	y (ft)	FILE	n	$\bar{u}$ (ft/s)	$\bar{v}$ (ft/s)	$\bar{U}$ (ft/s)	RMS u (ft/s)	RMS v (ft/s)	RMS U (ft/s)	MIN U (ft/s)	MAX U (ft/s)	ϕ
14	0.4	27	2,392	-0.752	0.148	0.827	0.404	0.287	0.386	0.061	1.928	168.9
	.6	28	2,400	-1.129	.024	1.209	.380	.391	.332	.146	2.183	178.8
	.8	29	2,400	-1.435	.007	1.551	.594	.507	.514	.058	2.993	179.7
	1.3	30	2,400	-1.689	.116	1.752	.561	.401	.521	.256	2.968	176.1
	1.8	31	2,400	-2.064	.301	2.130	.464	.399	.436	.356	3.266	171.7
	2.3	32	2,400	-2.326	.537	2.403	.396	.250	.380	1.271	3.293	167.0
15	.4	33	2,400	.457	-.367	.597	.163	.131	.177	.054	1.116	321.3
	.6	34	2,400	.294	-.249	.416	.204	.106	.169	.031	.890	319.8
	.8	35	2,400	.419	-.317	.586	.298	.129	.194	.015	1.080	322.9
	1.3	36	2,400	.584	-.324	.679	.187	.138	.194	.175	1.194	331.0
	1.8	37	2,400	.276	-.181	.557	.435	.317	.297	.028	1.868	326.8
	2.3	38	2,400	.412	-.231	.539	.251	.247	.236	.015	1.200	330.8
16	.4	41	2,400	.131	-.168	.353	.333	.186	.258	.000	2.872	308.1
	.6	42	2,400	.328	-.187	.516	.379	.267	.301	.010	3.169	330.3
	.8	46	2,400	.428	-.343	.592	.217	.205	.198	.011	1.361	321.3
	1.3	47	2,400	.555	-.336	.678	.210	.201	.212	.045	1.183	328.8
	1.8	48	2,400	.519	-.152	.636	.340	.289	.295	.021	1.609	343.7
	2.3	49	2,383	-.122	.028	.603	.501	.474	.357	.014	2.214	167.0
17	.4	50	2,400	.023	.036	.200	.225	.094	.147	.005	1.302	57.6
	.6	51	2,400	.059	-.120	.217	.163	.135	.125	.000	.889	296.0
	.8	52	2,400	.340	-.214	.458	.233	.188	.202	.049	1.074	327.9
	1.3	53	2,388	.447	-.266	.580	.260	.248	.250	.018	1.424	329.3
	1.8	54	2,400	.496	-.274	.648	.261	.283	.221	.042	1.278	331.1
	2.3	55	2,400	-.004	-.078	.654	.535	.513	.358	.005	1.914	267.3

Table A-1. Two-component velocity data for 1,820 cubic feet per second flow condition—*Continued*

Profile	y (ft)	FILE	n	$\bar{u}$ (ft/s)	$\bar{v}$ (ft/s)	$\bar{U}$ (ft/s)	RMS u (ft/s)	RMS v (ft/s)	RMS U (ft/s)	MIN U (ft/s)	MAX U (ft/s)	ϕ
18	0.4	0	2,400	-0.891	0.437	1.018	0.221	0.236	0.229	0.356	1.738	153.9
	.6	1	2,395	-.959	.477	1.102	.243	.238	.222	.429	1.762	153.5
	.8	2	2,400	-1.134	.326	1.203	.261	.204	.232	.599	1.873	164.0
	1.3	3	2,400	-1.443	.321	1.500	.289	.253	.284	.727	2.488	167.5
	2.3	4	2,394	-1.618	.632	1.756	.429	.217	.403	.801	2.844	158.7
19	.4	5	2,400	-.054	-.025	.235	.204	.181	.150	.005	1.076	204.9
	.6	6	2,400	-.141	.177	.447	.271	.394	.283	.007	1.500	128.4
	.8	7	2,400	-.535	.827	1.039	.300	.487	.467	.035	2.349	122.9
	1.3	8	2,400	-1.252	.626	1.430	.267	.307	.280	.423	2.202	153.4
	2.3	9	2,400	-1.253	.766	1.485	.210	.245	.236	.985	2.285	148.6
20	.4	10	2,400	.249	.873	.941	.265	.242	.260	.118	1.944	74.1
	.6	11	2,400	-.301	.735	.833	.262	.212	.225	.161	1.530	112.3
	.8	12	2,400	-.595	1.009	1.219	.286	.371	.326	.239	2.380	120.5
	1.3	13	2,400	-.918	.968	1.358	.250	.194	.188	.924	2.043	133.5
	2.3	14	2,400	-.906	1.135	1.469	.183	.265	.234	.790	2.230	128.6
21	.4	15	2,400	-.839	.689	1.097	.153	.163	.164	.681	1.691	140.6
	.6	17	2,400	-.900	.693	1.148	.166	.154	.152	.747	1.860	142.4
	.8	18	2,400	-.975	.707	1.217	.141	.193	.157	.757	1.717	144.0
	1.3	19	2,400	-1.136	.750	1.371	.155	.177	.172	.741	2.044	146.6
	2.3	21	2,400	-1.250	.622	1.405	.190	.174	.208	.861	1.953	153.5
22	.4	23	2,400	-1.197	.879	1.499	.212	.200	.208	.876	2.556	143.7
	.6	24	2,400	-1.367	.945	1.677	.165	.235	.173	1.175	2.327	145.3
	.8	25	2,400	-1.582	.963	1.884	.235	.389	.301	1.109	3.265	148.7
	1.3	26	2,395	-1.785	1.067	2.099	.197	.305	.223	1.303	2.950	149.1
	2.3	27	2,400	-2.072	1.136	2.371	.262	.259	.311	1.702	3.319	151.3
	3.3	71	2,400	-1.813	1.914	2.643	.215	.291	.306	1.882	4.232	133.5

Table A-1. Two-component velocity data for 1,820 cubic feet per second flow condition—*Continued*

Profile	y (ft)	FILE	n	$\bar{u}$ (ft/s)	$\bar{v}$ (ft/s)	$\bar{U}$ (ft/s)	RMS u (ft/s)	RMS v (ft/s)	RMS U (ft/s)	MIN U (ft/s)	MAX U (ft/s)	ϕ
23	0.4	28	2,400	-1.388	0.806	1.634	0.335	0.327	0.351	0.377	2.698	149.8
	.6	29	2,400	-1.551	.834	1.780	.216	.296	.255	.929	2.805	151.8
	.8	30	2,393	-1.531	1.158	1.941	.207	.311	.237	1.260	2.951	142.9
	1.3	31	2,393	-1.507	1.046	1.849	.229	.244	.237	1.152	2.680	145.2
	2.3	32	2,400	-1.558	1.301	2.046	.181	.276	.208	1.556	2.632	140.1
	3.3	72	2,400	-1.695	1.162	2.066	.153	.246	.202	1.416	2.660	145.6
24	.4	33	2,400	-1.413	.720	1.605	.272	.228	.252	.977	2.400	153.0
	.6	34	2,400	-1.444	.666	1.608	.288	.216	.272	1.006	2.591	155.3
	.8	35	2,400	-1.503	.702	1.674	.376	.222	.371	.594	2.552	155.0
	1.3	37	2,400	-1.585	.562	1.693	.211	.177	.196	1.205	2.593	160.5
	2.3	38	2,400	-1.470	.750	1.658	.204	.179	.219	.967	2.216	153.0
	3.3	73	2,400	-1.762	.876	1.979	.231	.244	.260	1.286	2.720	153.6
25	.4	39	2,400	.180	-.101	.255	.159	.104	.117	.000	.616	330.8
	.6	40	2,400	.212	-.076	.305	.228	.132	.165	.007	.986	340.4
	.8	41	2,400	-.091	-.001	.319	.356	.175	.253	.005	2.054	180.5
	1.3	43	2,400	-.718	.100	.802	.535	.219	.466	.020	2.121	172.1
	2.3	44	2,400	-.805	.072	.894	.843	.223	.784	.000	2.850	174.9
26	.4	45	2,400	-.339	-.311	.517	.200	.261	.229	.025	1.562	222.5
	.6	46	2,400	-.755	.015	.851	.333	.410	.354	.067	2.878	178.9
	.8	47	2,400	-.696	.295	.802	.297	.301	.327	.039	1.793	157.1
	1.3	48	2,400	-1.832	.557	1.927	.310	.261	.343	1.027	2.809	163.1
	2.3	49	2,400	-1.915	.616	2.020	.187	.207	.210	1.410	2.607	162.2
27	.4	50	2,400	-1.261	-.060	1.285	.250	.230	.244	.461	1.954	182.7
	.6	51	2,400	-1.318	.107	1.350	.305	.271	.306	.393	2.304	175.4
	.8	52	2,400	-1.431	.261	1.476	.311	.253	.310	.674	2.260	169.7
	1.3	53	2,400	-1.107	.322	1.161	.192	.151	.204	.578	1.903	163.8
	2.3	54	2,400	-1.149	.324	1.202	.205	.151	.217	.646	2.001	164.2

Table A-1. Two-component velocity data for 1,820 cubic feet per second flow condition—*Continued*

Profile	y (ft)	FILE	n	$\bar{u}$ (ft/s)	$\bar{v}$ (ft/s)	$\bar{U}$ (ft/s)	RMS u (ft/s)	RMS v (ft/s)	RMS U (ft/s)	MIN U (ft/s)	MAX U (ft/s)	ϕ
28	0.4	55	2,400	-0.424	0.070	0.482	0.246	0.229	0.257	0.010	1.601	17.6
	.6	56	2,400	-.580	-.054	.652	.231	.293	.231	.022	1.502	185.4
	.8	57	2,400	-.506	.016	.581	.307	.271	.295	.015	1.535	178.2
	1.3	58	2,400	-.871	.192	.921	.432	.234	.435	.010	2.188	167.6
	2.3	59	2,400	-1.568	.415	1.633	.322	.181	.314	.475	2.502	165.2
29	.4	60	2,400	-1.228	-.107	1.261	.270	.266	.271	.627	2.404	185.0
	.6	61	2,400	-1.107	-.043	1.148	.348	.299	.347	.313	3.008	182.2
	.8	62	2,400	-1.110	.203	1.171	.262	.305	.254	.460	2.117	169.6
	1.3	63	2,400	-1.713	.525	1.813	.377	.287	.385	.700	2.821	163.0
	2.3	64	2,390	-2.105	.527	2.178	.237	.191	.239	1.620	2.969	166.0
30	.4	65	2,400	-1.769	.070	1.785	.265	.235	.268	.996	3.593	177.7
	.6	66	2,393	-1.722	.103	1.737	.294	.212	.298	1.087	2.784	176.6
	.8	67	2,400	-1.862	.125	1.880	.234	.231	.237	1.151	2.590	176.2
	1.3	68	2,400	-1.878	.307	1.913	.241	.198	.243	1.325	2.868	17.7
	2.3	69	2,400	-1.934	.515	2.012	.253	.212	.259	1.409	2.875	165.1
31	.4	74	2,400	-1.413	.396	1.475	.205	.143	.198	.849	2.040	164.4
	.6	76	2,400	-1.456	.263	1.489	.238	.175	.243	.635	2.123	169.7
	.8	79	2,400	-1.488	.436	1.565	.233	.206	.232	.949	2.425	163.7
	1.3	80	2,400	-1.941	.578	2.034	.232	.204	.245	1.426	2.736	163.4
	2.3	81	2,400	-1.527	.550	1.635	.158	.181	.141	1.221	2.040	160.2
	4.3	82	2,400	-1.703	.908	1.941	.189	.237	.228	1.420	2.963	151.9
32	.4	85	2,400	-.500	-.050	.525	.130	.149	.125	.150	.942	185.7
	.6	86	2,400	-.502	-.004	.530	.157	.172	.159	.088	1.152	180.4
	.8	87	2,400	-.761	.146	.796	.193	.199	.207	.355	1.485	169.2
	1.3	88	2,400	-1.278	.316	1.326	.159	.160	.157	.836	2.261	166.1
	2.3	89	2,400	-1.729	.421	1.786	.212	.158	.215	1.230	2.562	166.3
	4.3	91	2,400	-1.741	.611	1.851	.141	.139	.135	1.440	2.228	160.7

Table A-1. Two-component velocity data for 1,820 cubic feet per second flow condition—*Continued*

Profile	y (ft)	FILE	n	$\bar{u}$ (ft/s)	$\bar{v}$ (ft/s)	$\bar{U}$ (ft/s)	RMS u (ft/s)	RMS v (ft/s)	RMS U (ft/s)	MIN U (ft/s)	MAX U (ft/s)	ϕ
33	0.4	0	2,400	-0.909	-0.040	0.927	0.189	0.178	0.190	0.485	1.519	182.5
	.6	1	2,400	-.962	.059	.976	.235	.149	.233	.483	1.649	176.5
	.8	2	2,400	-1.198	.036	1.214	.258	.190	.257	.496	1.954	178.3
	1.3	3	2,400	-1.377	.236	1.413	.338	.209	.338	.698	2.577	170.3
	2.3	4	2,400	-1.364	.438	1.446	.188	.197	.191	.814	1.943	162.2
	4.3	5	2,400	-1.312	.624	1.472	.162	.246	.176	1.031	1.946	154.6
34	.4	6	2,400	-1.101	.039	1.122	.179	.213	.177	.724	1.984	178.0
	.6	8	2,400	-1.172	.031	1.187	.213	.187	.213	.777	1.788	178.5
	.8	9	2,400	-1.346	.091	1.377	.246	.282	.253	.812	2.219	176.1
	1.3	10	2,400	-1.325	.285	1.368	.150	.183	.152	.890	1.874	167.9
	2.3	11	2,400	-1.346	.458	1.432	.227	.187	.235	.697	1.984	161.2
	4.3	12	2,400	-1.543	.636	1.675	.184	.169	.203	1.240	2.369	157.6
35	.4	13	2,400	-1.198	.036	1.236	.296	.299	.295	.514	2.141	178.3
	.6	14	2,400	-1.087	.349	1.176	.227	.323	.276	.464	2.112	162.2
	.8	15	2,400	-1.155	.307	1.225	.250	.266	.244	.639	1.955	165.1
	1.3	16	2,400	-1.336	.545	1.472	.254	.346	.314	.756	2.703	157.8
	2.3	17	2,400	-1.509	.533	1.615	.205	.236	.226	.928	2.247	160.6
	4.3	18	2,400	-1.613	.843	1.832	.226	.243	.258	1.001	2.555	152.4
36	.4	19	2,400	-1.242	.432	1.343	.286	.270	.283	.659	2.120	160.8
	.6	20	2,400	-1.446	.468	1.544	.343	.277	.345	.796	2.795	162.1
	.8	21	2,400	-1.415	.467	1.509	.282	.244	.287	.748	2.390	161.7
	.8	22	2,400	-1.368	.535	1.484	.268	.242	.289	.689	2.288	158.6
	1.3	23	2,400	-1.612	.565	1.722	.273	.222	.276	1.035	2.469	160.7
	2.3	24	2,400	-1.585	.703	1.747	.239	.236	.258	.968	2.531	156.1
	4.3	25	2,400	-2.008	.908	2.213	.253	.276	.311	1.680	3.525	155.7

Table A-1. Two-component velocity data for 1,820 cubic feet per second flow condition—*Continued*

Profile	y (ft)	FILE	n	$\bar{u}$ (ft/s)	$\bar{v}$ (ft/s)	$\bar{U}$ (ft/s)	RMS u (ft/s)	RMS v (ft/s)	RMS U (ft/s)	MIN U (ft/s)	MAX U (ft/s)	ϕ
37	0.4	26	2,400	-1.368	0.558	1.520	0.352	0.407	0.402	0.620	2.852	157.8
	.6	27	2,400	-1.513	.477	1.635	.369	.415	.388	.694	2.669	162.5
	.8	28	2,400	-1.594	.530	1.709	.337	.354	.374	.799	2.744	161.6
	1.3	29	2,394	-1.920	.662	2.061	.404	.377	.426	.913	3.081	161.0
	2.3	30	2,393	-2.406	.917	2.599	.357	.329	.333	1.651	3.476	159.1
	4.3	31	2,393	-2.279	1.100	2.542	.272	.303	.324	1.845	3.872	154.2
38	.4	32	2,400	-.607	.071	.654	.118	.250	.146	.302	1.265	173.3
	.6	33	2,400	-.659	-.062	.691	.162	.198	.161	.314	1.275	185.4
	.8	34	2,400	-1.181	.121	1.208	.335	.223	.336	.443	2.242	174.2
	1.3	35	2,395	-1.450	.269	1.480	.147	.120	.140	1.070	1.946	169.5
	2.3	37	2,400	-1.662	.557	1.762	.191	.185	.200	1.245	2.461	161.5
	4.3	38	2,400	-1.711	.574	1.813	.169	.184	.182	1.241	2.312	161.5
39	.4	39	2,400	-1.185	.013	1.205	.271	.221	.273	.584	2.186	179.4
	.6	40	2,400	-1.280	.082	1.296	.220	.186	.223	.828	1.976	176.4
	.8	41	2,400	-1.258	.127	1.279	.181	.183	.174	.737	1.819	174.2
	1.3	42	2,400	-1.570	.286	1.607	.246	.199	.256	.966	2.228	169.7
	2.3	43	2,400	-1.451	.400	1.515	.228	.174	.224	.963	2.009	164.6
	4.3	44	2,400	-1.585	.659	1.736	.202	.274	.219	1.241	2.468	157.4
40	.4	45	2,400	-1.103	-.187	1.158	.295	.296	.294	.540	2.506	189.6
	.6	46	2,400	-1.307	-.142	1.350	.294	.308	.298	.658	2.266	186.2
	.8	47	2,400	-1.179	-.036	1.207	.262	.258	.265	.597	1.978	181.8
	1.3	48	2,400	-1.320	.105	1.352	.229	.274	.230	.825	1.979	175.4
	2.3	49	2,400	-1.715	.264	1.761	.258	.312	.270	.914	2.446	171.3
	4.3	50	2,400	-1.838	.715	1.985	.281	.212	.272	1.320	2.804	158.8

Table A-1. Two-component velocity data for 1,820 cubic feet per second flow condition—*Continued*

Profile	y (ft)	FILE	n	$\bar{u}$ (ft/s)	$\bar{v}$ (ft/s)	$\bar{U}$ (ft/s)	RMS u (ft/s)	RMS v (ft/s)	RMS U (ft/s)	MIN U (ft/s)	MAX U (ft/s)	ϕ
41	0.4	51	2,400	-0.700	0.066	0.755	0.340	0.266	0.332	0.035	1.884	174.6
	.6	52	2,400	-1.073	.155	1.120	.332	.285	.333	.134	2.216	171.8
	.8	53	2,400	-1.501	.098	1.543	.411	.312	.386	.171	2.375	176.3
	1.3	54	2,400	-1.949	.379	2.007	.272	.286	.266	1.311	2.871	169.0
	2.3	55	2,400	-2.114	.457	2.180	.314	.285	.321	1.201	3.132	167.8
	4.3	56	2,400	-2.394	.751	2.528	.276	.333	.303	1.853	3.522	162.6
42	.4	57	2,400	-1.157	.049	1.181	.334	.233	.336	.401	3.650	177.6
	.6	58	2,400	-1.464	.211	1.510	.415	.278	.395	.307	2.569	171.8
	.8	60	2,400	-1.418	.398	1.507	.336	.323	.339	.660	2.720	164.3
	1.3	61	2,400	-2.059	.616	2.181	.350	.381	.362	1.171	3.101	163.3
	2.3	62	2,400	-2.162	.697	2.289	.313	.292	.327	1.398	3.323	162.1
	4.3	63	2,400	-2.358	1.060	2.602	.324	.331	.359	1.696	3.576	155.8
43	.4	64	2,400	-.833	.342	.925	.223	.210	.223	.421	1.823	157.7
	.6	65	2,400	-1.332	.431	1.419	.269	.255	.289	.644	2.306	162.1
	.8	66	2,400	-1.571	.417	1.653	.276	.305	.281	.870	2.371	165.1
	1.3	67	2,400	-1.855	.376	1.899	.224	.159	.225	1.307	2.542	168.6
	2.3	68	2,400	-1.940	.504	2.010	.195	.165	.199	1.485	2.487	165.4
	4.3	69	2,400	-2.090	.683	2.205	.208	.182	.217	1.718	2.863	161.9
44	.4	71	2,400	-.842	.225	.902	.325	.224	.319	.091	1.775	165.1
	.6	72	2,400	-1.280	.393	1.358	.276	.223	.274	.601	2.180	163.0
	.8	73	2,400	-1.563	.504	1.653	.243	.205	.256	.826	2.404	162.1
	1.3	74	2,400	-1.837	.526	1.921	.275	.205	.282	1.058	2.708	164.0
	2.3	75	2,400	-1.975	.583	2.068	.174	.197	.187	1.530	2.599	163.6
	4.3	76	2,400	-1.893	.663	2.011	.139	.154	.144	1.635	2.536	160.7

Table A-1. Two-component velocity data for 1,820 cubic feet per second flow condition—*Continued*

Profile	y (ft)	FILE	n	$\bar{u}$ (ft/s)	$\bar{v}$ (ft/s)	$\bar{U}$ (ft/s)	RMS u (ft/s)	RMS v (ft/s)	RMS U (ft/s)	MIN U (ft/s)	MAX U (ft/s)	ϕ
45	0.4	77	2,400	-1.077	0.514	1.212	0.225	0.248	0.255	0.477	2.195	154.5
	.6	78	2,400	-1.321	.540	1.444	.269	.247	.291	.533	2.287	157.8
	.8	79	2,400	-1.360	.511	1.467	.222	.228	.246	.869	2.164	159.4
	1.3	80	2,400	-1.740	.567	1.841	.253	.212	.262	1.121	2.707	161.9
	2.3	82	2,400	-1.952	.681	2.073	.249	.154	.250	1.326	2.969	160.8
	4.3	83	2,400	-1.727	.652	1.854	.173	.169	.168	1.353	2.398	159.3
46	.4	84	2,400	-1.451	.347	1.512	.273	.257	.284	.660	2.711	166.6
	.6	85	2,400	-1.442	.478	1.533	.211	.225	.235	.741	2.205	161.7
	.8	86	2,400	-1.027	.640	1.230	.183	.278	.250	.592	2.332	148.0
	1.3	87	2,400	-1.583	.447	1.661	.309	.253	.323	.546	2.551	164.2
	2.3	88	2,400	-2.049	.575	2.140	.205	.222	.198	1.574	3.301	164.3
	2.3	89	2,400	-1.729	.566	1.827	.232	.178	.241	1.242	2.616	161.9
	4.3	90	2,384	-1.818	.733	1.965	.214	.139	.211	1.547	2.476	158.0
47	.4	91	2,400	-.842	.306	.920	.226	.201	.218	.431	1.790	160.0
	.6	92	2,400	-.922	.315	1.002	.265	.240	.273	.514	2.160	161.2
	.8	93	2,400	-1.000	.249	1.051	.273	.203	.269	.377	1.914	166.0
	1.3	95	2,400	-1.459	.417	1.536	.314	.267	.337	.791	2.430	164.1
	2.3	96	2,395	-1.927	.633	2.036	.239	.211	.262	1.260	2.652	161.8
	4.3	97	2,400	-2.076	.897	2.268	.194	.187	.205	1.637	2.837	156.6
48	.4	98	2,400	-.959	.445	1.077	.265	.243	.296	.288	1.903	155.1
	.6	99	2,400	-1.161	.539	1.294	.232	.219	.258	.522	2.354	155.1
	.8	100	2,400	-1.251	.458	1.350	.273	.257	.303	.480	2.400	159.9
	1.3	101	2,400	-1.548	.430	1.623	.268	.242	.278	.780	2.322	164.5
	2.3	102	2,400	-1.733	.560	1.830	.193	.160	.183	1.035	2.364	162.1
	4.3	103	2,400	-1.737	.780	1.916	.210	.201	.195	1.191	2.911	155.8

Table A-1. Two-component velocity data for 1,820 cubic feet per second flow condition—*Continued*

Profile	y (ft)	FILE	n	$\bar{u}$ (ft/s)	$\bar{v}$ (ft/s)	$\bar{U}$ (ft/s)	RMS u (ft/s)	RMS v (ft/s)	RMS U (ft/s)	MIN U (ft/s)	MAX U (ft/s)	ϕ
49	0.4	0	2,400	-1.232	0.508	1.460	0.354	0.530	0.222	0.935	2.057	157.6
	.6	1	2,400	-1.180	.495	1.366	.319	.420	.219	.738	1.963	157.3
	.8	2	2,400	-1.099	.028	1.440	.785	.548	.230	.743	2.066	178.5
	1.3	3	2,400	-1.478	.980	1.815	.285	.331	.202	1.350	2.546	146.5
50	.6	7	2,400	-1.178	.497	1.289	.226	.157	.218	.687	1.909	157.1
	.8	8	2,400	-1.323	.535	1.437	.269	.174	.274	.695	2.193	158.0
	1.3	9	2,400	-1.518	.541	1.622	.210	.179	.208	1.074	2.141	160.4
	2.3	10	2,400	-1.852	.651	1.972	.200	.182	.195	1.411	2.513	160.6
	4.3	11	2,400	-2.171	.879	2.352	.324	.198	.310	1.572	3.219	158.0
51	.4	12	2,400	-.881	.320	.961	.269	.230	.284	.367	1.984	160.0
	.6	13	2,400	-1.212	.439	1.307	.253	.221	.257	.644	2.255	160.1
	.8	14	2,400	-1.157	.380	1.235	.237	.217	.247	.685	2.124	161.8
	1.3	15	2,400	-1.313	.410	1.389	.237	.207	.249	.753	2.271	162.7
	2.3	16	2,393	-1.800	.546	1.891	.223	.201	.224	1.224	2.447	163.1
	4.3	17	2,400	-1.720	.680	1.854	.172	.129	.173	1.451	2.477	158.4
52	.4	18	2,400	-.779	.306	.866	.318	.249	.337	.149	1.935	158.6
	.6	19	2,400	-1.121	.432	1.223	.290	.238	.298	.585	2.043	158.9
	.8	20	2,400	-1.006	.332	1.080	.228	.222	.239	.525	1.915	161.8
	1.3	21	2,400	-1.141	.352	1.210	.309	.233	.336	.189	2.431	162.9
	2.3	22	2,400	-1.538	.448	1.609	.217	.166	.231	.945	2.452	163.8
	4.3	23	2,400	-2.066	.869	2.249	.191	.196	.197	1.694	3.047	157.2
53	.4	25	2,400	-.199	.015	.304	.205	.227	.202	.000	1.091	175.8
	.6	26	2,400	-.460	.069	.549	.267	.286	.261	.021	1.596	171.5
	.8	27	2,400	-.739	.163	.811	.280	.300	.288	.177	1.709	167.6
	1.3	28	2,400	-.955	.181	1.020	.353	.320	.363	.138	1.940	169.3
	2.3	29	2,400	-1.505	.478	1.588	.243	.193	.258	.684	2.182	162.4
	4.3	30	2,400	-1.881	.698	2.013	.147	.162	.151	1.655	2.598	159.6

Table A-1. Two-component velocity data for 1,820 cubic feet per second flow condition—*Continued*

Profile	y (ft)	FILE	n	$\bar{u}$ (ft/s)	$\bar{v}$ (ft/s)	$\bar{U}$ (ft/s)	RMS u (ft/s)	RMS v (ft/s)	RMS U (ft/s)	MIN U (ft/s)	MAX U (ft/s)	ϕ
54	0.4	31	2,393	-0.864	-0.274	0.920	0.291	0.161	0.292	0.298	2.237	197.6
	.6	32	2,400	-.873	-.317	.943	.249	.145	.234	.326	1.841	200.0
	.8	33	2,400	-1.846	-.694	1.980	.390	.170	.385	1.017	3.006	200.6
	1.3	34	2,400	-1.777	-.531	1.874	.403	.272	.407	.315	2.830	196.6
	2.3	35	2,400	-1.792	-.251	1.832	.393	.286	.395	.364	2.778	188.0
	4.3	36	2,400	-1.550	-.019	1.576	.472	.271	.465	.439	2.675	180.7
55	.4	37	2,400	-.273	.542	.738	.364	.425	.371	.028	2.290	116.7
	.6	38	2,400	-.317	.498	.735	.338	.445	.346	.057	1.865	122.5
	.8	39	2,400	-.411	.535	.793	.291	.440	.323	.000	1.865	127.5
	1.3	40	2,400	-.260	.167	.539	.246	.456	.272	.000	1.491	147.4
	2.3	41	2,400	-.028	-.197	.362	.226	.280	.195	.007	1.034	262.0
	4.3	42	2,400	.088	-.200	.345	.207	.238	.168	.000	.924	293.8
56	.4	43	2,400	-.554	.864	1.077	.276	.377	.335	.204	2.077	122.7
	.6	44	2,400	-.763	.797	1.161	.416	.371	.423	.050	2.263	133.7
	1.3	45	2,400	-.674	.883	1.152	.295	.335	.326	.247	2.628	127.4
	2.3	46	2,400	-.626	.685	.986	.376	.463	.493	.021	2.350	132.4
	4.3	47	2,400	-.849	.447	1.060	.402	.518	.477	.176	2.739	152.2
57	.4	49	2,400	-.560	.122	.715	.280	.464	.334	.024	2.321	167.7
	.6	50	2,400	-.519	.049	.647	.311	.374	.299	.014	1.482	174.7
	.8	51	2,400	-.546	.333	.785	.292	.466	.308	.045	1.721	148.6
	1.3	52	2,400	-.660	.602	1.002	.383	.531	.472	.059	2.772	137.6
	2.3	53	2,400	-.795	.640	1.098	.300	.475	.390	.005	2.249	141.2
	4.3	54	2,400	-.310	.037	.549	.297	.465	.316	.005	1.792	173.3

Table A-1. Two-component velocity data for 1,820 cubic feet per second flow condition—*Continued*

Profile	*y* (ft)	FILE	*n*	$\bar{u}$ (ft/s)	$\bar{v}$ (ft/s)	$\bar{U}$ (ft/s)	RMS *u* (ft/s)	RMS *v* (ft/s)	RMS *U* (ft/s)	MIN *U* (ft/s)	MAX *U* (ft/s)	ϕ
58	0.4	55	2,400	-0.598	0.369	0.779	0.415	0.322	0.404	0.011	2.081	148.3
	.6	56	2,400	-.843	.571	1.067	.350	.348	.376	.111	2.099	145.9
	.8	57	2,400	-1.023	.491	1.178	.430	.341	.448	.288	2.370	154.4
	1.3	58	2,387	-1.434	.857	1.707	.386	.382	.414	.557	2.909	149.1
	2.3	59	2,400	-1.269	1.010	1.686	.452	.490	.484	.482	3.254	141.5
	4.3	60	2,400	-1.516	.869	1.779	.379	.422	.458	.543	3.051	150.2
59	.4	61	2,400	-.968	.055	1.002	.322	.248	.319	.352	2.033	176.7
	.6	62	2,400	-1.045	.100	1.065	.263	.173	.258	.312	1.697	174.5
	.8	63	2,400	-1.333	.163	1.355	.372	.180	.371	.324	2.271	173.0
	1.3	64	2,400	-1.492	.211	1.521	.321	.211	.325	.647	2.441	172.0
	2.3	65	2,400	-1.901	.266	1.929	.269	.192	.273	.965	2.804	172.0
	4.3	66	2,400	-2.075	.555	2.157	.263	.190	.260	1.308	3.130	165.0
60	.4	1	2,400	-.364	.711	.907	.428	.321	.319	.204	1.812	117.1
	.6	2	2,400	-.712	.863	1.203	.514	.331	.420	.315	2.569	129.5
	.8	3	2,383	-.605	.835	1.088	.341	.319	.311	.145	2.038	125.9
	1.3	4	2,400	-.924	1.025	1.458	.447	.436	.411	.525	2.609	132.1
	2.3	5	2,400	-1.004	1.014	1.496	.470	.527	.544	.257	2.873	134.7
	4.3	6	2,400	-.996	.992	1.483	.485	.733	.741	.162	3.068	135.1
61	.4	7	2,400	-.633	.964	1.276	.452	.466	.352	.311	2.336	123.3
	.6	8	2,400	-.866	.896	1.335	.482	.433	.435	.211	2.685	134.0
	.8	9	2,400	-.677	1.017	1.297	.395	.386	.339	.231	2.246	123.6
	1.3	10	2,400	-.509	1.014	1.206	.416	.406	.412	.119	2.426	116.6
	2.3	11	2,393	-.945	.892	1.378	.464	.469	.474	.183	2.712	136.7
	4.3	12	2,400	-1.439	1.357	2.006	.326	.412	.403	.912	2.986	136.7

Table A-1. Two-component velocity data for 1,820 cubic feet per second flow condition—*Continued*

Profile	y (ft)	FILE	n	$\bar{u}$ (ft/s)	$\bar{v}$ (ft/s)	$\bar{U}$ (ft/s)	RMS u (ft/s)	RMS v (ft/s)	RMS U (ft/s)	MIN U (ft/s)	MAX U (ft/s)	ϕ
62	0.4	13	2,395	-0.787	0.809	1.229	0.334	0.516	0.373	0.297	2.754	134.2
	.6	14	2,391	-.767	.784	1.169	.335	.467	.408	.095	2.566	134.4
	.8	15	2,394	-.998	.831	1.380	.433	.494	.460	.132	2.577	140.2
	1.3	16	2,400	-.789	.906	1.266	.325	.483	.423	.378	2.729	131.1
	2.3	17	2,400	-.861	.597	1.096	.346	.374	.397	.020	2.780	145.3
	4.3	18	2,389	-1.428	1.114	1.883	.478	.606	.575	.132	3.310	142.1
63	.4	19	2,400	-.975	.807	1.399	.434	.607	.449	.362	2.944	140.4
	.6	20	2,400	-.917	.888	1.334	.305	.471	.409	.419	2.951	135.9
	.8	21	2,400	-.933	.858	1.338	.301	.465	.349	.015	2.578	137.4
	1.3	22	2,400	-1.163	.994	1.595	.469	.499	.517	.179	2.867	139.5
	2.3	23	2,392	-1.499	1.047	1.861	.365	.386	.406	.514	2.983	145.1
	4.3	24	2,400	-1.667	1.105	2.026	.367	.434	.468	.487	3.544	146.5
64	.4	25	2,400	-.630	.459	.856	.441	.265	.372	.056	1.790	143.9
	.6	26	2,400	-1.214	.636	1.418	.509	.322	.480	.260	2.922	152.3
	.8	27	2,400	-1.057	.575	1.243	.365	.291	.350	.303	2.239	151.5
	1.3	28	2,385	-1.313	.561	1.450	.332	.237	.321	.432	2.328	156.9
	2.3	29	2,400	-1.388	.558	1.507	.297	.177	.293	.656	2.285	158.1
	4.3	30	2,400	-1.420	.596	1.547	.190	.177	.210	1.019	2.319	157.2
65	.4	31	2,400	-.881	.295	.988	.327	.353	.345	.191	2.228	161.5
	.6	32	2,400	-1.065	.378	1.173	.351	.331	.367	.277	2.508	160.5
	.8	33	2,400	-.748	.238	.819	.315	.262	.336	.164	2.310	162.4
	1.3	34	2,400	-.582	.276	.665	.165	.189	.189	.205	1.225	154.6
	2.3	35	2,400	-.761	.331	.847	.283	.183	.292	.302	1.920	156.5
	4.3	36	2,396	-1.111	.420	1.196	.175	.164	.191	.645	1.811	159.3

Table A-1. Two-component velocity data for 1,820 cubic feet per second flow condition—*Continued*

Profile	y (ft)	FILE	n	$\bar{u}$ (ft/s)	$\bar{v}$ (ft/s)	$\bar{U}$ (ft/s)	RMS u (ft/s)	RMS v (ft/s)	RMS U (ft/s)	MIN U (ft/s)	MAX U (ft/s)	ϕ
66	0.4	37	2,387	-0.447	-0.012	0.572	0.278	0.364	0.287	0.049	1.862	181.6
	.6	38	2,400	-.729	.194	.846	.362	.399	.380	.021	2.514	165.1
	.8	39	2,386	-1.068	.396	1.202	.407	.394	.416	.200	2.534	159.7
	1.3	40	2,393	-1.699	.654	1.841	.320	.281	.326	.933	2.950	159.0
	2.3	41	2,386	-1.859	.713	2.013	.361	.318	.378	.962	3.068	159.0
	4.3	42	2,400	-1.653	.591	1.765	.276	.227	.306	.846	2.754	160.3
67	.4	43	2,400	-.336	.252	.594	.446	.325	.357	.010	1.959	143.2
	.6	44	2,400	-.630	.272	.793	.475	.368	.450	.016	2.613	156.7
	.8	45	2,400	-.750	.221	.856	.444	.318	.420	.034	2.258	163.6
	1.3	46	2,400	-1.308	.483	1.442	.560	.339	.543	.061	3.006	159.7
	2.3	47	2,400	-1.731	.786	1.920	.375	.299	.399	.753	2.959	155.6
	4.3	48	2,400	-1.901	.929	2.125	.328	.262	.372	1.072	3.551	154.0
68	.4	50	2,400	-.535	-.297	.647	.258	.200	.251	.000	1.353	209.0
	.6	51	2,400	-.721	-.162	.769	.223	.219	.228	.241	1.454	192.6
	.8	52	2,379	-.753	-.100	.790	.238	.216	.237	.170	1.814	187.6
	1.3	53	2,400	-.989	.083	1.044	.335	.334	.346	.190	2.141	175.2
	2.3	54	2,360	-.833	.412	1.009	.391	.461	.460	.005	2.590	153.7
	4.3	55	2,400	-.702	.373	.926	.346	.488	.366	.069	2.047	152.0
69	.4	56	2,400	-.945	-.105	.968	.307	.173	.305	.391	1.827	186.4
	.6	58	2,400	-.892	-.021	.913	.226	.194	.226	.312	2.145	181.3
	.8	59	2,400	-1.194	.091	1.220	.297	.223	.291	.565	1.901	175.6
	1.3	60	2,394	-1.497	.292	1.540	.388	.233	.399	.553	2.746	169.0
	2.3	62	2,400	-1.445	.378	1.501	.161	.161	.173	.738	1.852	165.3
	4.3	63	2,400	-2.138	.715	2.262	.266	.166	.252	1.342	3.121	161.5

Table A-1. Two-component velocity data for 1,820 cubic feet per second flow condition—*Continued*

Profile	y (ft)	FILE	n	$\bar{u}$ (ft/s)	$\bar{v}$ (ft/s)	$\bar{U}$ (ft/s)	RMS u (ft/s)	RMS v (ft/s)	RMS U (ft/s)	MIN U (ft/s)	MAX U (ft/s)	ϕ
70	0.4	65	2,400	-0.716	-0.036	0.749	0.286	0.207	0.278	0.110	1.464	182.9
	.6	66	2,400	-1.006	.017	1.035	.306	.240	.304	.257	1.762	179.1
	.8	67	2,400	-1.126	.178	1.178	.296	.293	.293	.439	2.063	171.0
	1.3	68	2,400	-1.357	.328	1.428	.399	.311	.406	.426	2.367	166.4
	2.3	69	2,400	-1.732	.624	1.852	.233	.214	.248	1.092	2.476	160.2
	4.3	70	2,400	-1.806	.818	1.988	.140	.148	.138	1.599	2.485	155.6
71	.4	0	2,386	.624	-.287	.727	.223	.275	.262	.127	1.345	335.3
	.6	1	2,400	.499	-.357	.659	.228	.193	.177	.051	1.203	324.4
	.8	2	2,400	.273	-.322	.512	.308	.192	.219	.005	1.068	310.3
	1.3	3	2,400	.176	-.089	.496	.394	.317	.222	.000	1.245	333.1
	2.3	4	2,400	.144	-.131	.550	.448	.356	.250	.005	1.571	317.8
	4.3	5	2,400	-1.472	.545	1.697	.641	.607	.603	.079	4.026	159.7
	.8	6	2,400	.411	-.208	.534	.217	.248	.189	.031	1.236	333.2
72	.4	7	2,400	.439	-.009	.533	.197	.300	.193	.035	1.001	358.9
	.6	8	2,400	.461	-.261	.606	.235	.276	.212	.005	1.222	330.5
	.8	9	2,400	.511	-.252	.608	.159	.227	.177	.011	1.561	333.7
	1.3	10	2,400	.522	-.317	.673	.269	.251	.235	.060	1.584	328.7
	2.3	11	2,388	.121	-.100	.710	.687	.479	.471	.010	3.400	320.6
	4.3	12	2,392	-1.580	.590	1.821	.855	.527	.733	.029	3.428	159.5
	6.3	13	2,400	-1.325	.524	1.506	.505	.494	.514	.074	2.795	158.4
73	.4	14	2,400	.148	.144	.536	.359	.467	.319	.007	2.450	44.1
	.6	15	2,400	-.042	.222	.445	.345	.306	.255	.005	1.309	100.6
	.8	16	2,400	-.001	.019	.554	.487	.415	.322	.015	1.737	91.6
	1.3	17	2,400	-.089	.043	.504	.368	.412	.246	.010	1.848	154.3
	2.3	18	2,400	-.726	.189	.915	.590	.495	.565	.005	2.673	165.4
	4.3	19	2,400	-2.172	.719	2.316	.501	.376	.514	.491	3.723	161.7

Table A-1. Two-component velocity data for 1,820 cubic feet per second flow condition—*Continued*

Profile	y (ft)	FILE	n	$\bar{u}$ (ft/s)	$\bar{v}$ (ft/s)	$\bar{U}$ (ft/s)	RMS u (ft/s)	RMS v (ft/s)	RMS U (ft/s)	MIN U (ft/s)	MAX U (ft/s)	ϕ
74	0.4	20	2,393	-1.801	0.333	1.853	0.308	0.272	0.302	0.930	2.758	169.5
	.6	21	2,400	-1.696	.265	1.742	.256	.303	.262	.997	2.580	171.1
	.8	22	2,400	-1.822	.290	1.872	.309	.304	.301	.855	2.712	171.0
	1.3	23	2,400	-2.028	.441	2.092	.272	.255	.264	1.294	3.055	167.7
	2.3	24	2,400	-1.965	.653	2.087	.409	.279	.422	.899	3.111	161.6
	4.3	25	2,400	-2.384	.920	2.574	.313	.312	.322	1.639	3.553	158.9
75	.4	26	2,400	-.777	.344	.879	.247	.276	.293	.198	2.316	156.1
	.6	27	2,400	-.804	.240	.877	.322	.272	.336	.087	1.795	163.4
	.8	28	2,400	-1.034	.338	1.126	.317	.327	.352	.403	2.054	161.9
	1.3	29	2,400	-1.553	.416	1.649	.363	.375	.369	.615	2.852	165.0
	2.3	30	2,392	-2.051	.727	2.198	.410	.314	.412	1.050	3.205	160.5
	3.3	31	2,400	-1.950	.676	2.074	.278	.224	.291	1.281	2.837	160.9
	5.3	32	2,389	-2.284	.977	2.502	.274	.301	.274	1.700	3.408	156.9
76	.4	33	2,400	-.517	.225	.603	.276	.212	.274	.018	1.389	156.5
	.6	34	2,400	-.688	.322	.808	.403	.228	.372	.185	2.209	154.9
	.8	35	2,400	-.829	.347	.936	.419	.232	.400	.262	2.792	157.3
	1.3	36	2,386	-1.155	.429	1.273	.361	.316	.359	.468	2.262	159.6
	2.3	37	2,400	-1.844	.650	1.976	.388	.313	.405	1.046	3.057	160.6
	3.3	38	2,400	-2.042	.927	2.260	.274	.299	.294	1.308	2.961	155.6
	5.3	39	2,400	-2.263	.992	2.485	.275	.287	.294	1.730	3.292	156.3
77	.4	40	2,390	-.994	.459	1.135	.344	.290	.335	.319	2.101	155.2
	.6	41	2,374	-1.204	.434	1.312	.370	.319	.395	.416	2.457	160.2
	.8	42	2,400	-1.389	.431	1.486	.417	.289	.405	.482	2.748	162.8
	1.3	43	2,392	-1.147	.338	1.216	.496	.260	.515	.187	2.617	163.6
	2.3	44	2,400	-1.195	.354	1.258	.192	.170	.192	.633	1.776	163.5
	3.3	45	2,400	-1.377	.459	1.463	.235	.206	.256	.740	2.208	161.6
	5.3	46	2,383	-1.632	.547	1.734	.373	.271	.410	.654	2.983	161.5

Table A-1. Two-component velocity data for 1,820 cubic feet per second flow condition—*Continued*

Profile	y (ft)	FILE	n	$\bar{u}$ (ft/s)	$\bar{v}$ (ft/s)	$\bar{U}$ (ft/s)	RMS u (ft/s)	RMS v (ft/s)	RMS U (ft/s)	MIN U (ft/s)	MAX U (ft/s)	ϕ
78	0.4	47	2,400	-0.683	0.366	0.825	0.288	0.294	0.296	0.149	2.266	151.8
	.6	48	2,400	-.748	.398	.877	.265	.253	.290	.166	1.703	152.0
	.8	49	2,400	-.825	.377	.937	.225	.260	.250	.278	1.896	155.4
	1.3	50	2,400	-.858	.370	.956	.200	.232	.228	.478	1.727	156.7
	2.3	51	2,400	-1.132	.376	1.210	.192	.211	.202	.666	1.814	161.7
	3.3	54	2,400	-1.968	.750	2.119	.259	.264	.288	1.129	2.957	159.1
	5.3	53	2,400	-2.246	1.050	2.491	.257	.283	.294	1.731	3.245	154.9
79	.4	55	2,400	-.263	.412	.659	.323	.452	.337	.014	1.928	122.5
	.6	56	2,400	-.537	.247	.881	.431	.641	.412	.018	2.137	155.3
	.8	57	2,400	-.624	.579	.981	.418	.512	.447	.028	2.258	137.2
	1.3	58	2,400	-1.105	.621	1.346	.387	.436	.367	.250	2.439	150.7
	2.3	59	2,400	-1.787	.622	1.912	.336	.275	.338	.779	3.310	160.8
	3.3	60	2,400	-1.878	.696	2.020	.311	.249	.301	1.305	3.006	159.7
	5.3	61	2,400	-2.441	1.035	2.664	.467	.286	.486	1.585	3.984	157.0
80	.4	63	2,375	.192	.112	.643	.325	.607	.331	.016	1.693	30.3
	.6	65	2,400	.135	.229	.443	.238	.338	.213	.000	1.341	59.5
	.8	66	2,400	-.004	.158	.553	.373	.481	.300	.000	1.606	91.6
	1.3	67	2,376	-.336	.270	.720	.399	.545	.352	.022	1.967	141.3
	2.3	69	2,400	-.749	.445	1.016	.453	.554	.489	.016	2.790	149.3
	3.3	70	2,381	-.902	.324	1.034	.504	.413	.523	.029	2.640	160.2
	5.3	71	2,400	-1.679	.657	1.837	.398	.356	.403	.442	2.970	158.6
81	.4	74	2,390	.039	-.336	.472	.309	.220	.189	.034	1.579	276.7
	.6	78	2,394	.138	-.163	.375	.259	.286	.233	.005	1.522	310.2
	.6	79	2,400	-.056	-.056	.354	.293	.266	.192	.000	1.143	225.5
	.8	80	2,400	-.052	.178	.447	.300	.394	.282	.011	1.676	106.4
	1.3	81	2,400	-.299	.149	.633	.556	.381	.407	.028	2.021	153.6
	2.3	82	2,373	-.507	.318	.713	.441	.392	.445	.010	2.291	147.9
	3.3	83	2,400	-1.054	.383	1.188	.470	.423	.494	.069	2.428	160.0
	5.3	84	2,400	-.983	.381	1.154	.565	.463	.558	.015	2.472	158.8

Table A-2. Two-component velocity data for 2,230 cubic feet per second flow condition

Profile	*y* (ft)	FILE	*n*	*u* (ft/s)	*v* (ft/s)	*U* (ft/s)	RMS *u* (ft/s)	RMS *v* (ft/s)	RMS *U* (ft/s)	MIN *U* (ft/s)	MAX *U* (ft/s)	ϕ	*u'v'* (ft/s)
1	0.4	12	2,400	-0.837	0.047	0.856	0.184	0.171	0.183	0.454	1.335	176.8	-0.002
	.6	14	2,389	-1.020	.043	1.039	.202	.191	.200	.507	1.585	177.6	-.012
	.8	15	2,400	-1.055	.113	1.068	.181	.123	.182	.608	1.509	173.9	-.003
	1.3	16	2,400	-1.158	.260	1.202	.154	.186	.152	.800	1.811	167.4	.007
	2.3	17	2,400	-1.080	.379	1.153	.124	.160	.144	.746	1.602	160.6	-.006
	4.3	18	2,400	-1.137	.477	1.242	.170	.155	.176	.840	1.907	157.2	-.004
2	.4	19	2,400	-1.125	-.052	1.137	.159	.159	.156	.690	1.718	182.7	-.008
	.6	20	2,400	-1.191	.059	1.208	.187	.192	.188	.665	1.943	177.2	-.004
	.8	21	2,400	-1.167	.140	1.185	.181	.149	.179	.684	1.683	173.2	.001
	1.3	22	1,508	-1.268	.257	1.327	.301	.246	.254	.413	3.220	168.5	.013
	2.3	23	2,400	-1.130	.232	1.170	.194	.189	.191	.403	1.632	168.4	-.002
	4.3	25	2,400	-1.379	.758	1.580	.127	.162	.150	1.147	2.032	151.2	-.005
3	.4	26	2,400	-1.001	.197	1.043	.272	.232	.286	.191	1.958	168.9	-.017
	.6	27	2,390	-1.155	.300	1.214	.249	.241	.267	.530	2.012	165.4	-.022
	.8	28	2,392	-1.258	.393	1.344	.301	.286	.323	.578	2.242	162.6	-.012
	1.3	29	2,386	-1.432	.689	1.610	.384	.324	.433	.621	2.699	154.3	-.057
	2.3	30	2,400	-1.545	.829	1.770	.277	.282	.315	.835	2.603	151.8	-.029
	4.3	32	2,400	-1.502	.745	1.683	.138	.165	.161	1.237	2.179	153.6	-.007
4	.4	33	2,382	-1.267	-.037	1.289	.324	.233	.324	.500	2.277	181.7	.016
	.6	34	2,400	-1.401	.256	1.468	.368	.366	.378	.558	2.417	169.7	.010
	.8	36	2,391	-1.713	.409	1.787	.417	.317	.427	.859	3.090	166.6	-.017
	1.3	37	2,393	-1.359	.434	1.450	.368	.265	.373	.510	2.393	162.3	-.009
	2.3	38	1,058	-1.656	.586	1.773	.193	.258	.213	1.175	2.240	160.5	-.007
	4.3	40	2,400	-2.066	.892	2.265	.253	.280	.282	1.215	3.181	156.6	-.017

Table A-2. Two-component velocity data for 2,230 cubic feet per second flow condition—*Continued*

Profile	y (ft)	FILE	n	u (ft/s)	v (ft/s)	U (ft/s)	RMS u (ft/s)	RMS v (ft/s)	RMS U (ft/s)	MIN U (ft/s)	MAX U (ft/s)	ϕ	u'v' (ft/s)
5	0.4	41	2,393	-1.835	0.294	1.881	0.374	0.283	0.368	0.871	2.980	170.9	0.004
	.6	42	2,400	-1.893	.406	1.953	.377	.262	.378	1.071	3.295	167.9	-.016
	.8	43	2,400	-2.168	.557	2.268	.434	.337	.406	1.200	3.452	165.6	.017
	1.3	44	2,400	-1.989	.736	2.151	.435	.336	.416	1.234	3.276	159.7	.014
	2.3	45	2,400	-2.213	.805	2.371	.232	.292	.247	1.519	3.089	160.0	-.005
	4.3	46	2,400	-2.462	1.007	2.682	.299	.391	.347	1.850	3.768	157.8	-.028
6	.4	47	2,400	-1.341	.425	1.425	.330	.264	.359	.524	2.416	162.4	-.041
	.6	49	2,400	-1.755	.341	1.823	.400	.377	.418	.803	2.932	169.0	-.047
	.8	50	2,376	-2.006	.469	2.085	.494	.336	.506	.735	3.540	166.9	-.058
	1.3	51	2,400	-1.829	.491	1.918	.451	.310	.454	.859	3.310	165.0	-.021
	2.3	52	2,393	-1.811	.521	1.907	.314	.292	.309	1.105	2.852	164.0	.006
	4.3	54	2,400	-2.868	1.039	3.070	.365	.389	.407	1.903	4.121	160.1	-.040
7	.4	56	2,381	-1.004	.021	1.039	.325	.275	.331	.309	2.505	178.8	-.013
	.6	57	2,400	-1.308	-.002	1.335	.404	.265	.402	.283	2.541	180.1	-.012
	.8	59	2,400	-1.699	.248	1.756	.312	.360	.308	1.071	2.788	171.7	.009
	1.3	61	2,400	-2.300	.319	2.349	.462	.358	.461	1.026	3.549	172.1	-.004
	2.3	62	2,400	-2.012	.727	2.163	.345	.373	.398	1.127	3.388	160.1	-.048
	4.3	63	2,400	-2.318	.889	2.510	.362	.401	.392	1.446	3.706	159.0	-.021
8	.4	64	2,400	-1.438	.036	1.496	.379	.439	.409	.441	2.685	178.6	-.039
	.6	65	2,400	-1.633	-.078	1.672	.312	.354	.314	.745	2.695	182.7	-.011
	.8	66	2,400	-1.661	.090	1.715	.342	.415	.339	.800	2.811	176.9	-.012
	1.3	67	2,400	-1.696	.234	1.767	.418	.452	.436	.734	2.843	172.1	-.023
	2.3	68	2,387	-1.767	.383	1.833	.469	.335	.490	.674	3.513	167.8	-.054
	4.3	71	2,400	-1.907	.765	2.070	.316	.271	.330	.875	2.947	158.2	-.017

Table A-2. Two-component velocity data for 2,230 cubic feet per second flow condition—*Continued*

Profile	*y* (ft)	FILE	*n*	*u* (ft/s)	*v* (ft/s)	*U* (ft/s)	RMS *u* (ft/s)	RMS *v* (ft/s)	RMS *U* (ft/s)	MIN *U* (ft/s)	MAX *U* (ft/s)	ϕ	*u'v'* (ft/s)
9	0.4	72	2,392	-1.215	0.211	1.260	0.269	0.245	0.255	0.333	2.013	170.2	0.016
	.6	73	2,400	-1.321	.194	1.362	.234	.272	.236	.699	2.097	171.6	.003
	.8	74	2,400	-1.593	.252	1.630	.264	.244	.265	.944	2.343	171.0	.004
	1.3	76	2,386	-1.737	.375	1.788	.283	.208	.289	1.140	2.663	167.8	-.011
	2.3	77	2,396	-1.899	.620	2.016	.335	.267	.332	1.249	2.892	161.9	-.002
	4.3	78	2,400	-1.703	.824	1.911	.242	.296	.273	1.059	2.697	154.2	-.011
10	.4	79	2,400	-1.229	.488	1.346	.384	.251	.384	.093	2.102	158.3	-.023
	.6	80	2,003	-1.067	.293	1.239	.558	.491	.491	.035	5.584	164.6	.021
	.8	81	2,400	-.924	-.117	.964	.257	.242	.251	.278	1.636	187.2	.001
	1.3	82	2,400	-1.339	.191	1.381	.334	.271	.327	.498	2.222	171.9	-.008
	2.3	83	2,400	-1.796	.368	1.847	.303	.210	.293	1.102	2.961	168.4	.010
	4.3	84	2,394	-1.699	.576	1.806	.342	.222	.352	1.043	2.781	161.3	-.024
		85	2,387	-1.811	.722	1.967	.262	.235	.243	1.239	2.779	158.3	.009
11	.4	0	2,394	-.668	.507	.870	.219	.262	.252	.235	1.707	142.8	-.011
	.6	1	2,400	-1.077	.399	1.190	.273	.325	.288	.443	2.110	159.7	-.005
	.8	2	2,389	-.974	.510	1.137	.209	.318	.243	.453	1.963	152.4	-.009
	1.3	3	2,164	-.997	.411	1.095	.279	.212	.291	.392	1.822	157.6	-.022
	2.3	4	2,400	-1.056	.630	1.252	.261	.273	.295	.594	2.111	149.2	-.020
	4.3	5	2,400	-1.160	.703	1.369	.196	.216	.225	.577	1.953	148.8	-.013
12	.4	6	2,400	-.869	.280	.966	.236	.351	.284	.394	2.075	162.2	-.013
	.6	7	2,400	-.934	.411	1.046	.279	.250	.297	.269	1.948	156.3	-.018
	.8	8	2,400	-1.082	.267	1.153	.320	.290	.313	.502	1.934	166.2	.006
	1.3	9	2,400	-1.084	.374	1.179	.235	.310	.278	.506	1.811	161.0	-.027
	2.3	10	2,400	-1.263	.505	1.375	.240	.211	.246	.408	1.992	158.2	-.007
	4.3	11	2,400	-1.263	.672	1.438	.173	.147	.177	1.066	2.125	152.0	-.005

Table A-2. Two-component velocity data for 2,230 cubic feet per second flow condition—*Continued*

Profile	*y* (ft)	FILE	*n*	*u* (ft/s)	*v* (ft/s)	*U* (ft/s)	RMS *u* (ft/s)	RMS *v* (ft/s)	RMS *U* (ft/s)	MIN *U* (ft/s)	MAX *U* (ft/s)	ϕ	*u'v'* (ft/s)
13	0.4	12	2,373	-0.702	0.273	0.794	0.268	0.246	0.263	0.139	1.489	158.7	-0.001
	.6	13	1,757	-1.026	.174	1.085	.297	.307	.295	.353	2.013	170.4	.002
	.8	15	2,400	-.991	.279	1.077	.254	.313	.251	.322	1.802	164.3	.006
	1.3	16	2,390	-.846	.246	.922	.248	.272	.247	.316	1.711	163.8	-.005
	2.3	17	2,400	-1.404	.316	1.473	.370	.290	.347	.655	2.376	167.3	.026
	4.3	19	2,400	-1.458	.728	1.640	.189	.187	.194	1.020	2.466	153.5	-.003
14	.4	21	2,306	-1.534	-.441	1.629	.324	.332	.329	.712	3.175	196.1	.007
	.6	22	2,157	-1.802	-.614	1.927	.269	.289	.262	1.021	2.512	198.8	-.009
	.8	24	2,400	-1.743	-.508	1.842	.325	.290	.303	.862	2.902	196.3	-.015
	1.3	25	2,390	-1.776	-.478	1.866	.311	.307	.303	1.036	2.757	195.1	-.008
	2.3	26	2,352	-1.945	-.294	1.981	.279	.234	.280	1.253	2.751	188.6	.007
	4.3	29	2,400	-2.272	-.225	2.294	.221	.221	.221	1.457	2.872	185.7	.006
15	.4	30	2,390	-1.443	-.333	1.519	.277	.324	.258	.980	2.426	193.0	-.019
	.6	31	2,400	-1.462	-.327	1.525	.253	.279	.246	.743	2.241	192.6	-.008
	.8	32	2,390	-1.601	-.237	1.638	.236	.243	.224	.998	2.293	188.4	-.013
	1.3	33	2,400	-1.630	-.208	1.654	.210	.190	.206	1.145	2.292	187.3	-.004
	2.3	34	2,400	-1.710	.184	1.731	.279	.195	.279	1.087	2.622	173.9	-.005
	4.3	35	2,389	-1.923	-.051	1.932	.180	.192	.184	1.217	2.557	181.5	.010
16	.4	36	1,143	-.962	-.437	1.093	.217	.257	.186	.677	1.703	204.4	-.019
	.6	37	2,400	-1.339	-.313	1.405	.218	.294	.227	.858	2.279	193.1	.005
	.8	38	2,400	-1.182	-.022	1.202	.249	.212	.248	.389	1.852	181.1	-.006
	1.3	39	2,388	-1.449	-.008	1.473	.253	.268	.256	.906	2.405	180.3	-.003
	2.3	40	1,525	-2.042	.322	2.085	.248	.281	.257	1.377	2.803	171.1	-.018
	4.3	41	2,388	-1.662	.468	1.740	.191	.213	.189	1.304	2.458	164.3	.002

Table A-2. Two-component velocity data for 2,230 cubic feet per second flow condition—*Continued*

Profile	*y* (ft)	FILE	*n*	*u* (ft/s)	*v* (ft/s)	*U* (ft/s)	RMS *u* (ft/s)	RMS *v* (ft/s)	RMS *U* (ft/s)	MIN *U* (ft/s)	MAX *U* (ft/s)	φ	*u'v'* (ft/s)
17	0.4	42	2,400	-1.128	-0.278	1.190	0.371	0.280	0.388	0.405	2.738	193.8	0.033
	.6	44	2,357	-2.424	.372	2.472	.371	.300	.358	1.502	3.408	171.3	.027
	.8	45	2,393	-2.341	.300	2.378	.376	.292	.378	1.556	3.720	172.7	.002
	1.3	46	2,308	-1.959	.268	1.988	.272	.222	.284	1.358	2.792	172.2	-.025
	2.3	47	2,387	-1.964	.420	2.017	.186	.183	.191	1.333	2.509	167.9	-.004
	4.3	48	2,400	-3.088	1.209	3.325	.439	.211	.422	2.156	4.333	158.6	-.006
18	.4	49	2,400	-1.613	.103	1.638	.305	.262	.302	.806	2.416	176.4	-.001
	.6	50	2,395	-1.994	.188	2.030	.297	.322	.293	.945	2.882	174.6	-.008
	.8	51	2,400	-2.020	.162	2.045	.364	.287	.370	1.029	2.886	175.4	-.033
	1.3	52	2,381	-1.560	.192	1.584	.225	.214	.236	.813	2.631	173.0	-.017
	2.3	53	2,400	-2.701	.818	2.837	.318	.276	.302	1.930	3.614	163.2	.015
	4.3	55	794	-3.094	.821	3.216	.213	.304	.210	2.568	3.685	165.1	.010
19	.4	56	2,348	-1.418	-.390	1.506	.416	.326	.419	.236	2.628	195.4	.013
	.6	58	2,334	-1.911	-.298	1.960	.367	.315	.363	1.115	3.105	188.9	.008
	.8	59	2,400	-1.678	-.026	1.698	.293	.263	.296	1.013	2.481	180.9	.003
	1.3	60	2,400	-1.669	.123	1.696	.224	.275	.224	.890	2.386	175.8	-.006
	2.3	62	2,384	-2.206	.675	2.323	.275	.290	.295	1.545	3.347	163.0	-.021
	4.3	63	2,400	-2.244	.942	2.443	.183	.223	.195	1.847	3.189	157.2	-.002
20	.4	64	2,385	-.509	-.021	.537	.197	.161	.189	.142	1.293	182.3	-.009
	.6	65	2,299	-1.241	-.139	1.269	.250	.234	.259	.332	2.131	186.4	.027
	.8	66	2,268	-1.291	-.013	1.386	.452	.325	.235	.458	2.483	180.6	.013
	1.3	67	2,400	-1.697	.171	1.725	.298	.259	.297	.917	2.654	174.2	.004
	2.3	68	2,400	-2.060	.566	2.153	.310	.300	.338	1.294	3.306	164.6	-.034
	4.3	69	2,395	-2.381	.878	2.553	.263	.291	.273	1.360	3.765	159.8	-.004

Table A-2. Two-component velocity data for 2,230 cubic feet per second flow condition—*Continued*

Profile	*y* (ft)	FILE	*n*	*u* (ft/s)	*v* (ft/s)	*U* (ft/s)	RMS *u* (ft/s)	RMS *v* (ft/s)	RMS *U* (ft/s)	MIN *U* (ft/s)	MAX *U* (ft/s)	ϕ	*u'v'* (ft/s)
21	0.4	70	2,400	-0.726	0.822	1.115	0.270	0.323	0.370	0.117	2.472	131.4	-0.050
	.6	71	2,393	-.785	.815	1.153	.259	.314	.342	.308	2.382	133.9	-.039
	.8	73	2,400	-.589	.485	.819	.256	.338	.302	.068	2.199	140.5	-.021
	1.3	74	2,400	-1.703	.475	1.813	.477	.443	.511	.329	3.296	164.4	-.094
	2.3	75	2,400	-2.542	.950	2.728	.309	.284	.314	1.725	3.596	159.5	-.010
	4.3	76	2,395	-2.559	1.209	2.839	.241	.287	.294	2.123	3.594	154.7	-.030
22	.4	0	2,400	-.595	.989	1.167	.178	.199	.207	.596	1.918	121.0	-.006
	.6	1	2,380	-.796	.886	1.215	.252	.245	.255	.583	2.015	131.9	-.001
	.8	2	2,393	-.817	.798	1.157	.169	.242	.230	.645	1.963	135.7	-.009
	1.3	3	2,400	-1.025	1.307	1.674	.174	.259	.226	1.133	2.365	128.1	.002
	2.3	4	2,400	-1.215	1.415	1.882	.241	.378	.372	.898	2.835	130.7	-.034
	4.3	5	2,395	-1.354	1.733	2.205	.157	.196	.188	1.571	2.871	128.0	-.002
23	.4	6	2,400	-.027	.342	.403	.191	.180	.156	.007	.823	94.5	.013
	.6	7	2,400	-.405	.730	.863	.215	.273	.269	.041	1.705	119.0	-.015
	.8	8	2,381	-.868	.903	1.274	.251	.308	.322	.287	2.356	133.9	-.029
	1.3	9	2,393	-1.199	.681	1.406	.236	.282	.243	.601	2.095	150.4	.000
	2.3	10	2,386	-1.068	.838	1.365	.161	.159	.175	.824	1.932	141.9	-.005
	4.3	11	2,383	-1.263	1.048	1.650	.165	.158	.158	1.007	2.125	140.3	.001
24	.4	12	2,400	-.540	.388	.734	.344	.221	.264	.087	1.623	144.3	.026
	.6	13	2,400	-.561	.331	.710	.338	.183	.259	.183	1.562	149.5	.027
	.8	14	2,400	-.606	.601	.914	.373	.263	.319	.186	2.177	135.2	.019
	1.3	15	2,400	-1.349	.759	1.573	.242	.291	.256	.754	2.292	150.7	.003
	2.3	16	2,395	-1.385	.967	1.704	.193	.270	.240	1.007	2.319	145.1	-.007

Table A-2. Two-component velocity data for 2,230 cubic feet per second flow condition—*Continued*

Profile	*y* (ft)	FILE	*n*	*u* (ft/s)	*v* (ft/s)	*U* (ft/s)	RMS *u* (ft/s)	RMS *v* (ft/s)	RMS *U* (ft/s)	MIN *U* (ft/s)	MAX *U* (ft/s)	φ	*u'v'* (ft/s)
25	0.4	19	2,384	-1.292	1.314	1.854	0.187	0.206	0.191	1.307	2.586	134.5	0.002
	.6	20	2,383	-1.511	1.319	2.019	.181	.259	.219	1.417	2.548	138.9	-.000
	.8	21	2,400	-1.441	1.286	1.941	.206	.223	.234	1.331	2.686	138.2	-.009
	1.3	22	2,389	-1.465	1.365	2.015	.237	.234	.242	1.188	2.686	137.0	-.003
	2.3	23	2,400	-1.709	1.576	2.330	.223	.201	.255	1.649	3.066	137.3	-.020
	4.3	25	2,400	-1.864	1.754	2.566	.176	.240	.235	1.830	3.213	136.7	-.012
26	.4	26	2,395	-.092	.639	.685	.241	.155	.170	.187	1.274	98.2	-.005
	.6	27	2,400	-.756	1.196	1.432	.239	.230	.253	.787	2.063	122.3	-.009
	.8	28	2,400	-1.456	1.335	1.992	.250	.363	.361	1.225	3.213	137.5	-.034
	1.3	29	2,400	-1.444	.995	1.766	.140	.250	.196	1.100	2.317	145.5	-.006
	2.3	32	2,400	-1.798	1.190	2.168	.266	.271	.309	1.552	3.009	146.5	-.026
	4.3	33	2,400	-2.149	1.461	2.612	.234	.327	.310	1.867	3.724	145.8	-.024
27	.4	34	2,400	-1.606	.827	1.829	.282	.283	.282	1.106	2.827	152.8	.000
	.6	35	2,400	-1.809	.767	1.982	.307	.228	.278	1.294	2.788	157.0	.011
	.8	36	2,400	-1.836	.772	2.007	.279	.248	.277	1.167	3.004	157.2	.001
	1.3	37	2,400	-1.988	.815	2.166	.212	.271	.203	1.538	2.770	157.7	.013
	2.3	38	2,400	-2.138	.988	2.370	.247	.274	.262	1.735	3.144	155.2	-.005
	4.3	39	2,400	-2.008	1.155	2.331	.175	.301	.235	1.773	3.071	150.1	-.010
28	.4	40	2,390	-1.712	.570	1.819	.309	.236	.312	.993	2.691	161.6	-.011
	.6	41	2,400	-1.812	.528	1.906	.263	.264	.262	1.050	2.767	163.8	.008
	.8	44	2,345	-1.341	.456	1.431	.212	.227	.237	.808	2.233	161.2	-.017
	1.3	45	2,395	-1.379	.287	1.421	.215	.191	.218	.921	2.218	168.3	-.004
	2.3	47	2,400	-2.191	.780	2.341	.242	.285	.267	1.421	3.162	160.4	-.015
	4.3	50	2,400	-1.939	1.007	2.197	.166	.237	.174	1.741	2.778	152.6	.005

Table A-2. Two-component velocity data for 2,230 cubic feet per second flow condition—*Continued*

Profile	y (ft)	FILE	n	u (ft/s)	v (ft/s)	U (ft/s)	RMS u (ft/s)	RMS v (ft/s)	RMS U (ft/s)	MIN U (ft/s)	MAX U (ft/s)	ϕ	$u'v'$ (ft/s)
29	0.4	51	2,395	-0.650	0.558	0.880	0.223	0.281	0.298	0.029	1.681	139.4	-0.035
	.6	52	2,400	-.704	.756	1.054	.271	.278	.326	.081	2.121	133.0	-.042
	.8	53	2,400	-1.144	.685	1.359	.361	.305	.391	.352	2.502	149.1	-.045
	1.3	54	2,400	-1.756	.136	1.781	.341	.262	.339	.930	2.640	175.6	-.007
	2.3	56	2,400	-1.835	.630	1.948	.199	.163	.195	1.388	2.634	161.1	.001
	4.3	57	2,400	-1.723	.870	1.938	.160	.198	.190	1.413	2.540	153.2	-.009
30	.4	58	2,392	-.935	.447	1.100	.559	.248	.487	.007	2.656	154.4	-.020
	.6	59	2,396	-1.291	.521	1.436	.514	.285	.470	.065	2.495	158.0	-.007
	.8	60	2,400	-1.744	.563	1.865	.536	.267	.489	.477	3.006	162.1	.018
	1.3	61	2,382	-2.443	.475	2.506	.348	.305	.358	1.407	3.820	169.0	-.031
	2.3	62	2,400	-2.710	.508	2.767	.347	.248	.361	1.954	3.881	169.4	-.035
	4.3	63	2,400	-1.980	.770	2.148	.611	.292	.595	.177	3.370	158.8	-.060
31	.4	64	2,400	-.674	-.514	.869	.248	.212	.265	.110	1.883	217.4	.020
	.6	65	2,355	-.384	-.191	.527	.291	.292	.276	.007	1.361	206.4	.017
	.8	66	2,400	-.519	.243	.711	.439	.386	.406	.000	2.261	155.0	.011
	1.3	67	2,400	-1.841	.593	1.966	.508	.343	.500	.188	3.338	162.2	-.035
	2.3	68	2,400	-2.333	.639	2.429	.300	.250	.323	1.611	3.241	164.7	-.032
	4.3	69	2,400	-2.535	.808	2.666	.286	.203	.305	1.901	3.566	162.3	-.025
32	.4	70	2,391	-.309	-.418	.739	.561	.373	.422	.031	2.321	233.5	.012
	.6	71	2,400	-.766	-.302	.945	.565	.375	.493	.031	2.797	201.5	.015
	.8	72	2,384	-1.020	-.281	1.165	.647	.388	.574	.028	3.022	195.4	.020
	1.3	73	2,384	-1.401	.037	1.470	.689	.350	.633	.000	2.972	178.5	-.055
	2.3	75	2,386	-2.098	.388	2.142	.301	.175	.290	1.099	3.041	169.5	.009
	4.3	76	2,400	-.272	-.088	.569	.422	.403	.313	.010	1.790	197.9	.041

Table A-2. Two-component velocity data for 2,230 cubic feet per second flow condition—*Continued*

Profile	*y* (ft)	FILE	*n*	*u* (ft/s)	*v* (ft/s)	*U* (ft/s)	RMS *u* (ft/s)	RMS *v* (ft/s)	RMS *U* (ft/s)	MIN *U* (ft/s)	MAX *U* (ft/s)	ϕ	*u'v'* (ft/s)
33	0.4	77	2,400	-0.806	-0.310	0.944	0.293	0.392	0.307	0.117	1.860	201.0	0.008
	.6	78	2,374	-.888	.044	.968	.432	.385	.435	.035	2.273	177.2	-.056
	.8	79	2,385	-1.016	.199	1.105	.480	.388	.481	.061	2.829	168.9	-.078
	1.3	80	2,400	-1.665	.413	1.739	.501	.290	.505	.341	2.936	166.1	-.061
	2.3	81	2,400	-2.284	.513	2.347	.299	.159	.296	1.510	3.334	167.3	-.002
	4.3	82	2,322	-2.163	.526	2.241	.383	.233	.366	.956	3.256	166.3	.004
34	.4	83	2,376	-1.824	-.127	1.844	.335	.233	.329	.875	2.872	184.0	-.016
	.6	84	2,382	-1.607	.035	1.621	.291	.209	.289	.620	2.299	178.7	-.010
	.8	85	2,400	-2.030	.221	2.061	.337	.288	.340	.826	3.390	173.8	-.013
	1.3	86	2,400	-1.991	.551	2.089	.279	.356	.328	1.393	3.369	164.5	-.034
	2.3	87	2,400	-2.115	.730	2.248	.204	.246	.234	1.643	3.005	161.0	-.017
	4.3	89	2,400	-2.453	.884	2.616	.247	.250	.282	1.934	3.695	160.2	-.026
35	.4	1	2,400	-.684	.111	.736	.264	.221	.239	.025	1.440	170.8	.015
	.6	2	2,400	-.772	.201	.844	.270	.274	.267	.161	1.678	165.4	.010
	.8	3	2,400	-.697	.233	.774	.270	.241	.267	.196	1.960	161.5	.000
	1.3	4	2,400	-1.031	.374	1.135	.376	.292	.378	.225	2.273	160.1	-.021
	2.3	5	2,400	-1.808	.635	1.929	.332	.202	.320	.579	2.778	160.7	-.007
	4.3	6	2,400	-1.518	.417	1.612	.492	.272	.441	.556	2.780	164.7	.028
36	.4	7	2,400	-.936	.226	.981	.334	.188	.335	.223	2.244	166.4	-.009
	.6	8	2,382	-1.787	.133	1.806	.296	.227	.299	.753	2.513	175.7	-.023
	.8	11	2,400	-1.781	.335	1.825	.242	.219	.249	1.078	2.575	169.3	-.008
	1.3	12	2,400	-1.969	.412	2.020	.206	.194	.209	1.374	2.512	168.2	-.003
	2.3	13	2,400	-1.924	.572	2.014	.141	.179	.149	1.597	2.490	163.4	-.002
	4.3	14	2,400	-2.072	.718	2.198	.108	.160	.121	1.820	2.690	160.9	-.002

Table A-2. Two-component velocity data for 2,230 cubic feet per second flow condition—*Continued*

Profile	*y* (ft)	FILE	*n*	*u* (ft/s)	*v* (ft/s)	*U* (ft/s)	RMS *u* (ft/s)	RMS *v* (ft/s)	RMS *U* (ft/s)	MIN *U* (ft/s)	MAX *U* (ft/s)	ϕ	*u'v'* (ft/s)
37	0.4	15	2,345	-1.550	0.384	1.602	0.158	0.147	0.168	1.045	2.007	166.1	-0.008
	.6	16	2,356	-1.442	.363	1.492	.174	.135	.176	.848	1.944	165.9	-.002
	.8	18	2,400	-2.043	.639	2.150	.189	.210	.194	1.212	2.628	162.6	-.002
	1.3	19	2,400	-1.886	.620	1.998	.256	.263	.289	1.396	2.673	161.8	-.033
	2.3	21	2,400	-2.017	.812	2.182	.186	.189	.194	1.617	2.871	158.1	-.003
	4.3	22	2,400	-2.018	.886	2.209	.148	.155	.158	1.760	2.801	156.3	-.004
38	.4	23	2,400	-.754	.194	.790	.183	.147	.191	.380	1.385	165.6	-.008
	.6	24	2,400	-1.352	.583	1.484	.255	.161	.240	.641	2.191	156.7	-.003
	.8	25	2,400	-1.457	.678	1.616	.214	.174	.218	.988	2.187	155.1	-.007
	1.3	26	2,393	-1.720	.785	1.895	.230	.163	.248	.843	2.529	155.5	-.019
	2.3	28	2,394	-1.839	.637	1.953	.160	.181	.174	1.348	2.501	160.9	-.008
	4.3	29	2,400	-1.748	.694	1.884	.096	.106	.097	1.619	2.204	158.3	.000
39	.4	31	2,400	-.482	.086	.504	.176	.099	.162	.055	.963	169.9	.006
	.6	33	2,400	-.109	-.156	.227	.133	.092	.104	.000	.694	235.2	-.001
	.8	34	2,400	-.143	.036	.210	.147	.120	.116	.011	.664	166.0	.006
	1.3	35	2,400	-1.510	.302	1.552	.278	.223	.297	.549	2.305	168.7	-.037
	2.3	36	2,400	-1.640	.566	1.741	.153	.161	.173	1.242	2.178	161.0	-.012
	4.3	37	2,400	-1.983	.711	2.112	.165	.151	.165	1.655	2.760	160.3	-.000
40	.4	38	2,400	-1.646	.277	1.695	.339	.299	.343	.728	2.629	170.4	-.011
	.6	39	2,400	-1.604	.371	1.660	.278	.218	.283	.684	2.365	167.0	-.017
	.8	40	2,400	-1.779	.530	1.862	.164	.161	.176	1.217	2.300	163.4	-.008
	1.3	41	2,400	-1.719	.438	1.779	.187	.141	.192	1.177	2.261	165.7	-.006
	2.3	42	2,392	-1.763	.546	1.849	.165	.134	.177	1.070	2.296	162.8	-.009
	4.3	43	2,400	-1.887	.683	2.011	.161	.123	.166	1.505	2.561	160.1	-.005
		44	2,400	-1.896	.643	2.008	.128	.161	.134	1.639	2.467	161.3	-.001

Table A-2. Two-component velocity data for 2,230 cubic feet per second flow condition—*Continued*

Profile	*y* (ft)	FILE	*n*	*u* (ft/s)	*v* (ft/s)	*U* (ft/s)	RMS *u* (ft/s)	RMS *v* (ft/s)	RMS *U* (ft/s)	MIN *U* (ft/s)	MAX *U* (ft/s)	φ	*u'v'* (ft/s)
41	0.4	45	2,400	-0.961	0.424	1.067	0.249	0.200	0.256	0.472	1.807	156.2	-0.012
	.6	46	2,400	-1.122	.407	1.211	.302	.218	.311	.387	2.204	160.1	-.021
	.8	47	2,400	-1.396	.488	1.495	.322	.241	.339	.647	2.535	160.7	-.030
	1.3	48	2,379	-1.214	.316	1.272	.250	.218	.257	.413	1.946	165.4	-.011
	2.3	49	2,400	-1.730	.608	1.843	.312	.193	.317	1.070	2.663	160.6	-.017
	4.3	50	2,383	-1.932	.728	2.071	.219	.175	.228	1.309	2.991	159.4	-.009
42	.4	51	2,400	-.941	.297	1.006	.313	.231	.336	.377	2.120	162.5	-.036
	.6	52	2,394	-1.227	.373	1.300	.277	.229	.290	.587	2.086	163.1	-.014
	.8	53	2,384	-1.071	.414	1.158	.329	.215	.362	.488	2.171	158.9	-.045
	1.3	55	2,394	-1.083	.412	1.170	.275	.205	.303	.447	2.051	159.2	-.031
	2.3	56	2,400	-1.205	.426	1.285	.275	.154	.284	.454	2.048	160.5	-.018
	4.3	57	2,400	-1.754	.655	1.878	.275	.176	.293	1.058	2.710	159.5	-.023
43	.4	58	2,400	-.431	.254	.528	.124	.164	.119	.259	.930	149.5	.007
	.6	59	2,400	-.521	.443	.703	.175	.148	.161	.226	1.408	139.6	.002
	.8	61	2,382	-1.487	.518	1.603	.228	.293	.222	.916	2.354	160.8	.005
	1.3	62	2,390	-1.278	1.017	1.654	.309	.295	.340	.840	2.700	141.5	-.023
	2.3	63	2,400	-1.278	.767	1.502	.306	.138	.279	.751	2.380	149.0	-.005
	4.3	64	2,400	-1.530	1.155	1.925	.277	.198	.293	1.121	2.559	143.0	-.024
44	.4	65	2,400	-1.412	.431	1.491	.295	.216	.299	.574	2.462	163.0	-.010
	.6	66	2,400	-1.545	.466	1.633	.348	.250	.351	.741	2.494	163.2	-.011
	.8	67	2,400	-1.646	.505	1.736	.328	.217	.324	.879	2.656	163.0	-.007
	1.3	68	2,400	-1.901	.514	1.984	.346	.253	.356	.969	3.138	164.9	-.021
	2.3	69	2,400	-2.301	.637	2.400	.413	.276	.430	1.380	3.590	164.5	-.043
	4.3	70	2,400	-2.333	.795	2.475	.304	.211	.294	1.567	3.509	161.2	-.001

Table A-2. Two-component velocity data for 2,230 cubic feet per second flow condition—*Continued*

Profile	*y* (ft)	FILE	*n*	*u* (ft/s)	*v* (ft/s)	*U* (ft/s)	RMS *u* (ft/s)	RMS *v* (ft/s)	RMS *U* (ft/s)	MIN *U* (ft/s)	MAX *U* (ft/s)	ϕ	*u'v'* (ft/s)
45	0.4	71	2,400	-1.211	0.470	1.320	0.306	0.233	0.303	0.713	2.542	158.8	0.002
	.6	72	2,400	-1.408	.517	1.518	.263	.231	.259	.800	2.174	159.8	.002
	.8	73	2,400	-1.521	.488	1.621	.336	.283	.343	.862	2.628	162.2	-.013
	1.3	74	2,400	-1.870	.599	1.978	.302	.235	.300	1.202	2.865	162.2	-.003
	2.3	75	2,377	-2.072	.624	2.173	.263	.203	.269	1.341	3.052	163.2	-.010
	4.3	77	2,400	-2.292	.870	2.460	.285	.213	.289	1.268	3.362	159.2	-.010
46	.4	0	2,400	-.016	-.101	.148	.106	.068	.067	.005	.403	260.8	-.000
	.6	1	2,400	.064	-.208	.249	.125	.102	.107	.005	.543	287.0	-.004
	.8	2	2,400	.161	-.305	.372	.151	.159	.169	.007	.901	297.8	-.011
	1.3	3	2,400	.245	-.305	.440	.212	.182	.194	.005	1.218	308.8	-.021
	2.3	4	2,386	.254	-.186	.402	.227	.250	.226	.010	1.321	323.8	-.014
	4.3	5	2,366	-.076	-.124	.476	.355	.420	.312	.015	2.114	238.3	-.055
47	.4	6	2,400	-1.064	-.261	1.337	.859	.549	.671	.025	3.566	193.8	-.248
	.6	7	2,400	-.755	-.216	1.180	.942	.569	.660	.021	3.186	196.0	-.334
	.8	8	2,400	-2.160	.027	2.280	.916	.608	.824	.397	4.542	179.3	-.301
	1.3	9	2,400	-2.562	.210	2.629	.663	.519	.637	.146	4.339	175.3	-.116
	2.3	10	2,400	-3.078	.857	3.207	.437	.267	.428	2.053	4.674	164.4	-.002
	4.3	11	2,400	-3.376	1.048	3.558	.436	.370	.405	2.423	4.818	162.8	.037
48	.4	12	2,400	.586	-.383	.751	.274	.277	.279	.005	2.980	326.9	.001
	.6	13	2,394	.723	-.399	.854	.215	.232	.232	.229	1.447	331.1	-.012
	.8	14	2,400	.663	-.341	.782	.206	.258	.233	.074	1.511	332.8	-.014
	1.3	15	2,400	.647	-.385	.783	.271	.223	.276	.015	1.741	329.2	-.017
	2.3	16	2,291	.673	-.376	.828	.297	.282	.278	.054	1.466	330.8	-.012
	4.3	17	2,400	-1.295	.714	1.641	.757	.716	.761	.081	3.253	151.1	-.306

Table A-2. Two-component velocity data for 2,230 cubic feet per second flow condition—*Continued*

Profile	*y* (ft)	FILE	*n*	*u* (ft/s)	*v* (ft/s)	*U* (ft/s)	RMS *u* (ft/s)	RMS *v* (ft/s)	RMS *U* (ft/s)	MIN *U* (ft/s)	MAX *U* (ft/s)	ϕ	*u'v'* (ft/s)
49	0.4	18	1,397	0.125	-0.067	0.332	0.298	0.177	0.174	0.000	1.194	331.8	0.007
	.6	19	2,400	.220	-.085	.410	.329	.235	.226	.005	1.183	338.8	.029
	.8	20	2,357	.504	-.286	.658	.332	.266	.290	.025	1.855	330.4	-.000
	1.3	21	2,400	.649	-.369	.839	.408	.319	.350	.033	1.861	330.4	-.019
	2.3	22	2,400	.201	-.290	.784	.512	.604	.371	.022	2.079	304.7	-.090
	4.3	23	2,400	-2.450	.963	2.659	.438	.426	.480	.673	4.371	158.5	-.084
50	.4	24	2,400	-1.473	.205	1.574	.626	.468	.588	.112	3.437	172.1	-.101
	.6	25	2,400	-1.598	-.040	1.768	.769	.624	.643	.122	3.201	181.4	-.161
	.8	26	2,392	-1.766	-.221	1.950	.981	.605	.832	.064	4.193	187.1	-.280
	1.3	27	2,400	-2.002	-.194	2.160	1.002	.586	.852	.014	4.093	185.5	-.264
	2.3	28	2,392	-3.018	.362	3.080	.553	.464	.524	1.690	4.609	173.2	.057
	4.3	29	2,400	-3.279	.823	3.396	.517	.300	.503	2.359	4.899	165.9	.015
51	.4	30	2,400	.890	-.507	1.034	.217	.161	.230	.328	1.710	330.3	-.014
	.6	31	2,400	.699	-.434	.875	.297	.219	.218	.246	1.514	328.2	.018
	.8	32	2,400	.743	-.408	.864	.231	.157	.223	.273	1.500	331.2	-.008
	1.3	33	2,400	.878	-.411	1.004	.249	.245	.235	.306	1.821	334.9	-.003
	2.3	34	2,400	.733	-.491	.916	.244	.261	.258	.000	1.666	326.2	-.011
	4.3	35	2,400	-.950	.442	1.260	.832	.631	.775	.010	3.782	155.1	-.227
52	.4	36	2,400	-.039	.317	.507	.354	.349	.304	.005	1.754	97.0	-.039
	.6	37	2,400	-.050	.343	.714	.483	.569	.409	.026	2.425	98.3	-.092
	.8	38	2,389	-.120	.273	.800	.572	.651	.447	.010	2.514	113.8	-.128
	1.3	39	2,400	-.554	.334	1.002	.586	.703	.504	.035	3.250	149.0	-.173
	2.3	40	2,400	-.920	.148	1.309	.872	.803	.748	.025	3.975	170.8	-.361
	4.3	41	2,400	-2.568	.823	2.718	.456	.333	.453	1.729	4.262	162.2	-.010

Table A-2. Two-component velocity data for 2,230 cubic feet per second flow condition—*Continued*

Profile	y (ft)	FILE	n	u (ft/s)	v (ft/s)	U (ft/s)	RMS u (ft/s)	RMS v (ft/s)	RMS U (ft/s)	MIN U (ft/s)	MAX U (ft/s)	φ	u'v' (ft/s)
53	0.4	42	2,400	-0.610	0.011	0.684	0.335	0.309	0.335	0.021	3.257	179.0	-0.012
	.6	44	2,400	-1.034	.093	1.098	.448	.329	.424	.090	2.607	174.9	-.029
	.8	45	2,400	-1.354	.128	1.406	.388	.339	.371	.149	2.516	174.6	.004
	1.3	46	2,400	-2.117	.080	2.153	.421	.374	.412	.890	3.213	177.8	.026
	2.3	47	2,400	-2.456	.493	2.529	.365	.345	.361	1.577	3.322	168.7	.005
	4.3	48	2,400	-2.857	.820	2.993	.404	.332	.384	1.707	4.259	164.0	.017
54	.4	50	2,265	-.961	.209	1.020	.301	.270	.302	.262	1.929	167.7	-.004
	.6	52	2,400	-1.023	.247	1.265	.674	.727	.699	.108	6.993	166.5	.051
	.8	53	2,400	-1.158	.345	1.383	.667	.611	.603	.061	6.283	163.4	-.052
	1.3	54	2,174	-1.460	.351	1.549	.412	.385	.417	.573	3.174	166.5	.016
	2.3	55	2,400	-2.168	.671	2.298	.467	.411	.506	.950	4.032	162.8	-.065
	4.3	56	2,327	-2.668	.902	2.838	.412	.368	.426	1.383	3.999	161.3	-.025
55	.4	58	2,400	.151	-.117	.454	.325	.327	.208	.011	1.175	322.2	-.004
	.6	59	2,400	.103	-.078	.360	.224	.311	.184	.010	1.091	322.7	-.008
	.8	60	2,400	.194	.176	.555	.413	.381	.276	.025	1.614	42.1	.018
	1.3	61	2,400	-.033	.002	.502	.385	.420	.271	.011	1.478	177.3	.018
	2.3	62	2,400	-.157	.029	.605	.463	.489	.336	.010	2.151	169.5	-.049
	3.3	63	2,400	-.482	.067	.806	.640	.501	.498	.022	2.218	172.1	-.105
	5.3	64	2,400	-1.383	.507	1.622	.785	.623	.737	.045	3.473	159.9	-.276
56	.4	65	2,400	.067	.029	.622	.441	.567	.367	.018	2.649	23.4	.115
	.6	66	2,400	.021	.434	.702	.459	.461	.345	.005	1.772	87.3	.028
	.8	67	2,400	-.230	.408	.851	.577	.627	.470	.000	2.484	119.5	-.021
	1.3	68	2,400	-.439	.500	.893	.571	.550	.525	.059	2.851	131.3	-.052
	2.3	69	2,400	-1.062	.513	1.298	.499	.579	.540	.028	2.821	154.2	-.109
	4.3	70	2,400	-1.887	.643	2.067	.615	.583	.649	.493	3.491	161.2	-.208
	6.3	71	2,353	-2.558	1.109	2.814	.413	.421	.452	1.264	3.997	156.6	-.051

Table A-2. Two-component velocity data for 2,230 cubic feet per second flow condition—*Continued*

Profile	*y* (ft)	FILE	*n*	*u* (ft/s)	*v* (ft/s)	*U* (ft/s)	RMS *u* (ft/s)	RMS *v* (ft/s)	RMS *U* (ft/s)	MIN *U* (ft/s)	MAX *U* (ft/s)	ϕ	*u'v'* (ft/s)
57	0.4	72	2,400	-0.857	0.799	1.388	0.618	0.701	0.565	0.062	3.330	137.0	0.032
	.6	73	2,400	-.937	.536	1.209	.592	.559	.606	.014	3.297	150.2	-.089
	.8	74	2,400	-1.379	.701	1.645	.513	.566	.523	.173	3.049	153.1	-.036
	1.3	75	2,400	-1.467	.641	1.694	.524	.520	.488	.280	2.889	156.4	-.001
	2.3	76	2,400	-2.059	.749	2.231	.436	.400	.416	1.101	3.342	160.0	-.010
	4.3	77	2,394	-2.497	1.032	2.717	.484	.261	.468	1.788	4.440	157.5	-.006
	6.3	78	2,400	-2.538	1.194	2.817	.340	.291	.357	1.892	3.770	154.8	-.019
58	.4	80	2,373	-.867	.373	.981	.311	.289	.331	.141	2.329	156.7	-.022
	.6	81	2,400	-1.206	.588	1.389	.389	.323	.356	.490	2.605	154.0	.022
	.8	82	2,391	-1.230	.492	1.366	.394	.328	.388	.428	2.839	158.2	-.001
	1.3	83	2,400	-1.466	.480	1.584	.435	.364	.441	.320	3.196	161.9	-.003
	2.3	84	2,400	-1.923	.601	2.053	.433	.376	.417	.998	3.075	162.6	.017
	4.3	85	2,400	-2.381	.836	2.540	.351	.309	.365	1.642	3.799	160.7	-.016
	6.3	86	2,400	-2.834	1.245	3.106	.287	.280	.310	2.010	3.893	156.3	-.018
59	.4	87	2,400	-1.198	.323	1.281	.291	.333	.305	.466	2.238	164.9	-.015
	.6	88	2,400	-1.499	.441	1.631	.446	.469	.446	.622	3.072	163.6	.019
	.8	89	2,400	-1.355	.472	1.473	.346	.383	.395	.581	2.748	160.8	-.049
	1.3	90	2,400	-1.888	.654	2.028	.424	.346	.427	.990	3.517	160.9	-.021
	2.3	91	2,400	-2.312	.771	2.465	.415	.378	.425	1.446	3.866	161.6	-.018
	4.3	92	2,400	-2.810	1.076	3.026	.409	.354	.439	1.835	4.136	159.0	-.043
	6.3	93	2,400	-2.928	1.295	3.218	.281	.352	.316	2.332	4.045	156.1	-.019
60	.4	94	2,213	-1.163	.483	1.314	.408	.364	.397	.238	2.673	157.5	.013
	.6	95	2,378	-1.278	.513	1.424	.391	.373	.399	.400	2.870	158.1	-.021
	.8	96	2,400	-1.580	.382	1.668	.554	.390	.565	.503	3.555	166.4	-.056
	1.3	97	2,400	-1.683	.631	1.828	.456	.330	.453	.571	3.060	159.5	-.019
	2.3	98	2,332	-2.054	.794	2.229	.507	.380	.528	.970	3.717	158.9	-.059
	4.3	99	2,322	-2.517	1.192	2.800	.364	.337	.404	1.754	3.942	154.7	-.042
	6.3	100	2,400	-2.695	1.431	3.062	.315	.354	.396	2.085	3.989	152.0	-.059

Table A-2. Two-component velocity data for 2,230 cubic feet per second flow condition—*Continued*

Profile	*y* (ft)	FILE	*n*	*u* (ft/s)	*v* (ft/s)	*U* (ft/s)	RMS *u* (ft/s)	RMS *v* (ft/s)	RMS *U* (ft/s)	MIN *U* (ft/s)	MAX *U* (ft/s)	ϕ	*u'v'* (ft/s)
61	0.4	101	2,400	-1.241	0.916	1.588	0.334	0.383	0.341	0.569	2.824	143.6	0.000
	.6	102	2,400	-1.441	1.008	1.815	.467	.479	.497	.453	3.198	145.0	-.027
	.8	103	2,400	-1.406	.741	1.645	.384	.445	.409	.370	2.948	152.2	-.025
	1.3	104	2,400	-1.647	.900	1.907	.405	.355	.418	.529	2.861	151.3	-.034
	2.3	105	2,400	-1.887	.995	2.151	.382	.318	.409	1.034	3.347	152.2	-.042
	4.3	106	2,400	-2.151	1.350	2.547	.204	.232	.239	1.747	3.220	147.9	-.012
62	.4	0	2,400	-.864	.842	1.343	.555	.464	.417	.074	2.547	135.8	.097
	.6	1	2,354	-.707	1.042	1.397	.528	.527	.435	.368	3.456	124.2	.027
	.6	2	2,400	-.741	.890	1.294	.455	.533	.399	.359	2.570	129.8	.094
	.8	3	2,400	-.690	1.121	1.415	.457	.521	.458	.211	3.405	121.6	.064
	1.3	4	2,400	-1.024	1.005	1.515	.430	.497	.443	.399	3.054	135.5	.018
	2.3	5	2,400	-1.388	1.153	1.848	.442	.457	.496	.776	3.576	140.3	-.059
	4.3	6	2,400	-1.431	1.228	1.934	.452	.560	.578	.372	3.296	139.4	-.115
	6.3	7	2,400	-1.360	.986	1.755	.621	.627	.721	.099	3.518	144.1	-.175
63	.4	8	2,393	-.520	.955	1.213	.510	.457	.424	.294	2.925	118.6	.069
	.6	9	2,400	-.664	.969	1.298	.513	.482	.439	.181	2.769	124.4	.065
	.8	10	2,400	-.507	.942	1.163	.436	.374	.350	.020	2.367	118.3	.025
	1.3	11	2,378	-.853	1.063	1.477	.628	.475	.543	.341	3.351	128.7	.013
	2.3	12	2,400	-1.046	1.048	1.586	.515	.610	.561	.090	2.908	135.0	-.026
	4.3	13	2,400	-1.252	1.084	1.738	.565	.733	.761	.005	3.352	139.1	-.244
64	.4	14	2,400	-.381	.597	.750	.324	.347	.404	.015	1.950	122.5	-.077
	.6	15	2,400	-.473	.809	.976	.325	.391	.429	.031	2.370	120.3	-.069
	.8	16	2,400	-.544	.978	1.151	.257	.436	.430	.154	2.538	119.1	-.032
	1.3	17	2,400	-.500	1.211	1.331	.289	.390	.426	.233	2.457	112.4	-.059

Table A-2. Two-component velocity data for 2,230 cubic feet per second flow condition—*Continued*

Profile	*y* (ft)	FILE	*n*	*u* (ft/s)	*v* (ft/s)	*U* (ft/s)	RMS *u* (ft/s)	RMS *v* (ft/s)	RMS *U* (ft/s)	MIN *U* (ft/s)	MAX *U* (ft/s)	ϕ	*u'v'* (ft/s)
65	0.4	18	2,400	-0.648	0.730	1.041	0.411	0.357	0.410	0.034	2.876	131.6	-0.024
	.6	19	2,400	-.741	.862	1.215	.445	.432	.449	.078	2.724	130.7	-.006
	.8	20	2,400	-.830	1.007	1.379	.423	.434	.409	.111	2.569	129.5	.006
	1.3	21	2,400	-.871	1.004	1.395	.488	.446	.507	.137	2.948	131.0	-.046
66	.4	22	2,400	-1.177	.828	1.497	.472	.465	.518	.279	3.055	144.9	-.085
	.6	23	2,400	-1.425	.763	1.675	.548	.470	.572	.380	3.535	151.8	-.054
	.8	24	2,400	-1.263	.701	1.512	.361	.456	.371	.443	2.652	151.0	.002
	.8	25	2,400	-1.316	.772	1.585	.372	.462	.411	.444	2.762	149.6	-.013
	1.3	26	2,400	-1.503	.972	1.849	.454	.515	.505	.580	3.518	147.1	-.044
67	.4	27	2,374	-.331	-.212	.702	.315	.640	.413	.005	1.946	212.6	.133
	.6	28	2,400	-.483	-.552	.948	.375	.638	.432	.038	2.128	228.8	.161
	.8	29	2,400	-.162	.208	.692	.326	.674	.389	.014	2.082	128.0	.079
	1.3	30	2,400	-.096	.400	.607	.301	.435	.283	.022	1.508	103.5	.006
	2.3	31	2,400	-.011	.302	.690	.343	.622	.347	.011	2.434	92.0	-.019
	4.3	33	2,400	-.017	.003	.308	.242	.258	.174	.000	.785	168.8	.015
68	.4	34	2,371	-.463	-.223	.810	.367	.646	.400	.014	1.948	205.7	.143
	.6	35	2,390	-.492	.079	.942	.371	.876	.516	.025	2.848	170.9	.102
	.8	36	2,400	-.355	.404	.912	.313	.877	.570	.031	2.934	131.3	.034
	1.3	37	2,400	-.296	.742	.917	.302	.545	.431	.039	2.076	111.8	-.036
69	.4	40	2,400	-1.432	-.457	1.527	.418	.282	.427	.383	2.756	197.7	.053
	.6	41	2,400	-1.550	-.369	1.658	.569	.435	.553	.144	3.101	193.4	.152
	.8	42	2,390	-1.553	-.446	1.650	.460	.349	.474	.208	2.988	196.0	.070
	1.3	43	2,400	-.996	.016	1.178	.571	.584	.523	.061	2.929	179.1	.099
	2.3	44	2,400	-.556	.489	.950	.445	.618	.474	.016	2.924	138.7	.082
	4.3	45	2,400	-.083	.006	.439	.322	.397	.274	.005	1.524	176.1	.013

Table A-2. Two-component velocity data for 2,230 cubic feet per second flow condition—*Continued*

Profile	*y* (ft)	FILE	*n*	*u* (ft/s)	*v* (ft/s)	*U* (ft/s)	RMS *u* (ft/s)	RMS *v* (ft/s)	RMS *U* (ft/s)	MIN *U* (ft/s)	MAX *U* (ft/s)	ϕ	*u'v'* (ft/s)
70	0.4	46	2,400	-1.329	-1.016	1.687	0.319	0.300	0.381	0.422	2.974	217.4	0.052
	.6	47	2,400	-1.831	-.970	2.083	.411	.271	.445	.550	3.487	207.9	.064
	.8	48	2,400	-1.878	-1.056	2.161	.303	.213	.328	1.244	3.114	209.4	.033
	1.3	49	2,400	-1.717	-1.026	2.011	.364	.326	.443	.221	3.047	210.9	.091
71	.4	50	2,400	-1.455	.106	1.476	.323	.219	.319	.704	2.590	175.8	.001
	.6	51	2,390	-1.755	.150	1.779	.389	.251	.391	.778	3.181	175.1	-.009
	.8	52	2,400	-1.873	.106	1.890	.358	.223	.354	.950	3.003	176.8	-.005
	1.3	53	2,400	-2.164	.198	2.189	.336	.260	.336	1.357	3.092	174.8	-.014
72	.4	54	2,400	-1.681	.336	1.739	.357	.297	.361	.740	2.941	168.7	-.014
	.6	55	2,400	-1.740	.395	1.802	.263	.258	.269	1.025	2.569	167.2	-.005
	.8	56	2,400	-1.964	.404	2.023	.332	.270	.335	1.046	2.972	168.4	-.010
	1.3	57	2,400	-1.953	.444	2.016	.346	.239	.352	1.143	2.953	167.2	-.024
73	.4	58	2,400	-.724	.286	.817	.274	.247	.270	.132	1.609	158.5	-.009
	.6	59	2,400	-1.388	.594	1.557	.392	.393	.406	.559	2.650	156.8	-.011
	.8	60	2,389	-1.273	.467	1.379	.315	.266	.325	.566	2.588	159.8	-.017
	1.3	61	2,400	-1.698	.533	1.797	.370	.278	.392	.894	2.951	162.6	-.035
	2.3	62	2,400	-2.182	.709	2.304	.289	.219	.298	1.524	3.113	162.0	-.014
	4.3	63	2,400	-2.033	.883	2.223	.253	.204	.282	1.472	3.066	156.5	-.025
74	.4	64	2,400	-.640	.256	.736	.268	.281	.290	.092	1.817	158.2	-.030
	.6	65	2,400	-.979	.287	1.072	.355	.339	.364	.150	1.970	163.6	-.045
	.8	66	2,400	-1.291	.358	1.395	.381	.395	.388	.437	2.515	164.5	-.050
	1.3	67	2,400	-1.594	.593	1.732	.406	.339	.414	.587	2.786	159.6	-.040
	2.3	68	2,400	-2.011	.660	2.132	.285	.266	.295	1.022	2.922	161.8	-.017
	4.3	69	2,394	-2.083	.858	2.258	.228	.165	.238	1.542	2.964	157.6	-.011

Table A-2. Two-component velocity data for 2,230 cubic feet per second flow condition—*Continued*

Profile	*y* (ft)	FILE	*n*	*u* (ft/s)	*v* (ft/s)	*U* (ft/s)	RMS *u* (ft/s)	RMS *v* (ft/s)	RMS *U* (ft/s)	MIN *U* (ft/s)	MAX *U* (ft/s)	φ	*u'v'* (ft/s)
75	0.4	70	2,400	-0.849	0.162	0.909	0.368	0.273	0.362	0.054	1.972	169.2	-0.026
	.6	71	2,400	-1.036	.252	1.100	.325	.255	.314	.274	2.048	166.3	-.009
	.8	72	2,400	-1.225	.411	1.324	.304	.296	.310	.540	2.339	161.5	-.011
	1.3	73	2,400	-1.368	.490	1.477	.362	.259	.356	.346	2.539	160.3	-.015
	2.3	74	2,390	-1.882	.736	2.027	.217	.169	.223	1.256	2.627	158.6	-.008
	4.3	75	2,393	-1.840	.815	2.016	.135	.119	.143	1.605	2.582	156.1	-.004
76	.4	76	2,400	-.926	.080	.988	.356	.327	.350	.173	2.076	175.1	-.065
	.6	77	2,400	-.790	-.119	.843	.313	.253	.301	.258	1.888	188.6	-.020
	.8	78	2,400	-1.066	-.076	1.104	.364	.254	.347	.309	2.082	184.1	-.035
	1.3	79	2,400	-1.422	.141	1.456	.320	.277	.322	.659	2.231	174.3	-.029
	2.3	80	2,400	-1.955	.514	2.032	.254	.225	.266	1.365	2.582	165.3	-.017
	4.3	81	2,400	-1.967	.677	2.084	.197	.140	.201	1.547	2.625	161.0	-.006
77	.4	82	2,400	-.699	-.125	.742	.232	.213	.230	.173	1.434	190.2	-.007
	.6	83	2,400	-.849	-.062	.897	.292	.291	.300	.241	2.336	184.2	-.035
	.8	84	2,400	-.988	.043	1.053	.334	.372	.345	.252	2.213	177.5	-.011
	1.3	85	2,400	-1.104	.161	1.170	.295	.358	.301	.362	2.095	171.7	.015
	2.3	86	2,400	-1.406	.609	1.637	.418	.610	.461	.263	3.334	156.6	.019
	4.3	87	2,400	-1.145	.215	1.295	.485	.532	.447	.201	2.563	169.4	.107
78	.4	88	2,400	-.834	.429	1.029	.424	.401	.402	.210	2.540	152.8	.026
	.6	89	2,400	-.984	.495	1.188	.368	.493	.424	.132	2.634	153.3	-.039
	.8	90	2,400	-1.305	.559	1.500	.498	.485	.498	.063	2.995	156.8	-.017
	1.3	91	2,400	-1.673	.764	1.881	.397	.423	.423	.672	3.379	155.5	-.042
	2.3	92	2,391	-1.967	.900	2.187	.330	.346	.358	1.264	3.277	155.4	-.028
	4.3	93	2,400	-2.456	1.177	2.736	.312	.298	.344	1.900	3.711	154.4	-.027
	6.3	94	2,400	-2.616	1.199	2.893	.273	.329	.309	2.056	4.017	155.4	-.018

Table A-2. Two-component velocity data for 2,230 cubic feet per second flow condition—*Continued*

Profile	*y* (ft)	FILE	*n*	*u* (ft/s)	*v* (ft/s)	*U* (ft/s)	RMS *u* (ft/s)	RMS *v* (ft/s)	RMS *U* (ft/s)	MIN *U* (ft/s)	MAX *U* (ft/s)	ϕ	*u'v'* (ft/s)
79	0.4	95	2,400	-1.635	0.736	1.821	0.362	0.342	0.385	0.834	3.034	155.8	-0.028
	.6	96	2,400	-1.595	.708	1.768	.336	.305	.358	.912	2.870	156.1	-.025
	.8	97	2,391	-1.642	.740	1.824	.325	.317	.355	1.031	2.886	155.8	-.024
	1.3	98	2,400	-1.905	.831	2.104	.357	.348	.377	1.213	3.334	156.4	-.022
	2.3	99	2,400	-2.423	1.044	2.659	.454	.361	.474	1.075	4.068	156.7	-.042
	4.3	100	2,400	-2.924	1.320	3.221	.356	.293	.363	1.860	4.057	155.7	-.017
	6.3	101	2,400	-2.740	1.298	3.048	.339	.315	.346	2.208	4.223	154.7	-.005

Table A-3. Two-component velocity data for 3,000 cubic feet per second flow condition

Profile	*y* (ft)	FILE	*n*	*u* (ft/s)	*v* (ft/s)	*U* (ft/s)	RMS *u* (ft/s)	RMS *v* (ft/s)	RMS *U* (ft/s)	MIN *U* (ft/s)	MAX *U* (ft/s)	φ	*u'v'* (ft/s)
1	0.4	0	2,400	-1.080	0.202	1.124	0.287	0.247	0.294	0.280	1.901	169.4	-0.007
	.6	1	2,400	-1.205	.044	1.249	.337	.340	.351	.521	2.240	177.9	.028
	.8	3	2,392	-1.232	.281	1.296	.363	.297	.369	.524	2.490	167.2	-.008
	1.3	4	2,400	-1.476	.509	1.588	.266	.312	.289	.781	2.327	161.0	-.017
	2.3	5	2,400	-1.636	.738	1.815	.330	.296	.350	.869	2.824	155.7	-.023
	4.3	6	2,400	-1.901	.969	2.150	.233	.257	.229	1.508	3.164	153.0	.004
	6.3	7	1,367	-2.041	.863	2.242	.249	.421	.346	.929	4.980	157.1	-.037
2	.4	9	2,383	-1.393	.420	1.477	.430	.279	.445	.435	3.063	163.2	-.041
	.6	10	2,381	-1.815	.531	1.931	.353	.417	.380	.826	3.172	163.7	-.026
	.8	11	2,400	-1.936	.601	2.059	.414	.377	.426	.676	3.214	162.8	-.029
	1.3	12	2,400	-1.870	.746	2.048	.365	.381	.370	1.140	3.338	158.3	-.006
	2.3	13	2,400	-2.147	1.139	2.451	.375	.327	.380	1.358	3.340	152.1	-.014
	4.3	15	2,377	-2.304	1.219	2.640	.322	.464	.374	1.622	3.912	152.1	-.010
	6.3	17	2,391	-2.174	1.204	2.504	.263	.359	.325	1.737	3.681	151.0	-.020
3	.4	18	2,400	-1.076	.066	1.116	.385	.284	.380	.283	2.424	176.5	-.006
	.6	19	2,390	-1.328	.224	1.387	.354	.325	.348	.491	2.668	170.4	.003
	.8	20	2,400	-1.643	.290	1.713	.392	.403	.405	.813	3.349	170.0	-.007
	1.3	21	2,400	-2.149	.541	2.253	.398	.423	.416	1.110	3.452	165.9	-.016
	2.3	23	2,381	-2.278	.989	2.512	.411	.389	.420	1.401	3.644	156.5	-.013
	4.3	24	2,400	-2.373	1.031	2.607	.294	.337	.310	1.881	3.621	156.5	-.006
	6.3	25	2,400	-2.650	1.262	2.946	.213	.288	.256	2.172	3.775	154.5	-.015
4	.4	26	2,366	-.894	.143	.954	.363	.314	.376	.166	2.219	170.9	-.034
	.6	27	2,400	-1.768	.566	1.893	.410	.406	.443	.732	3.384	162.3	-.054
	.8	28	2,357	-2.051	.746	2.213	.469	.382	.485	.964	3.497	160.0	-.034
	1.3	29	2,400	-2.178	.985	2.413	.317	.366	.352	1.515	3.577	155.7	-.026
	2.3	30	2,400	-2.627	1.159	2.892	.354	.337	.341	1.841	3.833	156.2	.007
	4.3	31	2,400	-2.584	1.300	2.901	.284	.266	.316	2.136	3.674	153.3	-.027
	6.3	32	2,400	-2.451	1.378	2.821	.208	.248	.223	2.002	3.563	150.7	-.003

Table A-3. Two-component velocity data for 3,000 cubic feet per second flow condition—*Continued*

Profile	*y* (ft)	FILE	*n*	*u* (ft/s)	*v* (ft/s)	*U* (ft/s)	RMS *u* (ft/s)	RMS *v* (ft/s)	RMS *U* (ft/s)	MIN *U* (ft/s)	MAX *U* (ft/s)	ϕ	*u'v'* (ft/s)
5	0.4	33	2,400	-2.064	0.809	2.248	0.446	0.423	0.489	0.873	3.770	158.6	-0.079
	.6	35	2,400	-2.003	.599	2.137	.483	.445	.486	.912	3.870	163.4	.003
	.8	36	2,400	-2.157	.540	2.261	.580	.405	.577	.973	3.980	166.0	-.020
	1.3	38	2,368	-2.114	.779	2.280	.521	.405	.559	.779	3.612	159.8	-.080
	2.3	42	2,393	-2.860	1.294	3.154	.360	.318	.373	2.028	4.107	155.7	-.021
	4.3	43	2,393	-2.854	1.311	3.156	.288	.389	.368	2.297	4.195	155.3	-.046
	6.3	44	2,394	-3.028	1.482	3.389	.276	.326	.260	2.691	4.331	153.9	.021
6	.4	45	2,400	-1.011	.013	1.069	.302	.342	.298	.298	1.954	179.3	-.007
	.6	46	2,400	-1.462	.077	1.527	.411	.446	.421	.487	3.060	177.0	-.055
	.8	47	2,400	-1.630	.162	1.675	.406	.353	.408	.491	2.999	174.3	-.023
	1.3	48	2,400	-2.215	.392	2.284	.399	.404	.408	.909	3.306	170.0	-.021
	2.3	50	2,400	-2.389	.711	2.521	.401	.390	.411	1.437	3.560	163.4	-.020
	4.3	52	2,400	-2.582	1.088	2.810	.375	.238	.387	1.555	3.808	157.2	-.031
	6.3	54	2,392	-2.946	1.266	3.222	.346	.313	.342	2.403	4.264	156.7	-.001
7	.4	55	2,400	-1.316	.205	1.367	.320	.325	.336	.547	2.326	171.2	-.034
	.6	57	2,400	-1.164	.161	1.206	.328	.275	.331	.468	2.204	172.2	-.008
	.8	59	2,400	-1.483	.137	1.521	.397	.301	.391	.542	2.428	174.7	-.019
	1.3	60	2,400	-1.703	.343	1.765	.344	.322	.353	.931	2.556	168.6	-.016
	2.3	61	2,393	-1.976	.661	2.108	.295	.322	.297	1.278	2.803	161.5	-.004
	4.3	62	2,400	-2.068	.961	2.290	.245	.217	.255	1.295	2.924	155.1	-.010
	6.3	64	2,400	-2.438	.963	2.633	.231	.266	.252	1.846	3.383	158.5	-.011
8	.4	65	2,400	-1.231	-.097	1.284	.319	.356	.324	.510	2.410	184.5	-.020
	.6	66	2,400	-1.296	-.039	1.346	.297	.364	.298	.332	2.301	181.7	-.040
	.8	67	2,400	-1.138	.119	1.180	.271	.291	.274	.450	2.083	174.0	-.012
	1.3	68	2,400	-1.629	.168	1.672	.394	.323	.385	.464	2.959	174.1	-.011
	2.3	70	2,400	-1.960	.519	2.048	.383	.319	.405	1.085	3.239	165.2	-.043
	4.3	73	2,400	-2.141	.822	2.307	.214	.272	.247	1.512	3.238	159.0	-.017
	6.3	75	2,400	-2.126	.671	2.246	.237	.298	.266	1.442	3.410	162.5	-.014

Table A-3. Two-component velocity data for 3,000 cubic feet per second flow condition—*Continued*

Profile	*y* (ft)	FILE	*n*	*u* (ft/s)	*v* (ft/s)	*U* (ft/s)	RMS *u* (ft/s)	RMS *v* (ft/s)	RMS *U* (ft/s)	MIN *U* (ft/s)	MAX *U* (ft/s)	φ	*u'v'* (ft/s)
9	0.4	76	2,388	-1.293	-0.487	1.459	0.306	0.465	0.301	0.810	2.641	200.7	-0.039
	.6	77	2,392	-1.526	-.238	1.589	.374	.346	.344	.813	2.461	188.9	-.040
	.8	78	2,400	-1.502	-.188	1.559	.304	.369	.302	.694	2.298	187.1	-.011
	1.3	79	2,400	-1.485	-.071	1.545	.409	.416	.405	.708	2.721	182.7	.020
	2.3	80	2,400	-1.781	-.188	1.827	.310	.374	.324	.869	4.989	186.0	.000
	4.3	82	2,392	-1.874	-.043	1.901	.239	.316	.237	1.080	2.638	181.3	.008
	6.3	83	2,400	-1.642	.288	1.695	.218	.308	.222	1.091	2.475	170.1	-.011
10	.4	84	2,393	-.605	.520	.848	.214	.324	.262	.020	1.740	139.3	-.002
	.6	85	2,383	-.679	.546	.970	.299	.446	.325	.060	1.864	141.2	-.043
	.8	86	2,394	-.547	.493	.805	.279	.371	.330	.010	2.178	138.0	-.030
	1.3	87	2,400	-.620	.719	1.036	.309	.588	.518	.005	2.712	130.8	-.111
	2.3	88	2,400	-.917	1.063	1.438	.306	.475	.472	.093	3.077	130.8	-.096
	4.3	89	2,400	-.762	.710	1.094	.259	.441	.385	.184	2.024	137.0	-.054
	6.3	91	2,400	-.780	.265	.926	.342	.433	.355	.048	2.366	161.2	-.009
11	.4	95	2,376	-1.130	-1.250	1.738	.397	.421	.390	.476	3.000	227.9	-.007
	.6	96	2,400	-1.774	-1.305	2.278	.474	.468	.327	1.447	3.322	216.3	-.025
	.8	97	2,400	-1.817	-.975	2.101	.389	.366	.353	.928	3.157	208.2	-.023
	1.3	98	2,400	-1.771	-.935	2.020	.307	.263	.307	.902	2.858	207.8	.010
12	.4	101	2,400	-1.190	-.481	1.315	.306	.274	.296	.523	2.234	202.0	-.006
	.6	102	2,382	-1.147	-.420	1.246	.259	.239	.250	.622	1.950	200.1	-.009
	.8	103	2,390	-1.740	-.408	1.827	.325	.359	.299	.747	2.791	193.2	-.045
	1.3	106	2,388	-2.400	-.676	2.537	.387	.431	.346	1.420	3.425	195.7	-.062
13	.4	107	2,400	-1.173	-.410	1.340	.480	.504	.483	.079	6.511	199.3	-.030
	.4	108	2,400	-1.513	-.589	1.654	.352	.340	.373	.695	2.777	201.3	.024
	.6	109	830	-1.219	-.184	1.676	1.247	1.448	1.537	.158	11.063	188.6	-.004
	.8	111	2,395	-1.924	-.176	1.968	.363	.374	.360	1.040	3.234	185.2	-.032
	1.3	112	2,374	-2.111	.162	2.141	.327	.323	.333	1.306	3.275	175.6	-.010

Table A-3. Two-component velocity data for 3,000 cubic feet per second flow condition—*Continued*

Profile	y (ft)	FILE	n	u (ft/s)	v (ft/s)	U (ft/s)	RMS u (ft/s)	RMS v (ft/s)	RMS U (ft/s)	MIN U (ft/s)	MAX U (ft/s)	ϕ	$u'v'$ (ft/s)
14	0.4	2	2,400	-2.445	0.444	2.681	0.815	0.688	0.349	1.402	3.884	169.7	0.275
	.6	5	2,144	-2.992	.644	3.083	.369	.379	.377	1.904	4.149	167.9	-.009
	.8	9	1,688	-3.541	.698	3.628	.370	.372	.371	2.527	4.723	168.8	.010
	1.3	10	2,105	-.268	.262	.920	1.157	.633	1.017	.018	1.043	135.6	.098
	2.3	12	2,400	-3.477	.174	3.713	.699	1.395	.873	1.992	14.139	177.1	-.642
	4.3	13	2,400	-3.984	.572	4.031	.408	.233	.417	2.319	5.215	171.8	-.037
	6.3	15	2,386	-3.269	-.040	3.480	1.174	.362	.292	2.553	4.436	180.7	-.050
15	.4	16	2,394	-1.688	-.085	1.744	.495	.413	.479	.338	3.271	182.9	-.061
	.6	17	2,400	-2.450	-.336	2.508	.419	.418	.419	1.274	3.995	187.8	.039
	.8	18	2,400	-2.530	.039	2.557	.368	.359	.358	1.159	3.599	179.1	-.005
	1.3	19	2,393	-2.477	.228	2.503	.282	.278	.283	1.655	3.373	174.7	-.013
	2.3	20	2,394	-2.463	.618	2.550	.276	.252	.291	1.762	3.803	165.9	-.020
	4.3	21	2,390	-2.602	.705	2.707	.267	.264	.278	2.004	3.381	164.8	-.013
	6.3	22	2,396	-3.012	.884	3.155	.297	.307	.290	2.190	4.055	163.7	.009
16	.4	23	2,400	-2.036	-.157	2.064	.434	.303	.434	.874	3.520	184.4	.001
	.6	24	2,395	-2.366	-.369	2.440	.541	.481	.553	.946	3.608	188.9	.065
	.8	25	2,362	-2.147	.099	2.168	.393	.284	.397	1.061	3.348	177.4	-.033
	1.3	30	2,395	-2.597	.175	2.635	.343	.412	.344	1.524	3.569	176.2	-.009
	2.3	31	2,372	-2.778	.549	2.851	.292	.356	.317	1.790	3.844	168.8	-.038
	4.3	29	2,400	-2.994	.942	3.156	.432	.320	.425	2.161	4.366	162.5	-.001
	6.3	32	2,382	-2.825	.950	2.992	.261	.286	.284	2.078	3.937	161.4	-.015
17	.4	33	2,400	-1.226	.051	1.279	.273	.370	.288	.584	2.637	177.6	.002
	.6	35	2,400	-2.059	.238	2.102	.417	.360	.424	.765	3.130	173.4	-.026
	.8	36	2,400	-2.166	.318	2.229	.398	.417	.395	1.169	3.381	171.7	-.017
	1.3	37	2,400	-2.488	.612	2.598	.388	.442	.401	1.409	3.650	166.2	-.012
	2.3	38	2,400	-2.582	.865	2.751	.306	.453	.383	1.774	3.974	161.5	-.067
	4.3	39	2,400	-2.830	1.099	3.053	.257	.363	.306	2.138	4.130	158.8	-.030
	6.3	40	2,395	-2.721	1.247	3.011	.334	.342	.347	2.150	4.150	155.4	-.010

Table A-3. Two-component velocity data for 3,000 cubic feet per second flow condition—*Continued*

Profile	*y* (ft)	FILE	*n*	*u* (ft/s)	*v* (ft/s)	*U* (ft/s)	RMS *u* (ft/s)	RMS *v* (ft/s)	RMS *U* (ft/s)	MIN *U* (ft/s)	MAX *U* (ft/s)	ϕ	*u'v'* (ft/s)
18	0.4	43	2,377	-1.359	-0.174	1.398	0.302	0.283	0.307	0.686	2.721	187.3	0.019
	.6	44	2,400	-1.740	.092	1.787	.441	.407	.450	.691	3.273	177.0	-.013
	.8	45	2,400	-1.771	.157	1.814	.425	.363	.426	.658	3.447	174.9	.006
	1.3	46	2,361	-2.356	.538	2.448	.435	.396	.440	1.205	3.771	167.1	-.020
	2.3	47	2,392	-2.599	.880	2.763	.343	.331	.356	1.854	4.019	161.3	-.019
	4.3	48	2,386	-2.737	1.076	2.950	.226	.267	.262	2.299	3.575	158.5	-.023
	6.3	49	2,400	-2.710	1.043	2.916	.241	.278	.253	2.213	3.714	158.9	-.005
19	.4	50	1,984	-2.295	.401	2.345	.735	.301	.751	.601	4.461	170.1	-.152
	.6	52	2,400	-.175	.162	.278	.113	.164	.139	.007	.927	137.3	-.009
	.8	53	2,400	-.146	-.058	.267	.167	.201	.145	.007	1.091	201.5	-.017
	1.3	54	2,400	-.003	-.271	.352	.196	.203	.171	.005	1.090	269.4	-.005
20	.4	55	2,383	-1.642	-.080	1.671	.405	.290	.398	.471	3.094	182.8	.033
	.6	56	2,387	-1.494	-.189	1.530	.439	.271	.439	.552	2.856	187.2	.034
	.8	57	2,400	-1.599	-.156	1.630	.373	.264	.365	.498	2.704	185.6	.015
	1.3	58	2,390	-1.453	.191	1.527	.484	.422	.477	.460	2.858	172.5	-.028
21	.4	61	2,400	-.731	.387	.906	.488	.385	.498	.014	2.637	152.1	-.112
	.6	62	2,400	-.800	.195	.944	.451	.441	.428	.049	2.163	166.3	-.031
	.8	63	2,400	-.997	.093	1.142	.519	.553	.523	.010	2.829	174.7	-.037
	1.3	64	2,400	-1.707	.242	1.809	.618	.524	.599	.040	3.803	171.9	-.060
22	.4	0	2,388	-.138	.214	.551	.398	.412	.298	.010	1.391	122.8	-.090
	.6	1	2,400	-.226	.186	.573	.488	.361	.353	.011	1.816	140.5	-.106
	.8	2	2,400	-.176	.043	.453	.359	.357	.291	.000	1.512	166.4	-.052
	1.3	3	2,400	-.511	.198	.812	.566	.491	.449	.007	2.086	158.8	-.158
	2.3	4	2,400	-1.088	.275	1.289	.673	.577	.621	.029	3.215	165.8	-.142
	4.3	5	2,400	-2.607	.867	2.773	.540	.395	.550	.579	4.038	161.6	-.073
	6.3	7	2,380	-2.740	1.160	2.995	.358	.334	.352	2.084	4.078	157.1	.006

Table A-3. Two-component velocity data for 3,000 cubic feet per second flow condition—*Continued*

Profile	*y* (ft)	FILE	*n*	*u* (ft/s)	*v* (ft/s)	*U* (ft/s)	RMS *u* (ft/s)	RMS *v* (ft/s)	RMS *U* (ft/s)	MIN *U* (ft/s)	MAX *U* (ft/s)	ϕ	*u'v'* (ft/s)
23	0.4	8	2,384	-0.873	-0.062	0.929	0.384	0.340	0.405	0.026	3.024	184.1	0.043
	.6	9	2,400	-1.081	.170	1.150	.407	.336	.391	.250	2.717	171.1	.047
	.8	10	2,400	-1.198	.253	1.271	.471	.313	.452	.254	2.633	168.1	.012
	1.3	11	2,400	-1.992	.377	2.067	.563	.371	.540	.740	3.841	169.3	.040
	2.3	12	2,392	-2.531	.765	2.667	.455	.371	.473	1.438	3.956	163.2	-.037
	4.3	13	2,400	-2.966	1.188	3.209	.357	.325	.379	1.757	4.193	158.2	-.026
	6.3	14	2,395	-2.889	1.301	3.184	.335	.336	.352	2.150	4.359	155.8	-.011

APPENDIX B:
Profile Position and Streambed Elevation

Table B-1. Profile position and streambed elevation for 1,820 cubic feet per second flow condition

[*x/b*, ratio of the downstream coordinate, in feet (origin is center of the upstream cylinder) to the cylinder diameter (3 feet); *y/b*, ratio of the cross-stream coordinate, in feet (origin is center of the upstream cylinder) to the cylinder diameter (3 feet)]

Profile	Streambed elevation (feet)	*x/b*	*y/b*	Profile	Streambed elevation (feet)	*x/b*	*y/b*
1	91.0	0.11	5.91	42	91.1	-2.32	5.54
2	90.7	.02	4.32	43	92.7	1.71	-1.73
3	91.7	-.38	2.64	44	92.7	1.95	-2.56
4	92.2	.07	1.22	45	93.5	1.88	-4.56
5	91.6	.05	1.04	46	93.6	4.53	-4.62
6	92.7	-.63	.09	47	92.5	4.67	-2.41
7	92.3	-1.04	.14	48	92.5	4.45	-1.35
8	92.6	-.39	.52	49	92.0	6.12	-.59
9	92.4	-.77	.67	50	92.2	6.04	-.93
10	91.8	-1.24	1.16	51	92.2	6.03	-1.48
11	92.4	-1.53	-.02	52	92.3	6.18	-2.40
12	92.0	.29	.73	53	92.6	6.07	-4.62
13	92.5	.66	1.08	54	92.1	6.66	-.56
14	92.0	1.15	1.51	55	92.0	6.96	.04
15	91.0	1.62	.54	56	91.2	6.66	.64
16	90.5	1.62	.87	57	92.0	7.62	.04
17	91.5	1.12	.71	58	91.5	7.62	1.04
18	92.5	-1.21	-1.34	59	92.0	7.62	-.96
19	92.4	-.62	-1.07	60	91.2	6.00	.65
20	92.3	-.37	-.67	61	91.3	6.04	.88
22	92.8	.14	-.67	62	91.3	6.13	1.12
23	93.3	-.08	-1.09	63	91.3	6.36	1.45
24	92.4	-.04	-1.43	64	90.6	6.39	2.60
25	92.7	.59	-.42	65	90.2	5.89	4.39
26	92.8	.79	-.93	66	91.0	8.28	5.96
27	92.8	1.09	-1.24	67	90.8	8.66	2.80
28	92.7	1.50	-.37	68	91.4	8.54	.17
29	92.8	1.56	-.80	69	92.0	8.25	-1.85
30	92.9	1.65	-1.21	70	92.2	8.42	-3.88
31	92.5	.05	-2.62	71	90.4	2.23	.61
32	92.4	-.26	-4.47	72	90.4	2.42	.74
33	92.0	-5.72	-4.58	73	90.6	2.52	1.17
34	92.0	-5.12	-2.87	74	91.9	2.20	2.42
35	92.1	-5.04	-.24	75	90.4	2.37	4.81
36	92.2	-5.82	1.92	76	90.4	2.36	5.96
37	91.3	-5.46	5.31	77	90.3	4.05	5.58
38	92.5	-2.36	-4.72	78	90.1	3.99	4.51
39	92.1	-2.38	-2.61	79	90.2	4.27	2.22
40	92.2	-2.32	-.22	80	90.1	4.28	1.22
41	91.8	-2.40	2.24	81	90.0	4.58	.83

Table B-2. Profile position and streambed elevation for 2,230 cubic feet per second flow condition

[*x/b*, ratio of the downstream coordinate, in feet (origin is center of the upstream cylinder) to the cylinder diameter (3 feet); *y/b*, ratio of the cross-stream coordinate, in feet (origin is center of the upstream cylinder) to the cylinder diameter (3 feet)]

Profile	Streambed elevation (feet)	x/b	y/b	Profile	Streambed elevation (feet)	x/b	y/b
1	91.7	-5.35	-4.98	41	92.4	4.17	-0.91
2	91.8	-4.90	-2.80	42	92.6	4.27	-.35
3	91.6	-4.97	-.22	43	91.9	6.01	-.70
4	91.8	-4.93	2.14	44	92.0	6.19	-1.06
5	90.8	-4.79	4.60	45	92.2	6.19	-1.58
6	91.2	-2.47	4.70	46	91.4	.53	.41
7	91.5	-2.20	2.48	47	92.6	.77	.89
8	91.9	-2.41	.13	48	90.9	1.44	.49
9	91.9	-2.02	-2.63	49	91.0	1.42	.67
10	92.8	-2.11	-4.81	50	92.1	1.14	1.10
11	92.4	-.68	-.06	51	90.5	2.00	.47
12	92.3	-.99	.03	52	90.6	2.14	1.10
13	92.2	-1.29	-.02	53	90.7	1.51	2.78
14	92.3	-.54	.60	54	90.0	1.91	4.64
15	92.5	-.77	.71	55	90.2	4.36	.62
16	91.8	-.89	1.35	56	90.0	4.26	1.34
17	92.6	.05	.68	57	90.6	4.68	2.37
18	93.2	.17	1.12	58	90.1	4.59	4.00
19	92.0	.20	1.62	59	90.2	6.11	4.78
20	91.0	-.10	2.62	60	90.5	6.02	2.93
21	90.7	.30	4.65	61	91.6	5.99	1.43
22	92.6	-.28	-.70	62	91.4	6.17	1.00
23	92.3	-.47	-.93	63	91.4	6.19	.67
24	92.3	-.64	-1.25	64	91.2	6.55	.43
25	92.8	.08	-.73	65	91.2	6.78	.66
26	92.7	.10	-1.07	66	91.7	7.31	1.01
27	92.7	.09	-1.62	67	91.9	6.82	-.12
28	92.5	.02	-2.57	68	92.0	6.98	-.02
29	92.6	.30	-4.57	69	92.0	7.63	-.05
30	92.7	.59	-.70	70	92.0	6.40	-.50
31	92.7	.85	-.90	71	92.2	6.53	-1.00
32	92.9	1.11	-.41	72	92.3	7.04	-1.50
33	92.8	1.15	-.72	73	92.3	6.23	-2.70
34	92.6	1.01	-1.19	74	92.4	6.35	-4.51
35	92.7	2.31	-.54	75	92.3	8.42	-4.02
36	92.7	1.98	-1.41	76	92.3	8.42	-2.70
37	93.4	2.15	-2.27	77	92.3	8.42	.03
38	93.7	2.31	-4.60	78	92.3	8.42	2.93
39	92.6	4.61	-4.62	79	92.3	8.42	4.78
40	92.8	4.34	-2.41				

Table B-3. Profile position and streambed elevation for 3,000 cubic feet per second flow condition

[*x/b*, ratio of the downstream coordinate, in feet (origin is center of the upstream cylinder) to the cylinder diameter (3 feet); *y/b*, ratio of the cross-stream coordinate, in feet (origin is center of the upstream cylinder) to the cylinder diameter (3 feet)]

Profile	Streambed elevation (feet)	*x/b*	*y/b*
1	91.6	-3.99	-0.66
2	91.8	-4.46	1.23
3	91.5	-3.73	2.51
4	91.0	-4.01	4.06
5	91.5	-1.95	4.18
6	91.4	-1.98	2.35
7	91.6	-2.74	.01
8	92.0	-1.88	.12
9	92.6	-.91	.08
10	92.5	-.63	-.10
11	92.2	-.37	.53
12	91.8	-.56	.74
13	91.6	-.98	1.21
14	92.6	-.03	.73
15	92.1	-.03	1.07
16	91.7	-.12	1.57
17	91.2	-.39	3.03
18	90.6	.20	4.07
19	92.4	.18	.67
20	91.7	.37	.83
21	91.4	.79	1.01
22	91.4	1.48	1.23
23	91.4	1.48	2.23

APPENDIX C: Streambed-Elevation Data from February 1991 Survey

Table C. Streambed-elevation data from February 1991 survey

[*x/b*, ratio of the downstream coordinate, in feet (origin is center of the upstream cylinder) to the cylinder diameter (3 feet); *y/b*, ratio of the cross-stream coordinate, in feet (origin is center of the upstream cylinder) to the cylinder diameter (3 feet)]

Streambed elevation (feet)	*x/b*	*y/b*	Streambed elevation (feet)	*x/b*	*y/b*
92.84	-0.48	-0.08	91.10	-0.39	3.76
92.37	-.31	-.50	91.89	-.40	3.03
93.41	-.13	-.65	91.57	-.36	2.23
93.32	-.10	-1.11	92.10	-.40	1.17
93.17	-.17	-1.34	92.72	-.28	.39
92.33	-.10	-1.43	92.65	.01	.54
92.20	-.17	-2.08	93.04	.51	.84
92.46	-.27	-3.16	92.46	.46	.98
92.37	-.23	-4.42	92.53	.19	1.61
92.12	-.48	-.91	92.09	.19	1.80
92.15	-.36	-1.24	91.90	.03	2.23
92.45	-1.10	-.17	92.55	.65	1.94
92.21	-1.10	-1.05	92.59	1.24	2.27
92.17	-1.20	-1.56	91.51	1.46	2.17
92.34	-1.26	-2.55	91.74	1.38	2.57
92.10	-1.21	-3.58	91.65	.59	2.43
92.31	-1.17	-4.36	92.19	1.37	1.31
92.37	-2.00	-.41	91.47	1.81	1.59
92.16	-2.11	-1.49	91.42	2.22	1.86
92.21	-2.22	-2.62	90.58	3.06	2.30
92.39	-2.04	-4.69	92.87	.92	-.34
92.09	-3.47	-.36	92.84	.50	-.51
91.90	-3.71	-1.70	92.81	1.46	-.31
92.37	-3.71	-2.87	92.84	2.53	-.30
92.17	-3.80	-5.11	92.97	3.85	-.28
92.71	-5.52	3.15	92.52	4.84	-.26
92.08	-5.63	2.31	91.95	5.66	-.27
91.87	-5.74	.77	92.13	5.89	-.51
92.03	-5.79	-.85	91.95	6.21	-.57
91.97	-6.21	-2.77	91.95	6.57	-.39
92.43	-6.23	-5.57	92.17	6.61	-1.15
92.24	-3.21	3.00	92.31	5.86	-1.32
92.14	-3.10	2.20	92.35	4.88	-1.36
92.16	-3.06	1.11	92.57	3.64	-1.40
92.21	-3.21	.14	92.66	2.39	-1.48
91.48	-1.10	3.54	93.42	1.86	-1.49
91.84	-1.39	2.45	92.63	1.04	-1.53
91.70	-1.47	1.47	92.39	.17	-1.72
92.08	-1.47	.51	92.49	.09	-2.55

Table C. Streambed-elevation data from February 1991 survey—*Continued*

Streambed elevation (feet)	*x/b*	*y/b*	Streambed elevation (feet)	*x/b*	*y/b*
92.64	1.42	-2.32	90.22	3.51	0.92
93.26	2.19	-2.34	90.68	3.55	1.42
93.00	2.68	-2.36	90.40	3.74	1.89
92.60	3.68	-2.38	90.44	3.89	2.50
92.64	4.82	-2.55	90.13	4.70	2.47
92.50	6.05	-2.33	90.76	4.96	2.39
92.19	7.00	-2.36	90.47	4.82	1.79
92.12	6.93	-3.35	90.62	4.76	1.34
92.12	6.04	-3.45	90.11	4.74	.85
92.45	4.78	-3.66	90.05	4.73	.33
92.77	3.44	-3.70	89.97	5.52	.34
93.52	2.82	-3.76	90.42	5.36	.94
92.71	2.04	-3.82	91.03	5.42	1.42
92.58	1.00	-3.77	91.15	5.35	2.00
92.75	.04	-4.07	90.62	5.65	2.66
91.23	.54	.26	90.67	6.39	2.63
92.97	.50	.88	91.05	7.20	2.19
92.78	.17	.50	90.88	6.54	1.79
91.80	.09	.57	91.26	6.33	1.28
92.19	.60	.99	90.98	6.21	.61
90.48	1.35	.32	91.67	6.63	.16
91.14	1.38	.74	92.95	7.05	.31
91.13	1.52	1.21	91.95	7.10	.04
91.77	2.19	1.53	91.73	7.59	.49
90.75	2.03	1.18	92.88	7.54	.63
90.50	2.04	.27	91.70	8.07	.51
90.26	2.60	.31	91.70	7.75	.98
90.47	2.63	.89	91.10	7.69	1.78
91.40	2.66	1.49	91.15	7.34	2.00
90.63	2.86	1.87	91.06	6.80	1.55
90.05	3.67	.35			

APPENDIX D:
Pier-Location Data

Table D. Pier-location data

[*x/b*, ratio of the downstream coordinate, in feet (origin is center of the upstream cylinder) to the cylinder diameter (3 feet); *y/b*, ratio of the cross-stream coordinate, in feet (origin is center of the upstream cylinder) to the cylinder diameter (3 feet)]

x/b	*y/b*	*x/b*	*y/b*
-0.50	0.00	6.66	0.12
-.49	-.09	6.64	.20
-.47	-.17	6.60	.28
-.43	-.25	6.55	.35
-.38	-.32	6.49	.42
-.32	-.38	6.42	.47
-.25	-.43	6.34	.50
-.17	-.47	6.25	.53
-.09	-.49	6.17	.53
.00	-.50	6.08	.53
.09	-.49	6.00	.50
.17	-.47	5.92	.47
.25	-.43	5.85	.42
.32	-.38	5.78	.35
.38	-.32	5.73	.28
.43	-.25	.43	.25
5.73	-.22	.38	.32
5.78	-.29	.32	.38
5.85	-.35	.25	.43
5.92	-.40	.17	.47
6.00	-.44	.09	.49
6.08	-.46	.00	.50
6.17	-.47	-.09	.49
6.25	-.46	-.17	.47
6.34	-.44	-.25	.43
6.42	-.40	-.32	.38
6.49	-.35	-.38	.32
6.55	-.29	-.43	.25
6.60	-.22	-.47	.17
6.64	-.14	-.49	.09
6.66	-.05	-.50	.00
6.67	.03		

APPENDIX E:
Near-Bed Velocity Data

Table E-1. Near-bed velocity data for 1,820 cubic feet per second flow condition

[$\bar{u}_1$, average x-component velocity, in feet per second, at 0.4 feet above the streambed; $\bar{u}_2$, average x-component velocity, in feet per second, at 0.6 feet above the streambed; $\bar{u}_3$, average x-component velocity, in feet per second, at 0.8 feet above the streambed; ϕ_1, direction of $\bar{u}_1$, in degrees, from the negative x-axis; ϕ_2, direction of $\bar{u}_2$, in degrees, from the negative x-axis; ϕ_3, direction of $\bar{u}_3$, in degrees, from the negative x-axis; $\bar{u}_a$, average x-component velocity, in feet per second, of the approach flow; $\bar{u}_{ave}$, average of $\bar{u}_1$, $\bar{u}_2$, and $\bar{u}_3$; ft/s, feet per second; --, not available]

Profile	$\bar{u}_1$ (ft/s)	$\bar{u}_2$ (ft/s)	$\bar{u}_3$ (ft/s)	ϕ_1 (degrees)	ϕ_2 (degrees)	ϕ_3 (degrees)	$\bar{u}_1 / \bar{u}_a$ (ft/s)	$\bar{u}_{ave} / \bar{u}_a$ (ft/s)
1	1.61	1.75	2.15	164	164	166	1.31	1.41
2	--	1.18	1.01	178	177	--	--	--
3	1.69	1.29	1.70	187	181	183	1.37	1.20
4	1.71	1.76	1.96	177	179	176	1.38	1.39
5	.65	2.19	2.17	67	181	179	.53	1.28
6	.87	.93	.92	181	194	191	.70	.69
7	.58	.90	1.08	193	201	197	.47	.66
8	1.76	1.58	1.37	232	221	218	1.43	1.21
9	1.20	1.23	1.51	205	199	193	.98	1.01
10	1.09	1.51	1.73	207	191	190	.88	1.11
11	1.17	1.07	1.36	183	178	184	.95	.92
12	1.58	2.19	2.13	176	175	174	1.28	1.51
13	1.66	2.23	2.02	186	176	180	1.35	1.51
14	.83	1.21	1.55	169	179	180	.67	.92
15	.60	.42	.59	321	320	323	.48	.41
16	.35	.52	.59	308	330	321	.29	.37
17	.20	.22	.46	58	296	328	.16	.22
18	1.02	1.10	1.20	154	154	164	.83	.85
19	.24	.45	1.04	205	128	123	.19	.44
20	.94	.83	1.22	74	112	121	.76	.77
21	--	--	--	--	--	--	--	--
22	1.50	1.68	1.88	144	145	149	1.22	1.30
23	1.63	1.78	1.94	150	152	143	1.32	1.37
24	1.60	1.61	1.67	153	155	155	1.30	1.25
25	.26	.30	.32	331	340	181	.21	.22
26	.52	.85	.80	223	179	157	.42	.56
27	1.28	1.35	1.48	183	175	170	1.04	1.05
28	.48	.65	.58	171	185	178	.39	.44
29	1.26	1.15	1.17	185	182	170	1.02	.92
30	1.79	1.74	1.88	178	177	176	1.45	1.38
31	1.48	1.49	1.56	164	170	164	1.20	1.16
32	.52	.53	.80	186	180	169	.43	.47
33	.93	.98	1.21	183	177	178	.75	.80
34	1.12	1.19	1.38	178	178	176	.91	.94
35	1.24	1.18	1.23	178	162	165	1.00	.93
36	1.34	1.54	1.51	161	162	161	1.09	1.13
37	1.52	1.64	1.71	158	162	162	1.23	1.25
38	.65	.69	1.21	173	185	174	.53	.65

Table E-1. Near-bed velocity data for 1,820 cubic feet per second flow condition—*Continued*

Profile	$\bar{u}_1$ (ft/s)	$\bar{u}_2$ (ft/s)	$\bar{u}_3$ (ft/s)	ϕ_1 (degrees)	ϕ_2 (degrees)	ϕ_3 (degrees)	$\bar{u}_1 / \bar{u}_a$ (ft/s)	$\bar{u}_{ave} / \bar{u}_a$ (ft/s)
39	1.21	1.30	1.28	179	176	174	0.98	0.97
40	1.16	1.35	1.21	190	186	182	.94	.95
41	.75	1.12	1.54	175	172	176	.61	.88
42	1.18	1.51	1.51	178	172	164	.96	1.07
43	.92	1.42	1.65	158	162	165	.75	1.02
44	.90	1.36	1.65	165	163	162	.73	1.00
45	1.21	1.44	1.47	155	158	159	.98	1.06
46	1.51	1.53	1.23	167	162	148	1.23	1.09
47	.92	1.00	1.05	160	161	156	.75	.76
48	1.08	1.29	1.35	155	155	160	.87	.95
49	1.46	1.37	1.44	158	157	179	1.18	1.09
50	--	1.29	1.44	157	158	--	--	--
51	.96	1.31	1.24	160	160	162	.78	.90
52	.87	1.22	1.08	159	159	162	.70	.81
53	.30	.55	.81	176	171	168	.25	.43
54	.92	.94	1.98	198	200	201	.75	.98
55	.74	.74	.79	117	122	128	.60	.58
56	1.08	1.16	--	123	134	--	.87	--
57	.71	.65	.79	168	175	149	.58	.55
58	.78	1.07	1.18	148	146	154	.63	.77
59	1.00	1.07	1.36	177	175	173	.81	.88
60	.91	1.20	1.09	117	130	126	.74	.82
61	1.28	1.34	1.30	123	134	124	1.03	1.00
62	1.23	1.17	1.38	134	134	140	1.00	.97
63	1.40	1.33	1.34	140	136	137	1.13	1.04
64	.86	1.42	1.24	144	152	151	.69	.90
65	.99	1.17	.82	162	160	162	.80	.76
66	.57	.85	1.20	182	165	160	.46	.67
67	.59	.79	.86	143	157	164	.48	.57
68	.65	.77	.79	209	193	188	.52	.56
69	.97	.91	1.22	186	181	176	.78	.79
70	.75	1.03	1.18	183	179	171	.61	.76
71	.73	.66	.51	335	324	310	.59	.49
72	.53	.61	.61	359	331	334	.43	.45
73	.54	.45	.55	44	101	92	.43	.39
74	1.85	1.74	1.87	170	171	171	1.50	1.40
75	.88	.88	1.13	156	163	162	.71	.74
76	.60	.81	.94	156	155	157	.49	.60
77	1.14	1.31	1.49	155	160	163	.92	1.01
78	.83	.88	.94	152	152	155	.67	.68
79	.66	.88	.98	123	155	137	.53	.65
80	.64	.44	.55	30	60	92	.52	.42
81	.47	.35	.45	277	225	106	.38	.33

Table E-2. Near-bed velocity data for 2,230 cubic feet per second flow condition

[$\bar{u}_1$, average *x*-component velocity, in feet per second, at 0.4 feet above the streambed; $\bar{u}_2$, average *x*-component velocity, in feet per second, at 0.6 feet above the streambed; $\bar{u}_3$, average *x*-component velocity, in feet per second, at 0.8 feet above the streambed; ϕ_1, direction of $\bar{u}_1$, in degrees, from the negative *x*-axis; ϕ_2, direction of $\bar{u}_2$, in degrees, from the negative *x*-axis; ϕ_3, direction of $\bar{u}_3$, in degrees, from the negative *x*-axis; $\bar{u}_a$, average *x*-component velocity, in feet per second, of the approach flow; $\bar{u}_{ave}$, average of $\bar{u}_1$, $\bar{u}_2$, and $\bar{u}_3$; ft/s, feet per second]

Profile	$\bar{u}_1$ (ft/s)	$\bar{u}_2$ (ft/s)	$\bar{u}_3$ (ft/s)	ϕ_1 (degrees)	ϕ_2 (degrees)	ϕ_3 (degrees)	$\bar{u}_1 / \bar{u}_a$ (ft/s)	$\bar{u}_{ave} / \bar{u}_a$ (ft/s)
1	0.86	1.04	1.07	177	178	174	0.74	0.76
2	1.14	1.21	1.18	183	177	173	.98	.91
3	1.04	1.21	1.34	169	165	163	.90	.93
4	1.29	1.47	1.79	182	170	167	1.11	1.17
5	1.88	1.95	2.27	171	168	166	1.63	1.57
6	1.42	1.82	2.08	162	169	167	1.23	1.37
7	1.04	1.33	1.76	179	180	172	.90	1.06
8	1.50	1.67	1.72	179	183	177	1.29	1.25
9	1.26	1.36	1.63	170	172	171	1.09	1.09
10	1.35	1.24	.96	158	165	187	1.16	.91
11	.87	1.19	1.14	143	160	152	.75	.82
12	.97	1.05	1.15	162	156	166	.84	.81
13	.79	1.08	1.08	159	170	164	.69	.76
14	1.63	1.93	1.84	196	199	196	1.41	1.39
15	1.52	1.53	1.64	193	193	188	1.31	1.20
16	1.09	1.40	1.20	204	193	181	.95	.95
17	1.19	2.47	2.38	194	171	173	1.03	1.55
18	1.64	2.03	2.05	176	175	175	1.42	1.47
19	1.51	1.96	1.70	195	189	181	1.30	1.33
20	.54	1.27	1.39	182	186	181	.46	.82
21	1.11	1.15	.82	131	134	141	.96	.79
22	1.17	1.21	1.16	121	132	136	1.01	.91
23	.40	.86	1.27	94	119	134	.35	.65
24	.73	.71	.91	144	149	135	.64	.61
25	1.85	2.02	1.94	135	139	138	1.60	1.49
26	.69	1.43	1.99	98	122	138	.59	1.06
27	1.83	1.98	2.01	153	157	157	1.58	1.50
28	1.82	1.91	1.43	162	164	161	1.57	1.32
29	.88	1.05	1.36	139	133	149	.76	.85
30	1.10	1.44	1.87	154	158	162	.95	1.13
31	.87	.53	.71	217	206	155	.75	.54
32	.74	.95	1.17	234	202	195	.64	.73
33	.94	.97	1.11	201	177	169	.82	.78
34	1.84	1.62	2.06	184	179	174	1.59	1.42
35	.74	.84	.77	171	165	162	.64	.60
36	.98	1.81	1.82	166	176	169	.85	1.19
37	1.60	1.49	2.15	166	166	163	1.39	1.35
38	.79	1.48	1.62	166	157	155	.68	1.00

Table E-2. Near-bed velocity data for 2,230 cubic feet per second flow condition—*Continued*

Profile	$\bar{u}_1$ (ft/s)	$\bar{u}_2$ (ft/s)	$\bar{u}_3$ (ft/s)	ϕ_1 (degrees)	ϕ_2 (degrees)	ϕ_3 (degrees)	$\bar{u}_1 / \bar{u}_a$ (ft/s)	$\bar{u}_{ave} / \bar{u}_a$ (ft/s)
39	0.50	0.23	0.21	170	235	166	0.44	0.24
40	1.69	1.66	1.86	170	167	163	1.47	1.34
41	1.07	1.21	1.49	156	160	161	.92	.97
42	1.01	1.30	1.16	162	163	159	.87	.89
43	.53	.70	1.60	149	140	161	.46	.73
44	1.49	1.63	1.74	163	163	163	1.29	1.25
45	1.32	1.52	1.62	159	160	162	1.14	1.15
46	.15	.25	.37	261	287	298	.13	.20
47	1.34	1.18	2.28	194	196	179	1.16	1.23
48	.75	.85	.78	327	331	333	.65	.61
49	.33	.41	.66	332	339	330	.29	.36
50	1.57	1.77	1.95	172	181	187	1.36	1.36
51	1.03	.88	.86	330	328	331	.89	.71
52	.51	.71	.80	97	98	114	.44	.52
53	.68	1.10	1.41	179	175	175	.59	.82
54	1.02	1.26	1.38	168	166	163	.88	.94
55	.45	.36	.56	322	323	42	.39	.35
56	.62	.70	.85	23	87	119	.54	.56
57	1.39	1.21	1.64	137	150	153	1.20	1.09
58	.98	1.39	1.37	157	154	158	.85	.96
59	1.28	1.63	1.47	165	164	161	1.11	1.13
60	1.31	1.42	1.67	157	158	166	1.14	1.13
61	1.59	1.81	1.64	144	145	152	1.37	1.30
62	1.34	1.29	1.41	136	130	122	1.16	1.04
63	1.21	1.30	1.16	119	124	118	1.05	.94
64	.75	.98	1.15	123	120	119	.65	.74
65	1.04	1.21	1.38	132	131	129	.90	.93
66	1.50	1.68	1.58	145	152	150	1.29	1.22
67	.70	.95	.69	213	229	128	.61	.60
68	.81	.94	.91	206	171	131	.70	.68
69	1.53	1.66	1.65	198	193	196	1.32	1.24
70	1.69	2.08	2.16	217	208	209	1.46	1.52
71	1.48	1.78	1.89	176	175	177	1.28	1.32
72	1.74	1.80	2.02	169	167	168	1.50	1.43
73	.82	1.56	1.38	158	157	160	.71	.96
74	.74	1.07	1.39	158	164	165	.64	.82
75	.91	1.10	1.32	169	166	161	.79	.86
76	.99	.84	1.10	175	189	184	.85	.75
77	.74	.90	1.05	190	184	177	.64	.69
78	1.03	1.19	1.50	153	153	157	.89	.96
79	1.82	1.77	1.82	156	156	156	1.57	1.39

Table E-3. Near-bed velocity data for 3,000 cubic feet per second flow condition

[$\bar{u}_1$, average x-component velocity, in feet per second, at 0.4 feet above the streambed; $\bar{u}_2$, average x-component velocity, in feet per second, at 0.6 feet above the streambed; $\bar{u}_3$, average x-component velocity, in feet per second, at 0.8 feet above the streambed; ϕ_1, direction of $\bar{u}_1$, in degrees, from the negative x-axis; ϕ_2, direction of $\bar{u}_2$, in degrees, from the negative x-axis; ϕ_3, direction of $\bar{u}_3$, in degrees, from the negative x-axis; $\bar{u}_a$, average x-component velocity, in feet per second, of the approach flow; $\bar{u}_{ave}$, average of $\bar{u}_1$, $\bar{u}_2$, and $\bar{u}_3$; ft/s, feet per second; --, not available]

Profile	$\bar{u}_1$ (ft/s)	$\bar{u}_2$ (ft/s)	$\bar{u}_3$ (ft/s)	ϕ_1 (degrees)	ϕ_2 (degrees)	ϕ_3 (degrees)	$\bar{u}_1/\bar{u}_a$ (ft/s)	$\bar{u}_{ave}/\bar{u}_a$ (ft/s)
1	1.12	1.25	1.30	169	178	167	0.85	0.82
2	1.48	1.93	2.06	163	164	163	1.12	1.23
3	1.12	1.39	1.71	177	170	170	.85	.95
4	.95	1.89	2.21	171	162	160	.72	1.14
5	2.25	2.14	2.26	159	163	166	1.71	1.49
6	1.07	1.53	1.68	179	177	174	.81	.96
7	1.37	1.21	1.52	171	172	175	1.04	.92
8	1.28	1.35	1.18	185	182	174	.98	.86
9	1.46	1.59	1.56	201	189	187	1.11	1.03
10	.85	.97	.81	139	141	138	.64	.59
11	1.74	2.28	2.10	228	216	208	1.32	1.37
12	1.31	1.25	1.83	202	200	193	1.00	.99
13	1.65	1.97	--	201	185	--	1.26	--
14	2.68	3.08	3.63	170	168	169	2.04	2.11
15	1.74	2.51	2.56	183	188	179	1.33	1.53
16	2.06	2.44	2.17	184	189	177	1.57	1.50
17	1.28	2.10	2.23	178	173	172	.97	1.26
18	1.40	1.79	1.81	187	177	175	1.06	1.12
19	2.34	.28	.27	170	137	202	--	--
20	1.67	1.53	1.63	183	187	186	1.27	1.08
21	.91	.94	1.14	152	166	175	.69	.67
22	.55	.57	.45	123	141	166	.42	.35
23	.93	1.15	1.27	184	171	168	.71	.75

APPENDIX F:
Velocity-Gradient Data and Computed-Streambed Stresses

Table F-1. Velocity-gradient data and computed-streambed stresses for 1,820 cubic feet per second flow condition

[$\bar{U}$, average velocity mangitude, in feet per second; z, distance of velocity measurement from streambed, in feet; Slope, slope of the regression line through the points given for that profie; R^2, coefficient of determination of the regression line; τ, profile boundary shear stress, in pounds per square foot; τ_o, approach flow boundary shear stress, in pounds per square foot; ft/s, feet per second; ft, feet; lbs/ft^2, pounds per square foot; --, not available]

Profile	$\bar{U}$ (ft/s)	z (ft)	Slope	R^2	τ (lbs/ft^2)	τ/τ_o
1	1.614	0.4	0.60	0.93	0.164	3.48
	1.747	.6	--	--	--	--
	2.153	.8	--	--	--	--
	2.359	1.3	--	--	--	--
2	1.010	.8	.47	1.00	.266	5.65
	1.459	1.3	--	--	--	--
3	1.285	.6	.51	.90	.230	4.89
	1.697	.8	--	--	--	--
	1.910	1.3	--	--	--	--
4	1.705	.4	1.02	.85	.056	1.19
	1.765	.6	--	--	--	--
	1.965	.8	--	--	--	--
6	.865	.4	2.73	.90	.008	.17
	.925	.6	--	--	--	--
	.921	.8	--	--	--	--
	1.043	1.3	--	--	--	--
7	.584	.4	.72	.97	.114	2.43
	.897	.6	--	--	--	--
	1.083	.8	--	--	--	--
	1.282	1.3	--	--	--	--
9	1.204	.4	.88	.91	.076	1.63
	1.232	.6	--	--	--	--
	1.507	.8	--	--	--	--
	1.694	1.3	--	--	--	--
10	1.088	.4	.57	.96	.180	3.83
	1.508	.6	--	--	--	--
	1.730	.8	--	--	--	--
	1.954	1.3	--	--	--	--
11	1.070	.6	.62	.97	.154	3.27
	1.355	.8	--	--	--	--
	1.611	1.3	--	--	--	--
12	1.580	.4	.29	1.00	.724	15.41
	2.195	.6	--	--	--	--
13	1.661	.4	.31	1.00	.621	13.20
	2.234	.6	--	--	--	--
14	.827	.4	.52	.96	.218	4.64
	1.209	.6	--	--	--	--
	1.551	.8	--	--	--	--
	1.752	1.3	--	--	--	--

Table F-1. Velocity-gradient data and computed-streambed stresses for 1,820 cubic feet per second flow condition —*Continued*

Profile	$\bar{U}$ (ft/s)	z (ft)	Slope	R^2	τ (lbs/ft²)	τ/τ_o
15	0.597	0.4	--	--	--	*0.00
	.416	.6	--	--	--	--
	.586	.8	--	--	--	--
	.679	1.3	--	--	--	--
16	.353	.4	1.52	0.96	0.025	.54
	.516	.6	--	--	--	--
	.592	.8	--	--	--	--
	.678	1.3	--	--	--	--
17	.200	.4	--	--	--	*.00
	.217	.6	--	--	--	--
	.458	.8	--	--	--	--
	.580	1.3	--	--	--	--
18	1.018	.4	.99	.94	.060	1.27
	1.102	.6	--	--	--	--
	1.203	.8	--	--	--	--
	1.500	1.3	--	--	--	--
19	.235	.4	.34	.87	.510	1.85
	.447	.6	--	--	--	--
	1.039	.8	--	--	--	--
20	.833	.6	.57	.84	.180	3.82
	1.219	.8	--	--	--	--
	1.358	1.3	--	--	--	--
22	1.499	.4	.83	.99	.086	1.82
	1.677	.6	--	--	--	--
	1.884	.8	--	--	--	--
	2.099	1.3	--	--	--	--
23	1.634	.4	.98	.98	.061	1.30
	1.780	.6	--	--	--	--
	1.941	.8	--	--	--	--
25	.255	.4	4.41	.96	.003	.06
	.305	.6	--	--	--	--
	.319	.8	--	--	--	--
26	.517	.4	.53	1.00	.210	4.48
	.851	.6	--	--	--	--
27	1.285	.4	1.49	.92	.026	.56
	1.350	.6	--	--	--	--
	1.476	.8	--	--	--	--
28	.482	.4	1.04	1.00	.055	1.16
	.652	.6	--	--	--	--
31	1.489	.6	.56	.94	.189	4.03
	1.565	.8	--	--	--	--
	2.034	1.3	--	--	--	--
32	.530	.6	.42	1.00	.335	7.12
	.796	.8	--	--	--	--
	1.326	1.3	--	--	--	--

Table F-1. Velocity-gradient data and computed-streambed stresses for 1,820 cubic feet per second flow condition —*Continued*

Profile	$\bar{U}$ (ft/s)	z (ft)	Slope	R^2	τ (lbs/ft²)	τ/τ_o
33	0.976	0.6	0.76	0.96	0.101	2.16
	1.214	.8	--	--	--	--
	1.413	1.3	--	--	--	--
34	1.122	.4	1.06	.87	.052	1.10
	1.187	.6	--	--	--	--
	1.377	.8	--	--	--	--
35	1.176	.6	1.04	.95	.054	1.14
	1.225	.8	--	--	--	--
	1.472	1.3	--	--	--	--
36	1.343	.4	1.29	.87	.035	.75
	1.544	.6	--	--	--	--
	1.496	.8	--	--	--	--
	1.722	1.3	--	--	--	--
37	1.520	.4	.89	.93	.074	1.58
	1.635	.6	--	--	--	--
	1.709	.8	--	--	--	--
	2.061	1.3	--	--	--	--
38	.654	.4	.61	.99	.158	3.37
	1.208	.8	--	--	--	--
	1.480	1.3	--	--	--	--
39	1.205	.4	1.09	.82	.049	1.04
	1.296	.6	--	--	--	--
	1.279	.8	--	--	--	--
	1.607	1.3	--	--	--	--
40	1.207	.8	1.45	1.00	.028	.59
	1.352	1.3	--	--	--	--
41	.755	.4	.40	.99	.372	7.91
	1.120	.6	--	--	--	--
	1.543	.8	--	--	--	--
	2.007	1.3	--	--	--	--
42	1.181	.4	.49	.91	.246	5.23
	1.510	.6	--	--	--	--
	1.507	.8	--	--	--	--
	2.181	1.3	--	--	--	--
43	.925	.4	.51	.95	.229	4.87
	1.419	.6	--	--	--	--
	1.653	.8	--	--	--	--
	1.899	1.3	--	--	--	--
44	.902	.4	.49	.97	.249	5.29
	1.358	.6	--	--	--	--
	1.653	.8	--	--	--	--
	1.921	1.3	--	--	--	--

Table F-1. Velocity-gradient data and computed-streambed stresses for 1,820 cubic feet per second flow condition—*Continued*

Profile	$\bar{U}$ (ft/s)	z (ft)	Slope	R^2	τ (lbs/ft^2)	τ/τ_o
45	1.212	0.4	0.81	0.95	0.090	1.92
	1.444	.6	--	--	--	--
	1.467	.8	--	--	--	--
	1.841	1.3	--	--	--	--
46	1.512	.4	3.14	.95	.006	.13
	1.533	.6	--	--	--	--
	1.661	1.3	--	--	--	--
47	.920	.4	2.29	1.00	.011	.24
	1.002	.6	--	--	--	--
	1.051	.8	--	--	--	--
48	1.077	.4	.95	.98	.065	1.38
	1.294	.6	--	--	--	--
	1.350	.8	--	--	--	--
	1.623	1.3	--	--	--	--
50	1.289	.6	1.02	.99	.057	1.21
	1.437	.8	--	--	--	--
	1.622	1.3	--	--	--	--
51	.961	.4	.51	1.00	.227	4.83
	1.307	.6	--	--	--	--
52	.866	.4	.49	1.00	.242	5.15
	1.223	.6	--	--	--	--
53	.304	.4	.69	.98	.125	2.66
	.549	.6	--	--	--	--
	.811	.8	--	--	--	--
	1.020	1.3	--	--	--	--
55	.738	.4	--	--	--	*.00
	.735	.6	--	--	--	--
	.793	.8	--	--	--	--
	.539	1.3	--	--	--	--
56	1.077	.4	2.09	1.00	.013	.29
	1.161	.6	--	--	--	--
57	.647	.6	.95	1.00	.065	1.39
	.785	.8	--	--	--	--
	1.002	1.3	--	--	--	--
58	.779	.4	.55	.97	.197	4.18
	1.067	.6	--	--	--	--
	1.178	.8	--	--	--	--
	1.707	1.3	--	--	--	--
59	1.002	.4	.85	.92	.082	1.74
	1.065	.6	--	--	--	--
	1.355	.8	--	--	--	--
	1.521	1.3	--	--	--	--
60	.907	.4	.60	1.00	.166	3.52
	1.203	.6	--	--	--	--

Table F-1. Velocity-gradient data and computed-streambed stresses for 1,820 cubic feet per second flow condition —*Continued*

Profile	$\bar{U}$ (ft/s)	z (ft)	Slope	R^2	τ (lbs/ft^2)	τ/τ_o
61	1.276	0.4	2.98	1.00	0.007	0.14
	1.335	.6	--	--	--	--
62	1.229	.4	.86	.38	.079	1.69
	1.169	.6	--	--	--	--
	1.380	.8	--	--	--	--
63	1.338	.8	1.03	.98	.055	1.17
	1.595	1.3	--	--	--	--
64	1.243	.8	1.02	1.00	.057	1.21
	1.450	1.3	--	--	--	--
65	.988	.4	.95	1.00	.065	1.38
	1.173	.6	--	--	--	--
66	.572	.4	.39	.98	.389	8.28
	.846	.6	--	--	--	--
	1.202	.8	--	--	--	--
	1.841	1.3	--	--	--	--
67	.594	.4	.56	.91	.186	3.95
	.793	.6	--	--	--	--
	.856	.8	--	--	--	--
	1.442	1.3	--	--	--	--
68	.647	.4	1.25	.93	.038	.80
	.769	.6	--	--	--	--
	.790	.8	--	--	--	--
	1.044	1.3	--	--	--	--
69	.913	.6	.54	.98	.204	4.34
	1.220	.8	--	--	--	--
	1.540	1.3	--	--	--	--
70	.749	.4	.76	.99	.102	2.18
	1.035	.6	--	--	--	--
	1.178	.8	--	--	--	--
	1.428	1.3	--	--	--	--
71	.727	.4	--	--	--	*.00
	.659	.6	--	--	--	--
	.512	.8	--	--	--	--
	.496	1.3	--	--	--	--
72	.533	.4	2.42	1.00	.010	.21
	.606	.6	--	--	--	--
73	.536	.4	--	--	--	*.00
	.445	.6	--	--	--	--
	.554	.8	--	--	--	--
	.504	1.3	--	--	--	--
74	1.742	.6	.96	1.00	.064	1.36
	1.872	.8	--	--	--	--
	2.092	1.3	--	--	--	--

Table F-1. Velocity-gradient data and computed-streambed stresses for 1,820 cubic feet per second flow condition —*Continued*

Profile	$\bar{U}$ (ft/s)	z (ft)	Slope	R^2	τ (lbs/ft^2)	τ/τ_o
75	0.877	0.6	0.43	1.00	0.317	6.75
	1.126	.8	--	--	--	--
	1.649	1.3	--	--	--	--
76	.603	.4	.76	.99	.101	2.15
	.808	.6	--	--	--	--
	.936	.8	--	--	--	--
	1.273	1.3	--	--	--	--
77	1.135	.4	.86	.99	.080	1.70
	1.312	.6	--	--	--	--
	1.486	.8	--	--	--	--
78	.825	.4	2.67	.98	.008	.18
	.877	.6	--	--	--	--
	.937	.8	--	--	--	--
79	.659	.4	.74	.98	.106	2.25
	.881	.6	--	--	--	--
	.981	.8	--	--	--	--
	1.346	1.3	--	--	--	--
80	.443	.6	--	--	--	*.00
	.553	.8	--	--	--	--
	.720	1.3	--	--	--	--
81	.354	.6	--	--	--	*.00
	.447	.8	--	--	--	--
	.633	1.3	--	--	--	--

*Assumed 0.

Table F-2. Velocity-gradient data and computed-streambed stresses for 2,230 cubic feet per second flow condition

[$\bar{U}$, average velocity mangitude, in feet per second; z, distance of velocity measurement from streambed, in feet; Slope, slope of the regression line through the points given for that profie; R^2, coefficient of determination of the regression line; τ, profile boundary shear stress, in pounds per square foot; τ_o, approach flow boundary shear stress, in pounds per square foot; ft/s, feet per second; ft, feet; lbs/ft^2, pounds per square foot; --, not available]

Profile	$\bar{U}$ (ft/s)	z (ft)	Slope	R^2	τ (lbs/ft^2)	τ/τ_o
1	0.856	0.4	1.48	0.95	0.027	0.31
	1.039	.6	--	--	--	--
	1.068	.8	--	--	--	--
	1.202	1.3	--	--	--	--
2	1.137	.4	2.44	.84	.010	.12
	1.208	.6	--	--	--	--
	1.185	.8	--	--	--	--
	1.327	1.3	--	--	--	--
3	1.043	.4	.90	1.00	.073	.85
	1.214	.6	--	--	--	--
	1.344	.8	--	--	--	--
	1.610	1.3	--	--	--	--
4	1.289	.4	.58	.93	.174	2.04
	1.468	.6	--	--	--	--
	1.787	.8	--	--	--	--
5	1.881	.4	.66	.81	.134	1.56
	1.953	.6	--	--	--	--
	2.268	.8	--	--	--	--
6	1.425	.4	.46	1.00	.283	3.31
	1.823	.6	--	--	--	--
	2.085	.8	--	--	--	--
7	1.039	.4	.41	.96	.346	4.04
	1.335	.6	--	--	--	--
	1.756	.8	--	--	--	--
8	1.496	.4	1.26	.94	.037	.43
	1.672	.6	--	--	--	--
	1.715	.8	--	--	--	--
9	1.260	.4	.86	.95	.079	.92
	1.362	.6	--	--	--	--
	1.630	.8	--	--	--	--
	1.788	1.3	--	--	--	--
11	.870	.4	.55	1.00	.194	2.27
	1.190	.6	--	--	--	--
12	.966	.4	1.58	.97	.023	.27
	1.046	.6	--	--	--	--
	1.153	.8	--	--	--	--
13	.794	.4	.82	.81	.087	1.01
	1.085	.6	--	--	--	--
	1.077	.8	--	--	--	--
14	1.629	.4	.59	1.00	.168	1.96
	1.927	.6	--	--	--	--

Table F-2. Velocity-gradient data and computed-streambed stresses for 2,230 cubic feet per second flow condition —*Continued*

Profile	$\bar{U}$ (ft/s)	z (ft)	Slope	R^2	τ (lbs/ft^2)	τ/τ_o
15	1.519	0.4	1.90	0.71	0.016	0.19
	1.525	.6	--	--	--	--
	1.638	.8	--	--	--	--
16	1.093	.4	.57	1.00	.182	2.12
	1.405	.6	--	--	--	--
17	1.190	.4	.14	1.00	3.112	36.34
	2.472	.6	--	--	--	--
18	1.638	.4	.45	1.00	.290	3.38
	2.030	.6	--	--	--	--
19	1.506	.4	.39	1.00	.391	4.57
	1.960	.6	--	--	--	--
20	.537	.4	.41	.91	.349	4.08
	1.269	.6	--	--	--	--
	1.386	.8	--	--	--	--
	1.725	1.3	--	--	--	--
22	1.167	.4	3.65	1.00	.004	.05
	1.215	.6	--	--	--	--
23	.403	.4	.35	1.00	.489	5.71
	.863	.6	--	--	--	--
	1.274	.8	--	--	--	--
24	.710	.6	.37	.98	.424	4.94
	.914	.8	--	--	--	--
	1.573	1.3	--	--	--	--
25	1.854	.4	1.07	1.00	.051	.60
	2.019	.6	--	--	--	--
26	.685	.4	.23	1.00	1.102	12.87
	1.432	.6	--	--	--	--
	1.992	.8	--	--	--	--
27	1.829	.4	1.54	.97	.025	.29
	1.982	.6	--	--	--	--
	2.007	.8	--	--	--	--
	2.166	1.3	--	--	--	--
29	.880	.4	.54	.97	.203	2.37
	1.954	.6	--	--	--	--
	1.359	.8	--	--	--	--
	1.781	1.3	--	--	--	--
30	1.100	.4	.35	.99	.471	5.50
	1.436	.6	--	--	--	--
	1.865	.8	--	--	--	--
	2.506	1.3	--	--	--	--
31	.527	.6	.21	.93	1.338	15.62
	.711	.8	--	--	--	--
	1.966	1.3	--	--	--	--

Table F-2. Velocity-gradient data and computed-streambed stresses for 2,230 cubic feet per second flow condition —*Continued*

Profile	$\bar{U}$ (ft/s)	z (ft)	Slope	R^2	τ (lbs/ft^2)	τ/τ_o
32	0.739	0.4	0.69	1.00	0.125	1.45
	.945	.6	--	--	--	--
	1.165	.8	--	--	--	--
	1.470	1.3	--	--	--	--
33	.968	.6	.40	.96	.360	4.20
	1.105	.8	--	--	--	--
	1.739	1.3	--	--	--	--
34	1.621	.6	.28	1.00	.727	8.49
	2.061	.8	--	--	--	--
35	.736	.4	1.63	1.00	.022	.26
	.844	.6	--	--	--	--
36	.981	.4	.41	.77	.350	4.09
	1.806	.6	--	--	--	--
	1.825	.8	--	--	--	--
	2.020	1.3	--	--	--	--
38	.790	.4	.43	.90	.311	3.63
	1.484	.6	--	--	--	--
	1.616	.8	--	--	--	--
	1.895	1.3	--	--	--	--
40	1.660	.6	.62	1.00	.154	1.79
	1.862	.8	--	--	--	--
41	1.067	.4	.67	.92	.132	1.54
	1.211	.6	--	--	--	--
	1.495	.8	--	--	--	--
42	1.006	.4	.60	1.00	.163	1.91
	1.300	.6	--	--	--	--
43	.528	.4	.23	.80	1.072	12.52
	.703	.6	--	--	--	--
	1.603	.8	--	--	--	--
44	1.491	.4	1.03	.99	.055	.65
	1.633	.6	--	--	--	--
	1.736	.8	--	--	--	--
	1.984	1.3	--	--	--	--
45	1.320	.4	.77	.98	.098	1.15
	1.518	.6	--	--	--	--
	1.621	.8	--	--	--	--
	1.978	1.3	--	--	--	--
46	.148	.4	1.63	.96	.022	.26
	.249	.6	--	--	--	--
	.372	.8	--	--	--	--
	.440	1.3	--	--	--	--
47	1.180	.6	.20	.82	1.420	16.58
	2.280	.8	--	--	--	--
	2.629	1.3	--	--	--	--

Table F-2. Velocity-gradient data and computed-streambed stresses for 2,230 cubic feet per second flow condition —*Continued*

Profile	$\bar{U}$ (ft/s)	z (ft)	Slope	R^2	τ (lbs/ft^2)	τ/τ_o
48	0.751	0.4	1.72	1.00	0.020	0.23
	.854	.6	--	--	--	--
49	.332	.4	.90	.95	.072	.84
	.410	.6	--	--	--	--
	.658	.8	--	--	--	--
	.839	1.3	--	--	--	--
50	1.574	.4	.86	1.00	.080	.93
	1.768	.6	--	--	--	--
	1.950	.8	--	--	--	--
	2.160	1.3	--	--	--	--
51	1.034	.4	--	--	--	*.00
	.875	.6	--	--	--	--
	.864	.8	--	--	--	--
	1.004	1.3	--	--	--	--
52	.507	.4	1.05	.99	.053	.62
	.714	.6	--	--	--	--
	.800	.8	--	--	--	--
	1.002	1.3	--	--	--	--
53	.684	.4	.34	.99	.493	5.76
	1.098	.6	--	--	--	--
	1.406	.8	--	--	--	--
	2.153	1.3	--	--	--	--
54	1.020	.4	.96	.98	.064	.75
	1.265	.6	--	--	--	--
	1.383	.8	--	--	--	--
	1.549	1.3	--	--	--	--
55	.454	.4	--	--	--	*.00
	.360	.6	--	--	--	--
	.555	.8	--	--	--	--
	.502	1.3	--	--	--	--
56	.622	.4	1.26	.93	.037	.43
	.702	.6	--	--	--	--
	.851	.8	--	--	--	--
57	1.209	.6	.53	.70	.207	2.42
	1.645	.8	--	--	--	--
	1.694	1.3	--	--	--	--
58	.981	.4	.84	1.00	.083	.97
	1.366	.8	--	--	--	--
	1.584	1.3	--	--	--	--
59	1.473	.8	.38	1.00	.406	4.74
	2.028	1.3	--	--	--	--

Table F-2. Velocity-gradient data and computed-streambed stresses for 2,230 cubic feet per second flow condition —*Continued*

Profile	$\bar{U}$ (ft/s)	z (ft)	Slope	R^2	τ (lbs/ft²)	τ/τ_o
60	1.314	0.4	0.91	0.96	0.071	0.83
	1.424	.6	--	--	--	--
	1.668	.8	--	--	--	--
	1.828	1.3	--	--	--	--
61	1.645	.8	.80	1.00	.091	1.06
	1.907	1.3	--	--	--	--
62	1.343	.4	2.52	.89	.009	.11
	1.346	.6	--	--	--	--
	1.415	.8	--	--	--	--
	1.515	1.3	--	--	--	--
63	1.163	.8	.67	1.00	.131	1.52
	1.477	1.3	--	--	--	--
64	.750	.4	.86	.99	.079	.92
	.976	.6	--	--	--	--
	1.151	.8	--	--	--	--
	1.331	1.3	--	--	--	--
65	1.041	.4	1.21	.86	.040	.47
	1.215	.6	--	--	--	--
	1.379	.8	--	--	--	--
	1.395	1.3	--	--	--	--
66	1.497	.4	.99	1.00	.060	.70
	1.675	.6	--	--	--	--
67	.702	.4	.71	1.00	.115	1.34
	.948	.6	--	--	--	--
68	.810	.4	1.33	1.00	.033	.39
	.942	.6	--	--	--	--
69	1.527	.4	1.83	.79	.018	.21
	1.658	.6	--	--	--	--
	1.650	.8	--	--	--	--
70	1.687	.4	.57	.93	.179	2.09
	2.083	.6	--	--	--	--
	2.161	.8	--	--	--	--
71	1.476	.4	.73	.99	.111	1.29
	1.779	.6	--	--	--	--
	1.890	.8	--	--	--	--
	2.189	1.3	--	--	--	--
72	1.739	.4	1.31	.79	.034	.40
	1.802	.6	--	--	--	--
	2.023	.8	--	--	--	--
	2.016	1.3	--	--	--	--
73	1.379	.8	.51	1.00	.230	2.68
	1.797	1.3	--	--	--	--

Table F-2. Velocity-gradient data and computed-streambed stresses for 2,230 cubic feet per second flow condition —*Continued*

Profile	$\bar{U}$ (ft/s)	z (ft)	Slope	R^2	τ (lbs/ft^2)	τ/τ_o
74	0.736	0.4	0.50	0.99	0.233	2.72
	1.072	.6	--	--	--	--
	1.395	.8	--	--	--	--
	1.732	1.3	--	--	--	--
75	.909	.4	.85	.97	.081	.94
	1.100	.6	--	--	--	--
	1.324	.8	--	--	--	--
	1.477	1.3	--	--	--	--
76	.843	.6	.55	1.00	.193	2.26
	1.104	.8	--	--	--	--
	1.456	1.3	--	--	--	--
77	.742	.4	1.14	.98	.045	.53
	.897	.6	--	--	--	--
	1.053	.8	--	--	--	--
	1.170	1.3	--	--	--	--
78	1.029	.4	.56	.97	.184	2.15
	1.188	.6	--	--	--	--
	1.500	.8	--	--	--	--
	1.881	1.3	--	--	--	--
79	1.768	.6	.92	.95	.070	.81
	1.824	.8	--	--	--	--
	2.104	1.3	--	--	--	--

*Assumed 0.

Table F-3. Velocity-gradient data and computed-streambed stresses for 3,000 cubic feet per second flow condition

$\bar{U}$, average velocity mangitude, in feet per second; z, distance of velocity measurement from streambed, in feet; Slope, slope of the regression line through the points given for that profie; R^2, coefficient of determination of the regression line; τ, profile boundary shear stress, in pounds per square foot; τ_o, approach flow boundary shear stress, in pounds per square foot; ft/s, feet per second; ft, feet; lbs/ft^2, pounds per square foot; --, not available]

Profile	$\bar{U}$ (ft/s)	z (ft)	Slope	R^2	τ (lbs/ft^2)	τ/τ_o
1	1.124	0.4	1.06	0.94	0.052	0.34
	1.249	.6	--	--	--	--
	1.296	.8	--	--	--	--
	1.588	1.3	--	--	--	--
2	1.477	.4	.48	.95	.251	1.66
	1.931	.6	--	--	--	--
	2.059	.8	--	--	--	--
3	1.116	.4	.44	.99	.307	2.02
	1.387	.6	--	--	--	--
	1.713	.8	--	--	--	--
	2.253	1.3	--	--	--	--
4	.954	.4	.31	.86	.614	4.05
	1.893	.6	--	--	--	--
	2.213	.8	--	--	--	--
	2.413	1.3	--	--	--	--
5	2.137	.6	1.01	.86	.057	.38
	2.261	.8	--	--	--	--
6	1.069	.4	.43	.98	.323	2.13
	1.527	.6	--	--	--	--
	1.675	.8	--	--	--	--
	2.284	1.3	--	--	--	--
7	1.206	.6	.59	.95	.168	1.11
	1.521	.8	--	--	--	--
	1.765	1.3	--	--	--	--
8	1.180	.8	.43	1.00	.319	2.11
	1.672	1.3	--	--	--	--
9	1.459	.4	1.35	1.00	.032	.21
	1.589	.6	--	--	--	--
10	.848	.4	1.45	1.00	.028	.18
	.970	.6	--	--	--	--
11	1.738	.4	.33	1.00	.551	3.63
	2.278	.6	--	--	--	--
12	1.315	.4	.33	.85	.527	3.48
	1.246	.6	--	--	--	--
	1.827	.8	--	--	--	--
	2.537	1.3	--	--	--	--
13	1.340	.4	.60	.96	.163	1.08
	1.676	.6	--	--	--	--
	1.968	.8	--	--	--	--
	2.141	1.3	--	--	--	--

Table F-3. Velocity-gradient data and computed-streambed stresses for 3,000 cubic feet per second flow condition —*Continued*

Profile	$\bar{U}$ (ft/s)	z (ft)	Slope	R^2	τ (lbs/ft^2)	τ/τ_o
14	2.681	0.4	0.31	0.97	0.600	3.96
	3.083	.6	--	--	--	--
	3.628	.8	--	--	--	--
15	1.744	.4	.31	.87	.614	4.05
	2.508	.6	--	--	--	--
	2.557	.8	--	--	--	--
16	2.064	.4	.47	1.00	.267	1.76
	2.440	.6	--	--	--	--
17	1.279	.4	.37	.90	.435	2.87
	2.102	.6	--	--	--	--
	2.229	.8	--	--	--	--
	2.598	1.3	--	--	--	--
18	1.398	.4	.48	.94	.254	1.67
	1.787	.6	--	--	--	--
	1.814	.8	--	--	--	--
	2.448	1.3	--	--	--	--
21	.906	.4	.47	.85	.262	1.73
	.944	.6	--	--	--	--
	1.142	.8	--	--	--	--
	1.809	1.3	--	--	--	--
22	.453	.8	.59	1.00	.170	1.12
	.812	1.3	--	--	--	--
23	.929	.4	.41	.90	.346	2.28
	1.150	.6	--	--	--	--
	1.271	.8	--	--	--	--
	2.067	1.3	--	--	--	--
[1]24	1.671	.4	.19	1.00	1.566	10.33
	1.530	.6	--	--	--	--
	1.630	.8	--	--	--	--
	2.345	1.3	--	--	--	--

[1]Profile 24 is a combination of data from profiles 19 and 20.

District Chief
Kentucky District
U.S. Geological Survey
Water Resources Division
2301 Bradley Avenue
Louisville, KY 40217-1807